ORNL/TM-6113

High Voltage Research (Breakdown Strengths of Gaseous and Liquid Insulators)

Semiannual Report (April 1–September 30, 1977)

OAK RIDGE NATIONAL LABORATORY
OPERATED BY UNION CARBIDE CORPORATION · FOR THE DEPARTMENT OF ENERGY

DISCLAIMER

Printed in the United States of America. Available from
National Technical Information Service
U.S. Department of Commerce
5285 Port Royal Road, Springfield, Virginia 22161
Price: Printed Copy $7.25; Microfiche $3.00

ORNL/TM-6113

Contract No. W-7405-eng-26
Activity No. HA 02 01 00 0

HEALTH AND SAFETY RESEARCH DIVISION

ATOMIC, MOLECULAR AND HIGH
VOLTAGE PHYSICS GROUP

HIGH VOLTAGE RESEARCH (BREAKDOWN STRENGTHS OF GASEOUS AND LIQUID INSULATORS)

Semiannual Report
(April 1-September 30, 1977)

L. G. Christophorou

D. R. James
R. Y. Pai
R. A. Mathis
M. O. Pace (part time)
D. W. Bouldin (part time)
A. A. Christodoulides (alien guest)
C. C. Chan (student)

Date Published: November 1977

NOTICE This document contains information of a preliminary nature. It is subject to revision or correction and therefore does not represent a final report.

OAK RIDGE NATIONAL LABORATORY
Oak Ridge, Tennessee 37830
operated by
UNION CARBIDE CORPORATION
for the
DEPARTMENT OF ENERGY

THIS PAGE

WAS INTENTIONALLY

LEFT BLANK

TABLE OF CONTENTS

		Page
	ABSTRACT	v
I.	INTRODUCTION	1
II.	BREAKDOWN STRENGTHS OF MULTICOMPONENT GAS MIXTURES (LOW PRESSURES)	2
III.	BREAKDOWN STRENGTHS OF MULTICOMPONENT GAS MIXTURES (HIGH PRESSURES)	12
IV.	BREAKDOWN STRENGTHS OF UNITARY GASES	14
V.	BASIC STUDIES	18
VI.	APPLIED STUDIES	25
VII.	ENVIRONMENTAL EFFECTS OF DIELECTRIC GASES: ANALYSIS OF THE BREAKDOWN PRODUCTS OF NEW GASEOUS INSULATORS	33
VIII.	APPARATUS	39
IX.	RADIOGRAPHY OF ENERGIZED GAS-INSULATED CABLES	55
X.	INTERNATIONAL SYMPOSIUM ON GASEOUS DIELECTRICS	56
XI.	PUBLICATIONS AND CONTACTS	57
XII.	REFERENCES	60
	APPENDICES	61

THIS PAGE

WAS INTENTIONALLY

LEFT BLANK

ABSTRACT

Direct current breakdown strength measurements on a large number of multicomponent gas mixtures at low ($\lesssim$ 1 atm) and high ($\lesssim$ 5 atm) pressures led to the discovery of many gas mixtures of electron-attaching gases and strongly electron-attaching gases with N_2 and C_3F_8 which are superior to SF_6. Of special significance are mixtures containing C_4F_6 (perfluoro-2-butyne). The breakdown strength of one such mixture (20% C_4F_6-80% SF_6) is $\sim$ 30% higher than pure SF_6 under identical conditions, both at low ($\sim$ 0.7 atm) and high (4.6 atm) pressures. Perfluorocyclohexene (C_6F_{10}) and C_5F_8 (perfluorocyclopentene) were found at low pressure ($\sim$ 0.2 atm) to be, respectively, $\sim$ 2.1 and 2.2 times better than SF_6 under comparable conditions; they both have a potential as additives in gas mixtures.

The effect of the inelastic electron scattering properties of a gas via negative ion resonances in the low-energy range (1 to $\sim$ 4 eV) on the breakdown strength has been demonstrated for H_2, N_2, and CO and binary mixtures of these with SF_6 and C_4F_6 (perfluoro-2-butyne). Electron attachment to C_4F_6 (perfluoro-1,3-butadiene), C_7F_8 (perfluorotoluene), and C_8F_{16} (perfluoro-1,3-dimethylcyclohexane) has been studied; the magnitude and energy dependence of the attachment rates and cross sections correlate with the respective DC breakdown strengths of these systems. Knowledge on low-energy electron-molecule interaction processes in dilute and in dense gases has been synthesized, discussed, and related to the breakdown strengths of gaseous dielectrics.

The construction of a new high pressure (to $\sim$ 11 atm), variable temperature (- 50°C to + 150°C) apparatus has been completed and a practical test facility utilizing cylindrical electrode geometries has

been put into operation; the first results on the latter apparatus were on SF_6-N_2 and c-C_4F_8—N_2 mixtures. Studies of environmental effects of dielectric gases, via their electron-impact-induced decompositions and analysis of their breakdown products, have begun using mass spectrometry and gas chromatography; C_4F_6 (perfluoro-2-butyne) seems to be resistant to electron-impact-induced decomposition indicating long-term stability. Calculations of the effects of radiography on an energized gas-insulated cable were performed, and on the basis of these calculations no effect of radiography is foreseen.

I. INTRODUCTION

The basic and applied aspects of gaseous dielectrics are studied comprehensively, and improved gaseous insulators are being developed for the nation's varied needs in high voltage insulation. The multiple needs in high voltage insulation dictate the development of a variety of gaseous insulating systems each appropriate for the specific need. It has been argued in our earlier reports and it is further emphasized in this report that such a variety of optimal insulators consists of multi-component gas mixtures (rather than a single gas system) carefully designed as to components and properties on the basis of detailed fundamental physicochemical knowledge, especially on low-energy electron-molecule interactions.

II. BREAKDOWN STRENGTHS OF MULTICOMPONENT GAS MIXTURES (LOW PRESSURES)

Our work on low-pressure multicomponent systems continued. Such experiments are singularly appropriate for screening a large number of gases and for studying synergistic behavior of gas combinations. Synergistic behavior may arise from cooperative effects of appropriate combinations of two or more electron-attaching components and/or from cooperative effects of combination of gases of appropriate electron scattering and electron-attaching properties. Such measurements—allowing faster, cheaper, and more accurate data acquisition than for high-pressure systems—enhance the breadth of our breakdown studies and provide a multiplicity of optional systems to be used for the varied needs of gaseous insulation. The importance of such studies at low pressures is strengthened by our earlier[1] and present (Section III) findings that the breakdown strength of the low-pressure multicomponent systems is not significantly different at higher total pressures within the Pd range we covered.

The general principles of choosing gases for multicomponent mixtures have been outlined in our earlier reports and are further discussed in Appendix III. The overall properties of mixtures of gases are determined by the cumulative effects of their components on the number and energy distribution of the free electrons in the mixture. Although knowledge of the basic cross sections of the component gases does not presently allow a detailed deduction of the basic properties of the corresponding multicomponent mixture, it can be used as a guide in tailoring promising mixtures for breakdown testing.

Binary Mixtures of Electron-Attaching Gases with N_2

In Table I the slope $\Delta V_s/\Delta(Pd)$, where V_s is the breakdown voltage and Pd is the product of the total gas pressure P and the electrode spacing d, is presented for a number of binary mixtures of electron-attaching gases with N_2. N_2 is used as the buffer gas, and SF_6, C_4F_6 (perfluoro-2-butyne), c-C_4F_8, C_4F_8 (perfluoro-2-butene), and C_3F_8 are used singly as electron-attaching gases. These data were presented graphically (for one 4.595 atm-mm Pd value) in our last report.[1] The overall data are presented here for completeness in our study of gas mixtures. The important aspect of these data, as pointed out earlier,[1] is the stronger saturation effect exhibited by the N_2-SF_6 mixtures compared with the rest for which the electron attachment cross section extends to much higher energies than for the SF_6-N_2 mixtures.

Multicomponent Mixtures Containing N_2 as the Basic Component

Table II lists $\Delta V_s/\Delta(Pd)$ for mixtures again containing N_2 as the buffer gas but with two or more electron-attaching components used in combination to bracket a wider energy range over which effective electron attachment occurs. There are two salient features of these mixtures:
(1) C_4F_6 is an extremely effective additive in N_2. In mixtures 4 through 10 with 70% N_2 those mixtures containing C_4F_6 are all better dielectrics than those without C_4F_6. Mixtures 11 through 17 show further evidence of the effectiveness of C_4F_6 as an additive. Twenty and 30% C_4F_6 mixtures are markedly better than the mixtures with less or no C_4F_6.
(2) A rather distinct synergistic effect is observed when C_3F_8 is used in combination with SF_6 and C_4F_6. Thus if we compare mixtures 11 and 13,

TABLE I

$\Delta V_s/\Delta(Pd)$ for Binary Mixtures of Electron-Attaching Gases with N_2; P_{total} = 500 Torr (Plane-Plane Electrode Geometry)

Mixture No.	Percentage of Gas						$\frac{\Delta V_s}{\Delta(Pd)}\left(\frac{kV}{atm\text{-}mm}\right)$
	N_2	SF_6	C_4F_6 †	$c\text{-}C_4F_8$	C_4F_8 ‡	C_3F_8	
1		100					8.83
2	95	5					5.09
3	95		5				6.01
4	95			5			4.37
5	95				5		4.40
6	95					5	3.74
7	90	10					6.10
8	90		10				6.80
9	90			10			4.51
10	90				10		4.98
11	90					10	4.12
12	80	20					6.44
13	80		20				8.64
14	80			20			5.39
15	80				20		6.19
16	80					20	4.69
17	70	30					7.29
18	70		30				10.23
19	70			30			6.09
20	70				30		7.18
21	70					30	5.22
22	60	40					7.76
23	60		40				12.23
24	60			40			6.77
25	60				40		8.30

†Perfluoro-2-butyne.

‡Perfluoro-2-butene.

TABLE II

$\Delta V_s/\Delta(Pd)$ for Multicomponent Mixtures Containing N_2 as the Basic Component; P_{total} = 500 Torr (Plane-Plane Electrode Geometry)

Mixture No.	Percentage of Gas						$\frac{\Delta V_s}{\Delta(Pd)}\left(\frac{kV}{atm\text{-}mm}\right)$
	N_2	SF_6	C_4F_6 †	$c\text{-}C_4F_8$	C_4F_8 ‡	C_3F_8	
1		100					8.83
2	80	10	10				7.69
3	80	10				10	6.36
4	70	10	10	10			8.11
5	70	10			10	10	7.05
6	70	10		20			6.85
7	70	10			20		7.50
8	70	10	10			10	8.28
9	70	10		10		10	6.88
10	70		10	10		10	7.94
11	60	10	20			10	10.32
12	60	10	10	10		10	8.42
13	60	20	20				9.46
14	50	10	20	10		10	11.04
15	50	20	20			10	10.41
16	50	10	20			20	10.41
17	50	20	30				11.61
18	50	10	30			10	12.03
19	30	30	20			20	11.13

†Perfluoro-2-butyne.

‡Perfluoro-2-butene.

changing 20% SF_6 to 10% SF_6 and 10% C_3F_8 improves the mixture by approximately 10%. Mixtures 17 and 18 show this effect also. This is seen clearly in Fig. 1 where V_s versus Pd is presented for mixtures 11, 13, 17, and 18. The breakdown strength of each of these mixtures is better than for pure SF_6.

These findings seem to indicate that the electron-capturing capability of SF_6 saturates markedly even at 10% admixture, so that increasing the percentage of SF_6 from 10 to 25% influences the electron attachment properties of the mixture less than 10% of C_3F_8 which captures electrons weakly but at higher energies[2] than either SF_6 or C_4F_6. Consistent with this argument are the data on mixtures 14 and 15. Changing from 20% SF_6 to 10% SF_6-10% c-C_4F_8 increases the dielectric strength even though c-C_4F_8, whose electron attachment cross section extends to higher energies than that for SF_6,[3] is not an effective additive by itself (see mixtures 4, 9, and 14 in Table I).

Experiments are continuing on mixtures of different proportions and compositions to further test these propositions. Those mixtures which show promise, such as 20% C_4F_6-10% SF_6-10% C_3F_8-60% N_2, will be tested at higher total pressures.

Mixtures Containing N_2 and/or CO_2

In Table III, $\Delta V_s/\Delta(Pd)$ are given for mixtures of gases using N_2 and CO_2 as major components. Pure N_2 is slightly better as a dielectric than pure CO_2. Except for mixtures containing c-C_4F_8 (see mixtures 4 and 5), N_2 is better as a buffer gas than CO_2. These data are being analyzed.

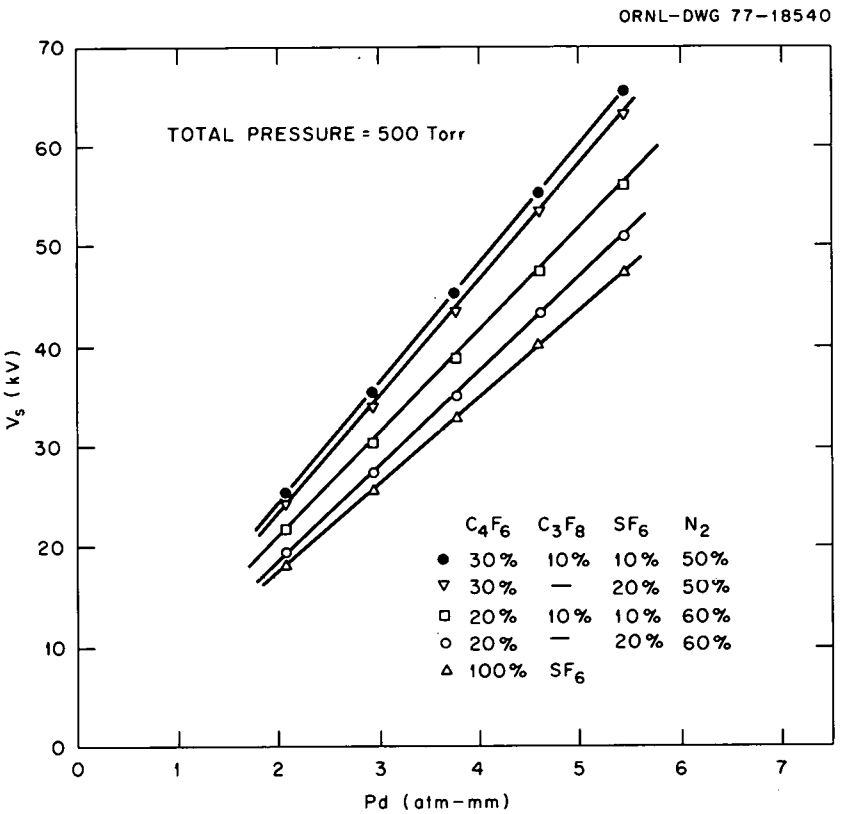

FIG. 1. V_s versus Pd for SF_6 and mixtures of N_2, C_4F_6, C_3F_8, and SF_6 at a total pressure of 500 torr (see text) (plane-plane electrode geometry).

TABLE III

$\Delta V_s/\Delta(Pd)$ for Mixtures Containing N_2 and/or CO_2; P_{total} = 500 Torr
(Plane-Plane Electrode Geometry)

Mixture No.	Percentage of Gas							$\frac{\Delta V_s}{\Delta(Pd)}\left(\frac{kV}{atm\text{-}mm}\right)$
	N_2	CO_2	SF_6	C_4F_6†	c-C_4F_8	C_4F_8‡	C_3F_8	
1			100					8.83
2	80			20				8.64
3		80		20				8.32
4	80				20			5.15
5		80			20			5.40
6	80					20		6.02
7		80				20		5.97
8	80						20	4.69
9		80					20	4.24
10	40	40	20					6.14
11	40	40		20				8.55
12	40	40			20			5.34
13	40	40				20		5.99
14	40	40					20	4.59
15	40	40	10				10	5.87
16	35	35		10		10	10	8.62
17	35	35	10			10	10	6.76
18	35	35	10	10			10	8.15
19	35	35	10	10		10		8.55
20	30	30			40			6.90
21	30	30	10	10		10	10	9.26

†Perfluoro-2-butyne.

‡Perfluoro-2-butene.

Multicomponent Mixtures Containing C_4F_6 (Perfluoro-2-Butyne)

In Table IV are listed breakdown strength data for mixtures of C_4F_6 with a number of gases. Some of these data were taken from the previous three tables in order to emphasize the unique effectiveness of C_4F_6 as additive in multicomponent mixtures. Except for three mixtures with very small percentages of C_4F_6, the rest of the mixtures which contain C_4F_6 have breakdown strengths greater than or equal to 90% that of SF_6. Interestingly, mixtures of C_4F_6 and SF_6 show a slight synergism: 50% SF_6-50% C_4F_6 has a relative breakdown strength of 1.75 compared with a weighted average value[1] of 1.6.

C_6F_{10} (Perfluorocyclohexene) as an Additive to N_2

C_6F_{10} has been found to be a good additive in N_2. Figure 2 shows the breakdown voltage V_s versus the percentage of C_6F_{10} in N_2 for Pd values of 0.1 and 0.3 atm-mm at a total pressure of 80 torr. There is no evidence for a saturation effect for this system. Calculation of the breakdown voltage for the mixture based on the weighted average method[1] was found to agree well with the experimental values indicating no synergism.

TABLE IV

DC Breakdown Strengths for Some Unitary and Multicomponent Mixtures Containing C_4F_6[†]

Percentage of Component Gas							Slope (kV/atm-mm)	Intercept (kV)	$(V_s)_{Relative}$[‡]
C_4F_6	iso-C_4F_8	c-C_4F_8	SF_6	C_3F_8	CO_2	N_2			
A. Unitary Systems									
100							19.74	- 0.61	2.21
	100						14.80	0.44	1.69
		100					10.94	0.38	1.25
			100				8.83	- 0.03	1.00
				100			7.47	1.23	0.93[§]
					100		2.72	1.89	0.37[‖]
						100	2.78	2.53	0.40
B. Binary Mixtures									
5						95	6.01	0.83	0.71
10						90	6.80	0.41	0.79
20						80	8.64	0.35	0.99
30						70	10.23	0.10	1.16
40						60	12.23	0.30	1.40
20					80		8.32	- 0.10	0.94
5			95				9.24	2.36	1.10[¶]
10			90				10.39	- 1.00	1.17[#]
20			80				11.71	- 0.79	1.30
50			50				14.09	6.89	1.75[#]
C. Tertiary Mixtures									
10			10			80	7.69	0.73	0.90
20			20			60	9.46	- 0.22	1.07
30			20			50	11.61	0.29	1.33
20					40	40	8.55	- 0.09	0.97
D. Four-Component Mixtures									
10			10	10		70	8.28	0.59	0.96
10		10	10			70	8.11	0.49	0.94
10		10		10		70	7.94	0.78	0.93
20			10	10		60	10.32	0.28	1.18
30			10	10		50	12.03	0.20	1.37
E. Five-Component Mixtures									
6.6		6.6	6.6	6.6		73.6	7.16	0.59	0.83
10		10	10	10		60	8.42	0.43	0.97
10			10	10	35	35	8.15	0.30	0.93
10	10		10		35	35	8.55	0.31	0.98
10	10			10	35	35	8.62	0.23	0.98
20		10	10	10		50	11.05	- 0.31	1.24

[†] Plane-plane uniform field geometry unless otherwise indicated. Total pressure is 500 torr unless otherwise noted.

[‡] Breakdown strength relative to SF_6 of 1.

[§] Sphere-plane geometry; P = 760 torr.

[‖] Data from H. Winkelnkemper, Z. Krasucki, J. Gerhold, T. W. Dakin, Electra 52, 67 (1977).

[¶] P = 2000 torr.

[#] P = 1000 torr.

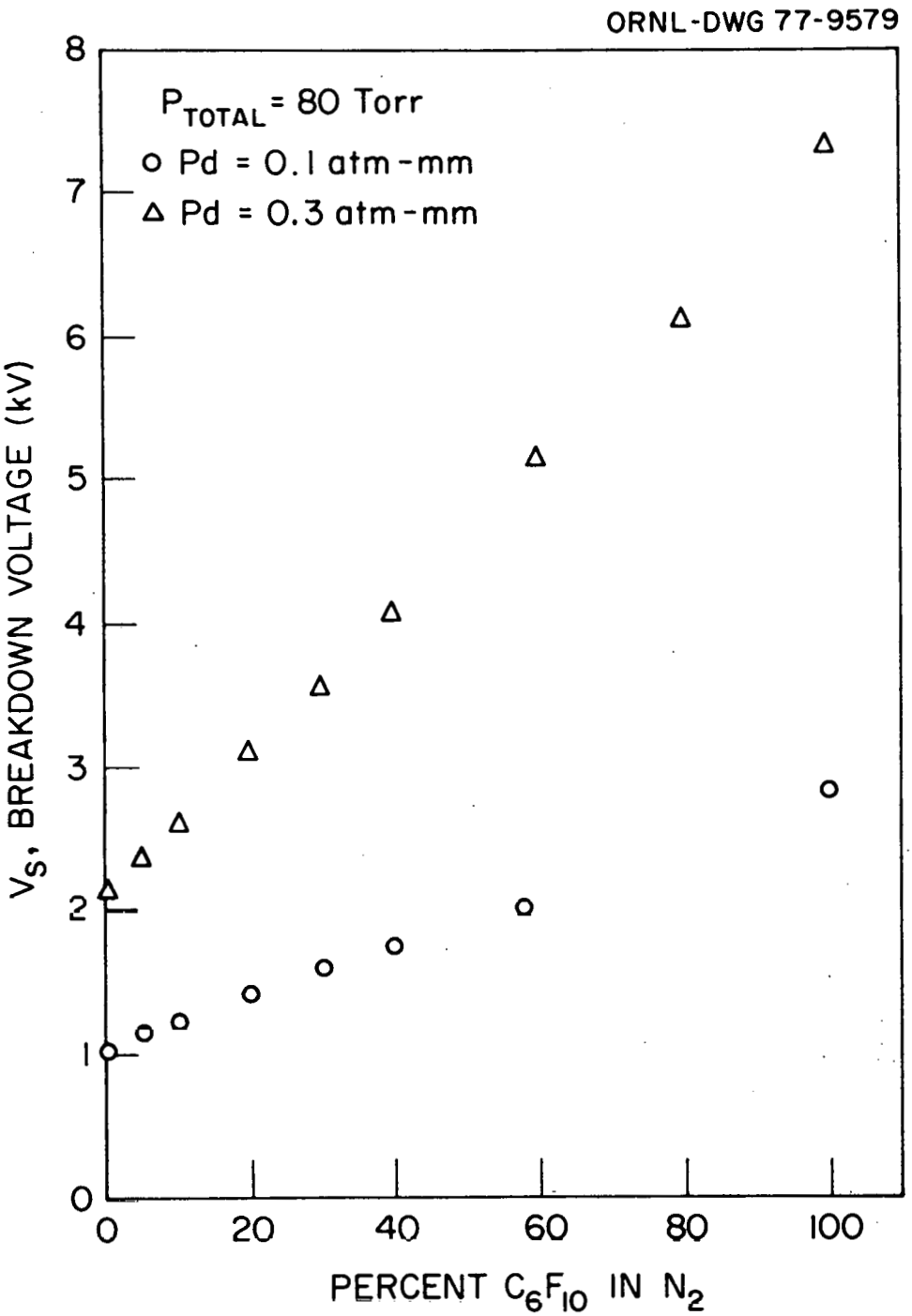

FIG. 2. Breakdown voltage, V_S, as a function of percent of C_6F_{10} in N_2 at the indicated pressure and Pd values (sphere-plane electrode geometry).

III. BREAKDOWN STRENGTHS OF MULTICOMPONENT GAS MIXTURES (HIGH PRESSURES)

Figure 3 shows the breakdown strength as a function of Pd for three different gases/mixtures: pure SF_6, 20% C_4F_6-80% SF_6, and 10% C_4F_6-40% SF_6-50% N_2. The breakdown strength of the 20% C_4F_6-80% SF_6 mixture is approximately 30% better than that of pure SF_6 under identical conditions. It compares well with our low-pressure (500 torr) data (see Table IV).

The 10% C_4F_6-40% SF_6-50% N_2 mixture has a dielectric strength which is approximately the same as that of pure SF_6, but it is estimated to be a cheaper gas (taking the cost of C_4F_6 to be $\sim$ 3 times that of SF_6). This gas would be expected to withstand impulse voltages better than pure SF_6.

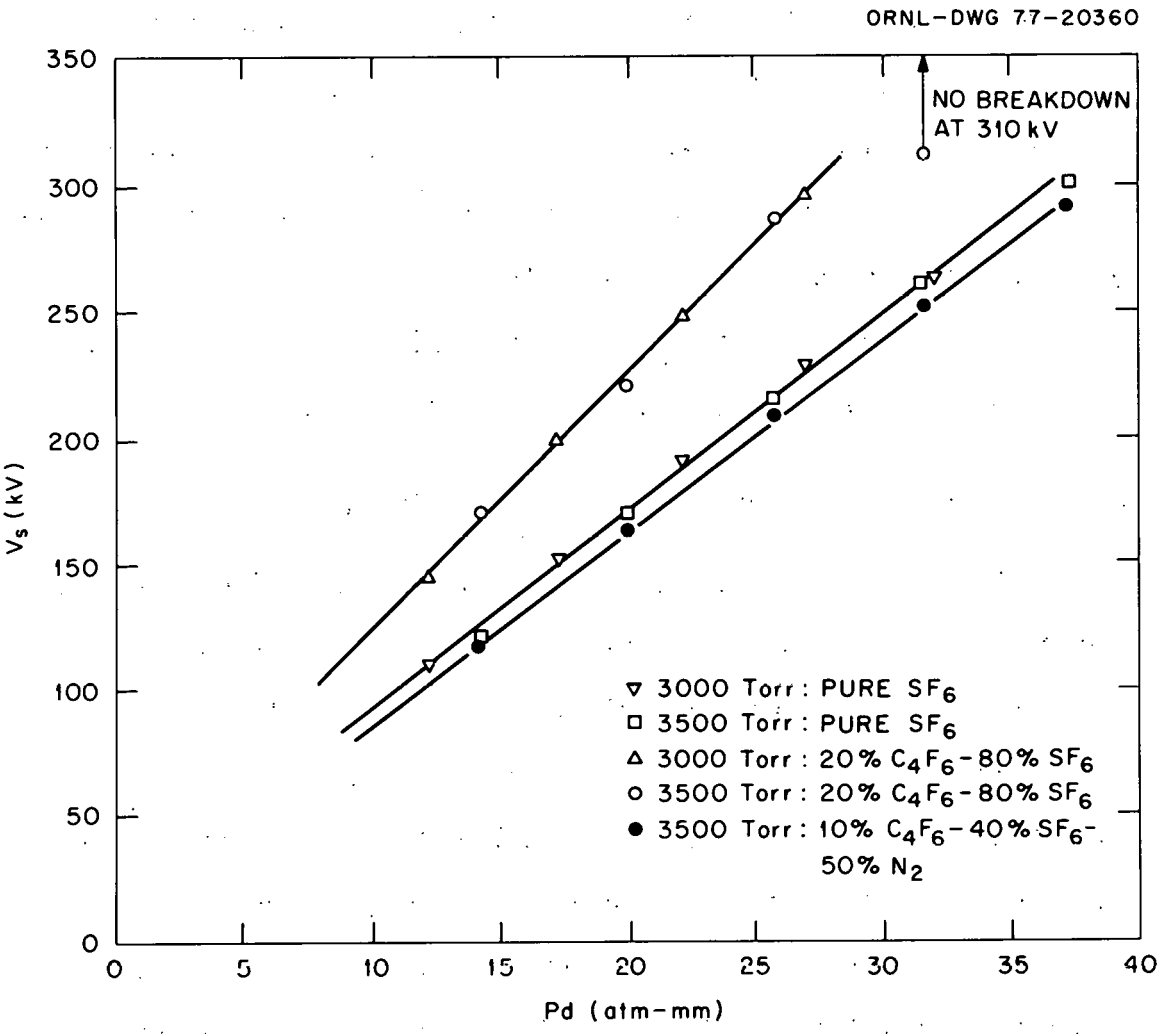

FIG. 3. Breakdown voltage, V_s, for pure SF_6 and for SF_6-C_4F_6 (hexafluoro-2-butyne) and SF_6-C_4F_6-N_2 mixtures as a function of Pd for pressures 3000 to 3500 torr (sphere-sphere electrode geometry).

IV. BREAKDOWN STRENGTHS OF UNITARY GASES

Important Physical Properties of Dielectric Gases

In Appendix I, the dielectric strengths and synonyms for the unitary gases investigated by us so far are listed along with their structural formulae. The search for new compounds (to be used primarily as additives in multicomponent systems) continues, guided on one hand by basic knowledge on molecular structure and electron-molecule interactions and on the other hand by the well-known physical, chemical, toxicological, engineering, and economic practical constraints.

Breakdown Strength of Perfluorocyclopentene (C_5F_8)

Perfluorocyclopentene (see structural formula in Appendix I) is another of the low-vapor-pressure fluorocarbons possessing a high dielectric strength. Its breakdown voltage as a function of Pd, measured in a sphere-plane electrode apparatus, is compared with those of several other previously measured compounds at low pressures in Fig. 4. Over the range of Pd covered ($0.5 \lesssim Pd \lesssim 2.0$ atm-mm), the breakdown strength of C_5F_8 is approximately 2.2 times higher than that for pure SF_6 under comparable conditions. This compound has a potential as an additive.

Breakdown Strength of SF_6 at High Pressures

Breakdown strength measurements of SF_6 at 2000 and 3000 torr have been made with two electrode geometries: plane-plane electrode design[3] and sphere-sphere electrode configuration (sphere diameter = 1-1/2 inches). The data are shown in Fig. 5. Both electrode geometries gave the same results within the statistical error which is smaller than the size of

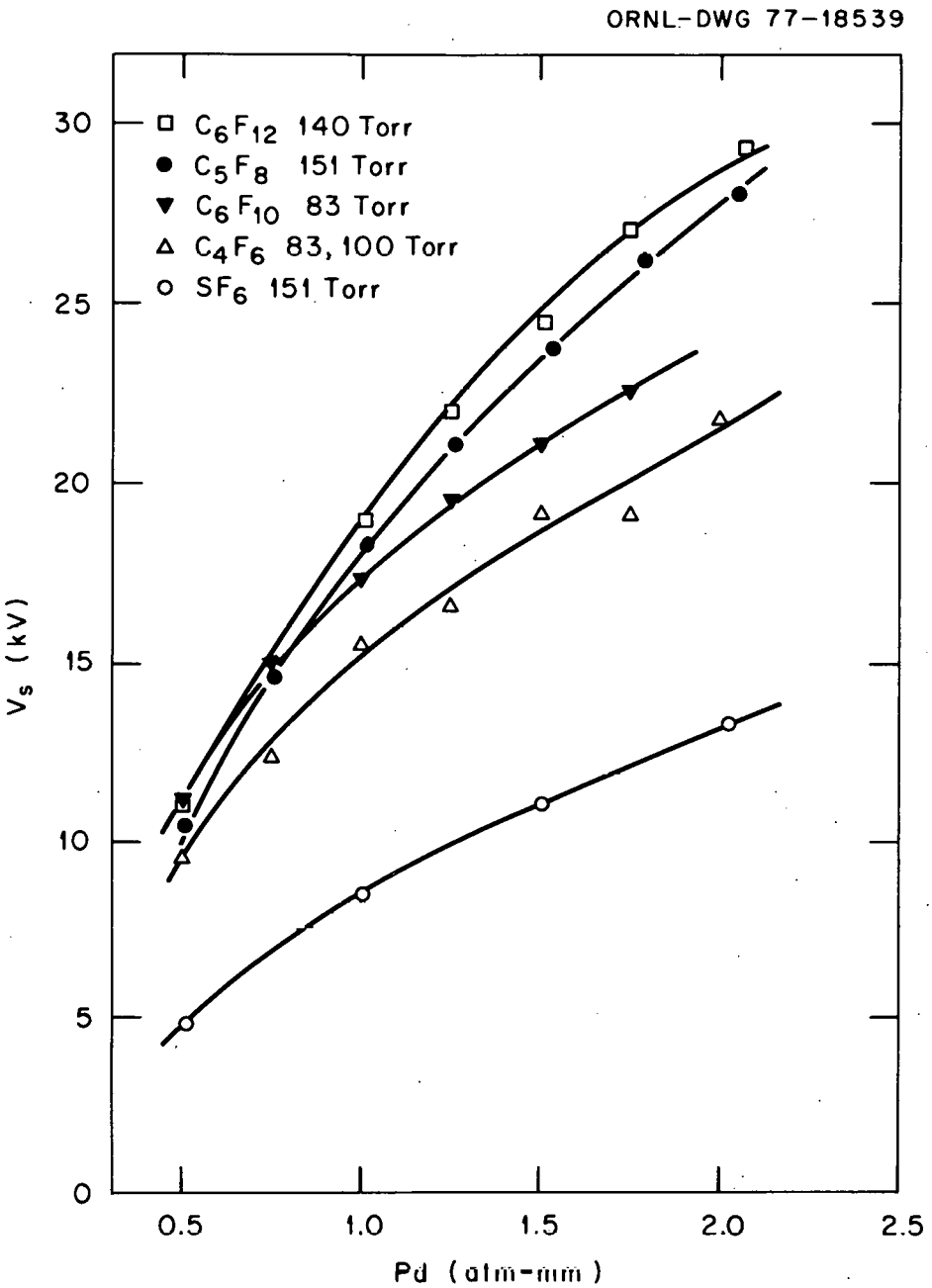

FIG. 4. Breakdown voltage, V_s, versus Pd for C_6F_{12}, C_5F_8, C_6F_{10}, C_4F_6, and SF_6 at the indicated pressures (sphere-plane electrode geometry).

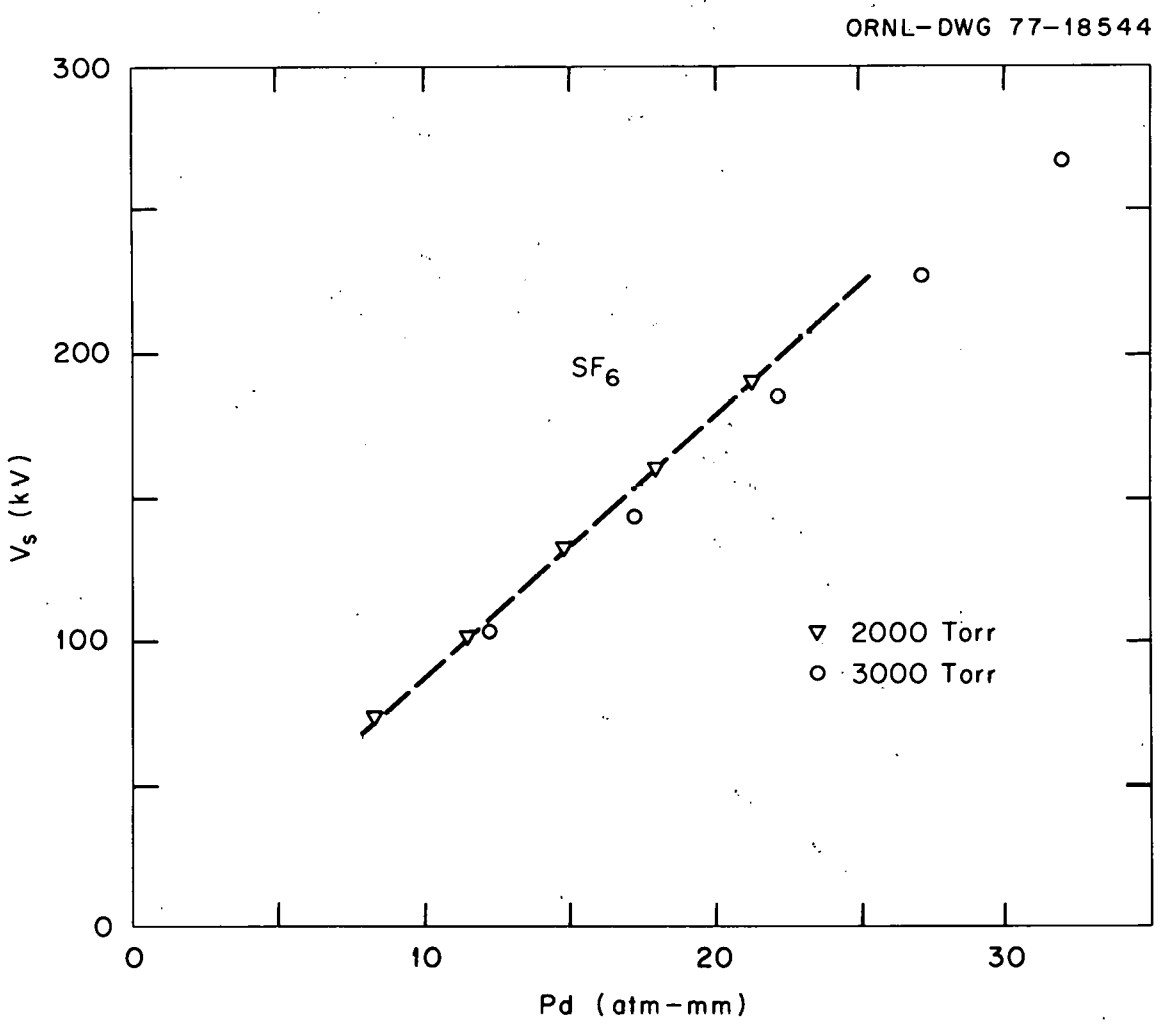

FIG. 5. V_s versus Pd for pure SF_6 at 2000 (▽) and 3000 (o) torr (see text).

the symbols in the figure. In this set of measurements, the breakdown strength at 3000 torr is slightly lower than that at 2000 torr, but it is somewhat higher than that we presented in our last report.[1] The earlier data seem to have been affected by the presence of corona due to faulty insulation in the high voltage lead inside the chamber. Improvements in the insulation eliminated the effect of corona in the present measurements.

V. BASIC STUDIES

Electron Attachment

In support of our breakdown strength studies on fluorocarbons and fluorocarbon mixtures, we have continued to measure the electron attachment rates as a function of mean electron energy, $\langle\varepsilon\rangle$, and to calculate from these the corresponding electron attachment cross sections as a function of electron energy, ε, for these compounds. In Fig. 6 the electron attachment rate, αw, is presented as a function of $\langle\varepsilon\rangle$ for C_7F_8 (perfluorotoluene), C_8F_{16} (perfluoro-1,3-dimethylcyclohexane), and C_4F_6 (perfluoro-1,3-butadiene). These were measured in mixtures with N_2 (see ref. 4, Chap. 4) except for C_4F_6 for which measurements were made in both N_2 and Ar as the carrier gas.[4] In the last case the agreement between the two sets of values is excellent. The measurements with C_7F_8 were difficult since this molecule tends to stick to the walls of the apparatus, and the measured attachment rates changed with time. For this reason the uncertainty in the data is large ($\sim$ 15%) preventing determination of the electron attachment cross sections as a function of electron energy via the swarm-unfolding method.[5]

The unfolded electron attachment cross sections as a function of electron energy are shown in Fig. 7 for C_8F_{16} and C_4F_6 (perfluoro-1,3-butadiene) along with those previously determined for SF_6 and C_4F_6 (perfluoro-2-butyne). The cross section for C_8F_{16} shows a peak at $\sim$ 0.2 eV and decreases monotonically beyond this energy to $\sim$ 1.2 eV. Below $\sim$ 0.1 eV, the cross section increases again with decreasing energy. The cross section for C_4F_6 (perfluoro-1,3-butadiene) is higher than that of the butyne isomer below $\sim$ 0.35 eV but is lower at higher energies (see Fig. 7).

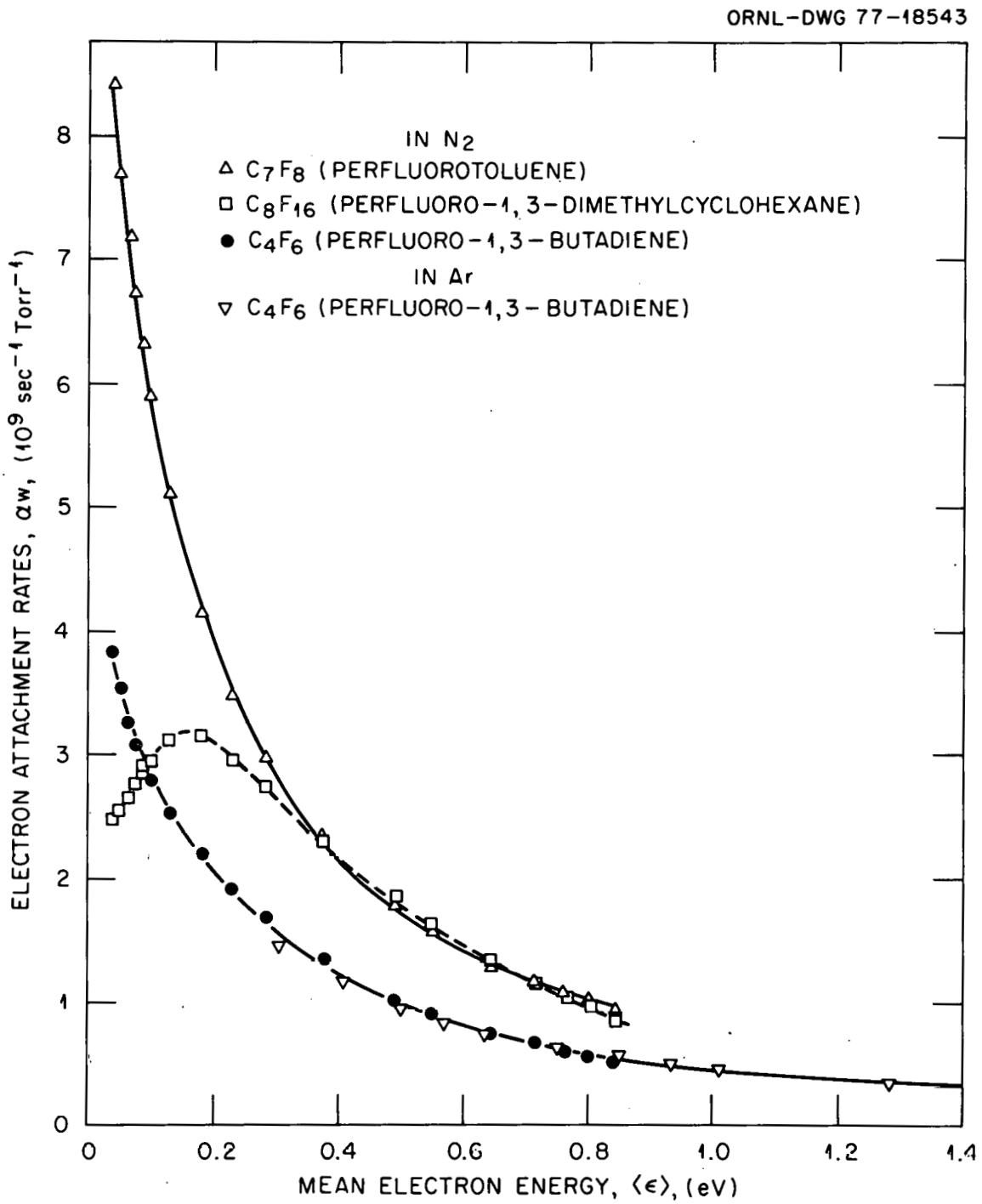

FIG. 6. Electron attachment rate, αw (in units of sec^{-1} $torr^{-1}$), as a function of mean electron energy, $\langle\varepsilon\rangle$ (in units of eV), for (△) C_7F_8 (perfluorotoluene), (□) C_8F_{16} (perfluoro-1,3-dimethylcyclohexane), and (●) C_4F_6 (perfluoro-1,3-butadiene) measured in mixtures with N_2 and (▽) C_4F_6 (perfluoro-1,3-butadiene) measured in mixtures with Ar.

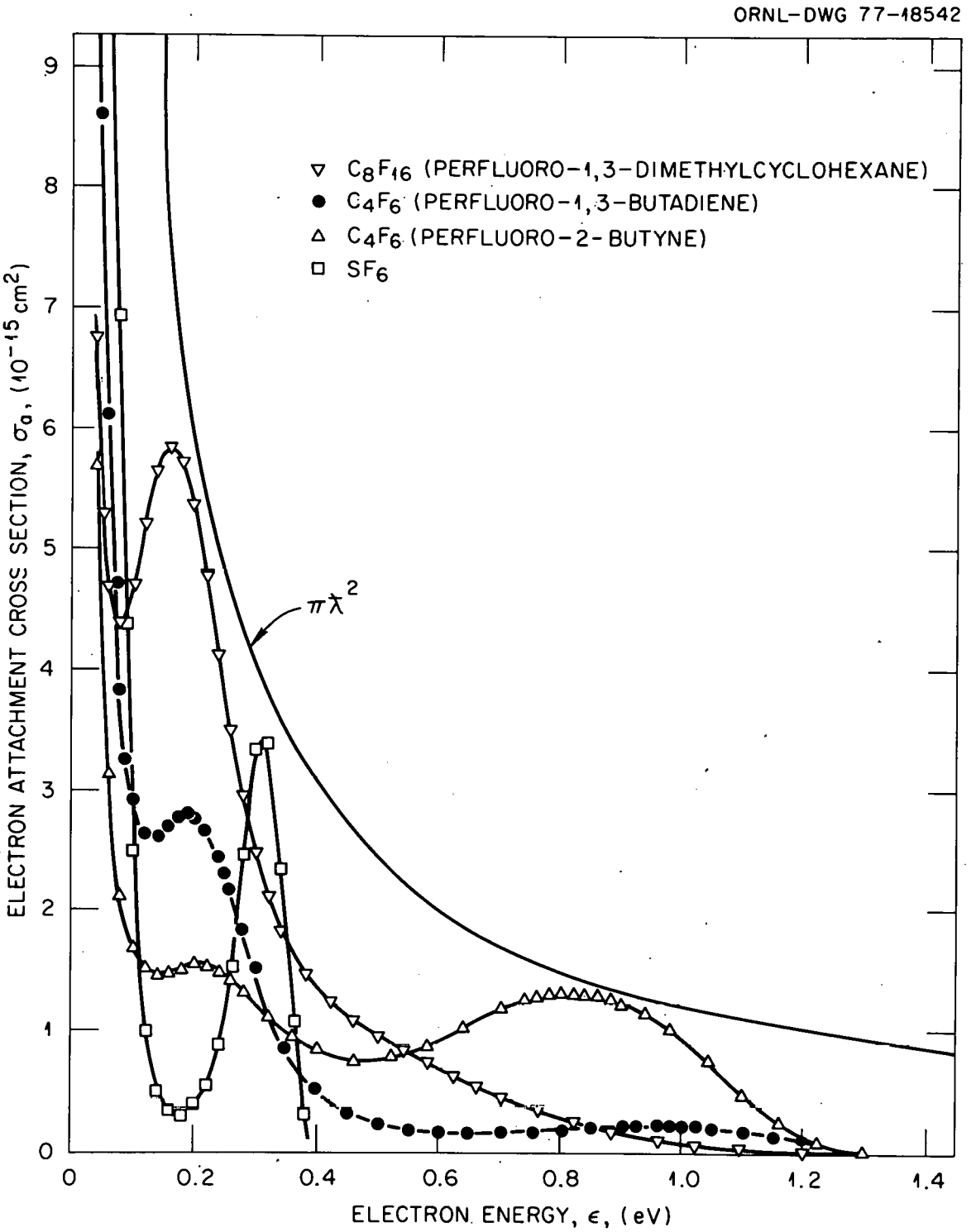

FIG. 7. Electron attachment cross sections as a function of electron energy for (▽) C_8F_{16} (perfluoro-1,3-dimethylcyclohexane), (●) C_4F_6 (perfluoro-1,3-butadiene), (△) C_4F_6 (perfluoro-2-butyne), and (□) SF_6 (see text).

The larger breakdown strength (Fig. 8 of ref. 1) of C_7F_8 compared with C_4F_6 (perfluoro-1,3-butadiene) is consistent with its higher electron attachment rate (Fig. 6) and the larger electron attachment cross section for C_4F_6 (perfluoro-2-butyne) in the energy range $\sim$ 0.4 to $\sim$ 1.2 eV compared with its isomer perfluoro-1,3-butadiene (Fig. 7) is also consistent with the higher breakdown strength of the former (see Table I of ref. 1). The high dielectric strength of all these compounds and C_8F_{16} (see Fig. 8 of ref. 1) accord well with our picture that large attachment rates (or cross sections) out to $\sim$ 1 to 2 eV greatly increase the dielectric strength of the gaseous insulator. It should be stressed, however, that other processes besides electron attachment could critically affect the breakdown strength of a gaseous dielectric (see earlier reports and Appendix III).

Elementary Electron-Molecule Interaction Processes

A comprehensive paper entitled "Elementary Electron-Molecule Interactions and Negative Ion Resonances at Subexcitation Energies and Their Significance in Gaseous Dielectrics" has been completed. In this paper recent knowledge on low-energy (mostly $\lesssim$ 10 eV) electron-molecule interaction processes in dilute and in dense gases has been synthesized, discussed, and related to the breakdown strength of gaseous dielectrics. In this paper, also, the optimal design of multicomponent gaseous insulators on the basis of such knowledge is discussed. The paper has been presented at the XIIIth International Conference on Phenomena in Ionized Gases, Berlin, September 11-17, 1977, and will be published in the conference proceedings (Vol. III [Invited Lectures]). It is added as Appendix III to this report.

Additionally, the role and need of electron impact ionization cross sections close to the ionization thresholds for dielectric gases has been documented. Plans to obtain such needed information and possibly also to measure directly the electron energy distribution functions at prebreakdown E/P values are being contemplated.

Effect of Negative Ion Resonances on Breakdown

In our last report[1] we presented preliminary data on the breakdown strengths of N_2, CO, and H_2 and binary mixtures of these with C_4F_6 (perfluoro-2-butyne) in an effort to test the effect of negative ion resonances, NIRs, exhibited by these systems on their breakdown strengths. On the basis of these results and the known electron scattering cross sections (Fig. 8), it was concluded that the higher the electron scattering cross section (mainly indirect through negative ion resonances) the better is the breakdown strength of the mixture, demonstrating in this way the direct effect of the inelastic scattering properties of the gas via negative ion resonances in the low-energy range ($\sim$ 1 to $\sim$ 4 eV) on the breakdown strength. These preliminary studies were extended to include mixtures of SF_6 as well as C_4F_6 with H_2, N_2, and CO and our findings are summarized in Table V. It is seen that the breakdown strength (relative to SF_6 of 1) for the unitary systems decreases in the order CO (0.5) > N_2 (0.4) > H_2 (0.25), that is, in the order the magnitude of the scattering cross sections due to NIRs shown in Fig. 8 decreases. The data for the binary mixtures (see Table V) behave similarly.

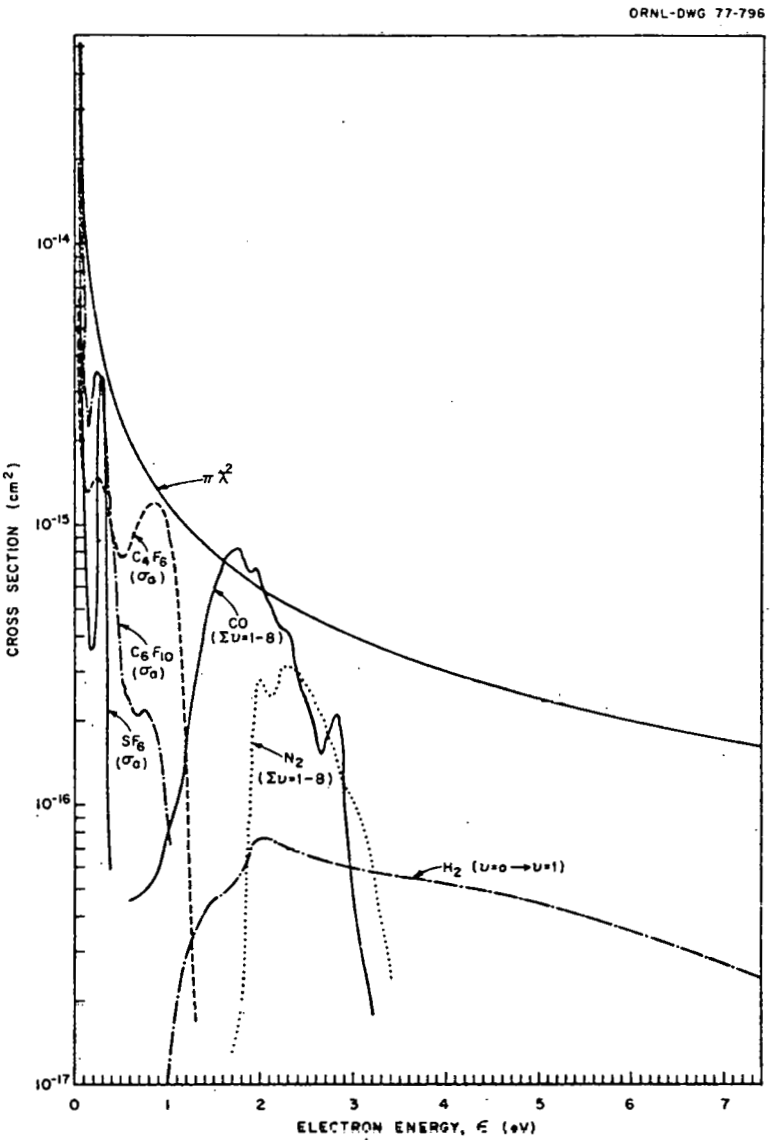

FIG. 8. Electron attachment cross sections, σ_a, as a function of electron energy, ε, for three electron-attaching gases, SF_6, C_4F_6, and C_6F_{10}.
Vibrational excitation cross sections via negative ion resonances: $CO(\Sigma_{\upsilon=1-8})$ is the sum of vibrational cross sections for the first eight individual states of CO as a function of electron energy (ref. 6); $N_2(\Sigma_{\upsilon=1-8})$ is the sum of vibrational cross sections for the first eight individual states of N_2 as a function of electron energy (ref. 6); $H_2(\upsilon=0\rightarrow\upsilon=1)$ is the cross section for excitation of the first vibrational level of H_2 (6) multiplied by 1.4 to correct the experimental data for nonisotropic electron scattering (see ref. 4, p. 347). Since the cross section for excitation of higher vibrational levels of H_2 is very much lower than for the $\upsilon=1$ level, one can conclude that the cross sections for vibrational excitation of CO, N_2, and H_2 via negative ion (shape) resonances decrease in the order $CO > N_2 > H_2$. $\pi\lambda^2$ is the maximum s-wave capture cross section (from ref. 1).

TABLE V

Effect of Negative Ion Resonances on Breakdown[†]

Percentage of Component Gas					Slope (kV/atm-mm)	Intercept (kV)	$(V_s)_R$ [‡]
C_4F_6	SF_6	H_2	N_2	CO			
10		90			4.39	0.82	0.55
10			90		6.18	0.66	0.73
10				90	6.71	1.02	0.82
33		67			8.76	0.68	1.01
33			67		8.93	1.41	1.10
33				67	10.74	0.61	1.22
66		34			15.05	0.55	1.66
66			34		14.16	0.22	1.52
66				34	16.12	0.49	1.76
	10	90			3.27	0.69	0.40
	10		90		4.83	1.18	0.60
	10			90	5.75	1.13	0.71
	33	67			4.79	1.13	0.59
	33		67		6.55	0.83	0.78
	33			67	7.18	1.04	0.86
	66	34			6.70	0.83	0.80
	66		34		7.56	1.03	0.91
	66			34	8.28	0.66	0.96
100					17.55	2.00	2.09
	100				8.49	0.87	1.00
		100			1.55	1.30	0.25
			100		2.74	1.56	0.40
				100	3.52	1.80	0.50

[†]Total pressure 2 atm; sphere-plane electrode geometry.

[‡]Breakdown strength relative to SF_6 of 1.

VI. APPLIED STUDIES

Breakdown Strengths of Gases/Mixtures with Cylindrical Electrodes

The apparatus described in Section VIII has been used to make breakdown measurements of SF_6-N_2 and c-C_4F_8—N_2 mixtures. Figures 9, 10, and 11 show our preliminary results for SF_6-N_2 mixtures on the breakdown voltages for inner stainless steel electrodes of respective radii, 1.4, 0.75, and 0.4 cm, each inside the outer cylinder of inner radius 2 cm. In all experiments the total pressure was 760 torr (1 atm), and the SF_6-N_2 concentration fraction was varied from 0 to 100% by pressure. The outer cylinder was at ground potential, and the inner cylinder was at either polarity of high voltage. Similar measurements were made for c-C_4F_8—N_2 mixtures, and Figs. 12 and 13 show some of our preliminary results for this system for inner electrode radii of 0.75 and 0.4 cm. Each data point in Figs. 9, 10, 11, 12, and 13 was the average of at least 10 breakdowns, and for each the random scatter (standard deviation ÷ mean) was less than 3%. Experiments are in progress with an inner electrode radius of 0.107 cm for which corona often precedes breakdown.

Our earlier uniform field breakdown strength data[1] on SF_6-N_2 and c-C_4F_8—N_2 mixtures are also presented in Figs. 9, 10, 11, 12, and 13. They have been normalized to the nonuniform field value of the V_s for pure N_2 in each of the figures. Although the normalized uniform and nonuniform field data are not dramatically different, it is interesting to see that the dependence of V_s on the amount of SF_6 in N_2 shows a stronger "saturation" effect in uniform than in nonuniform fields. In the uniform field case, the SF_6-N_2 mixtures which contain more than 40 to 50% of SF_6 showed little additional improvement in V_s. In the

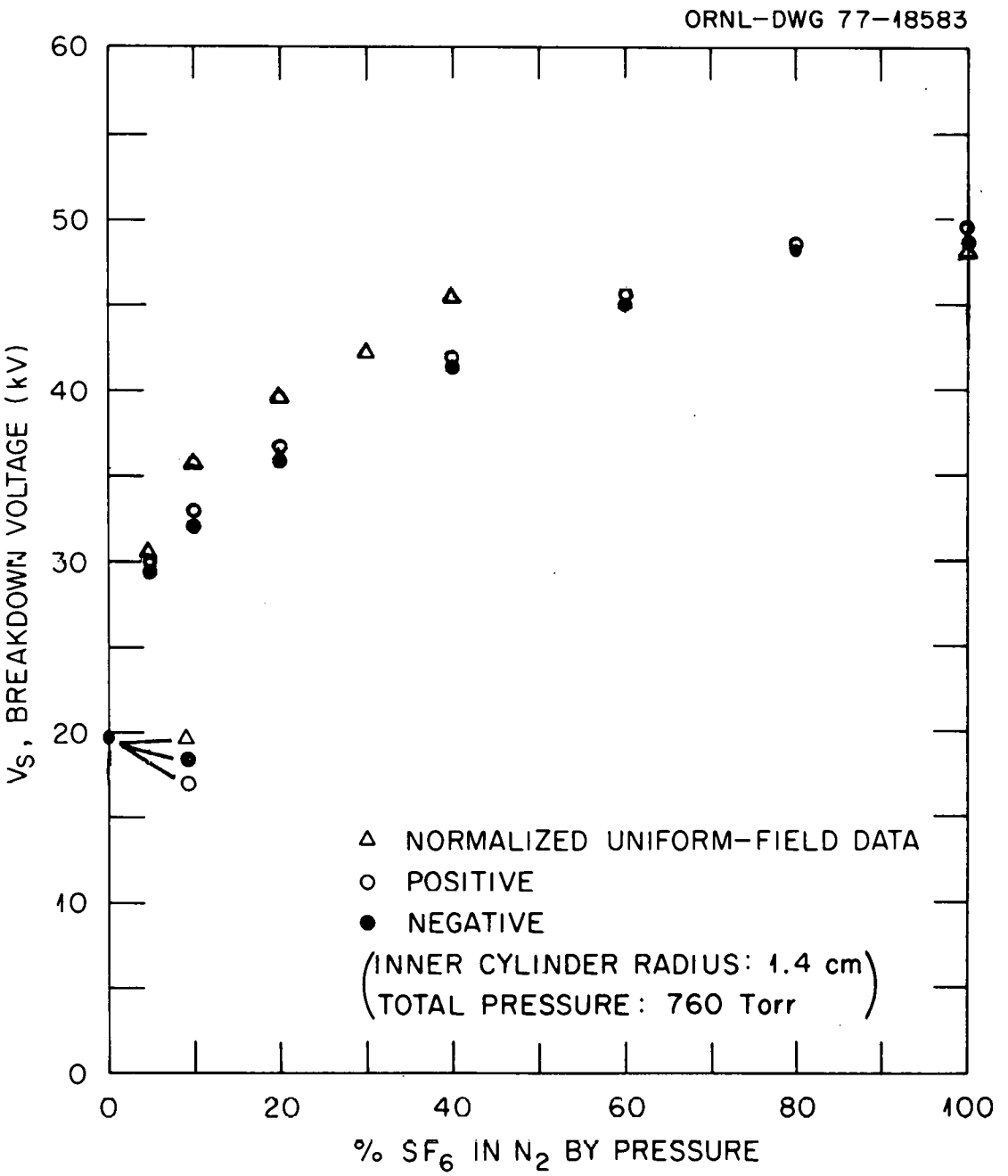

FIG. 9. Breakdown voltages for SF_6-N_2 mixtures with cylindrical electrode radii 1.4 and 2 cm. (o) inner electrode at positive potential, (●) inner electrode at negative potential, (△) normalized uniform field data.

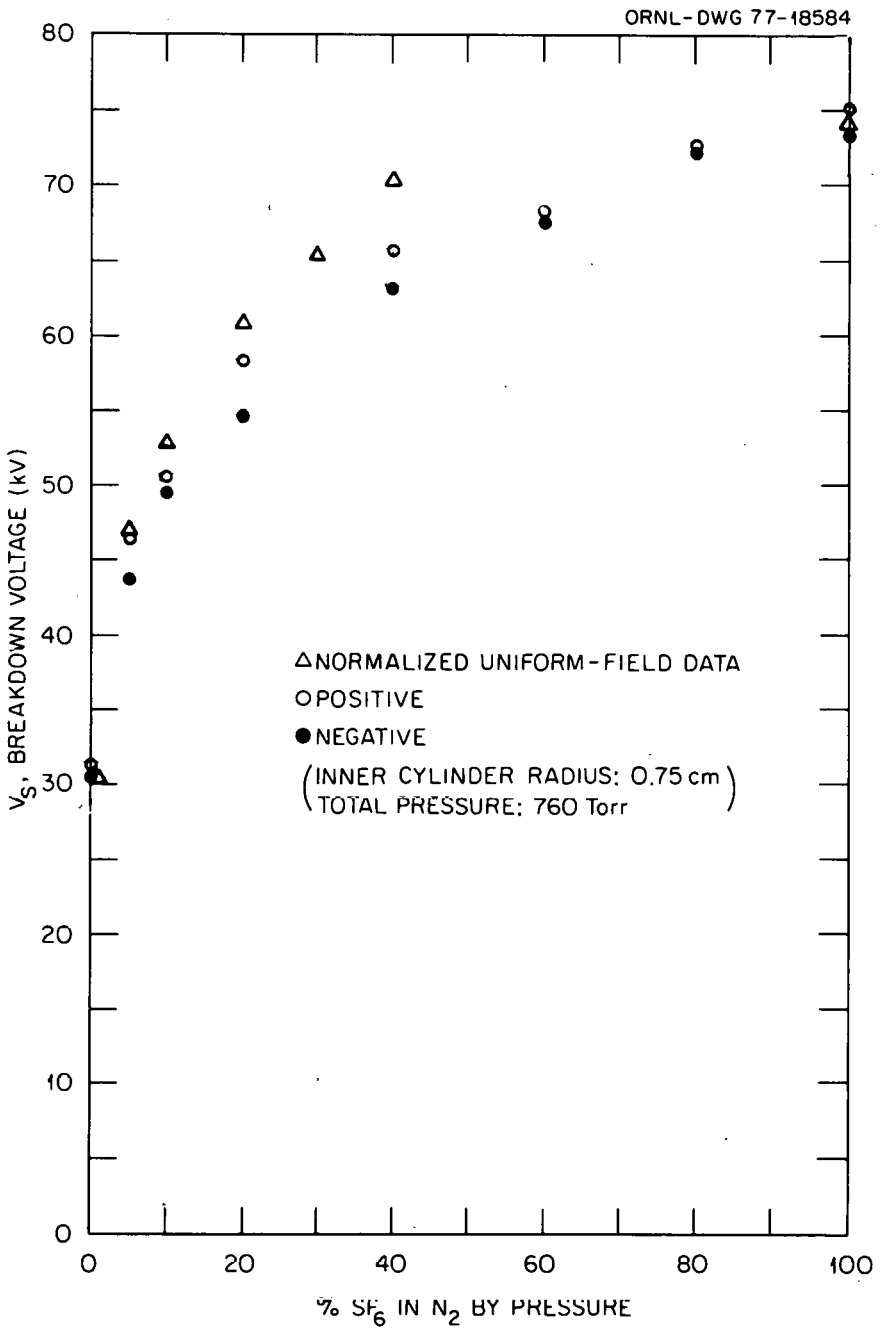

FIG. 10. Breakdown voltages for SF_6-N_2 mixtures with cylindrical electrode radii 0.75 and 2 cm. (o) inner electrode at positive potential, (●) inner electrode at negative potential, (△) normalized uniform field data.

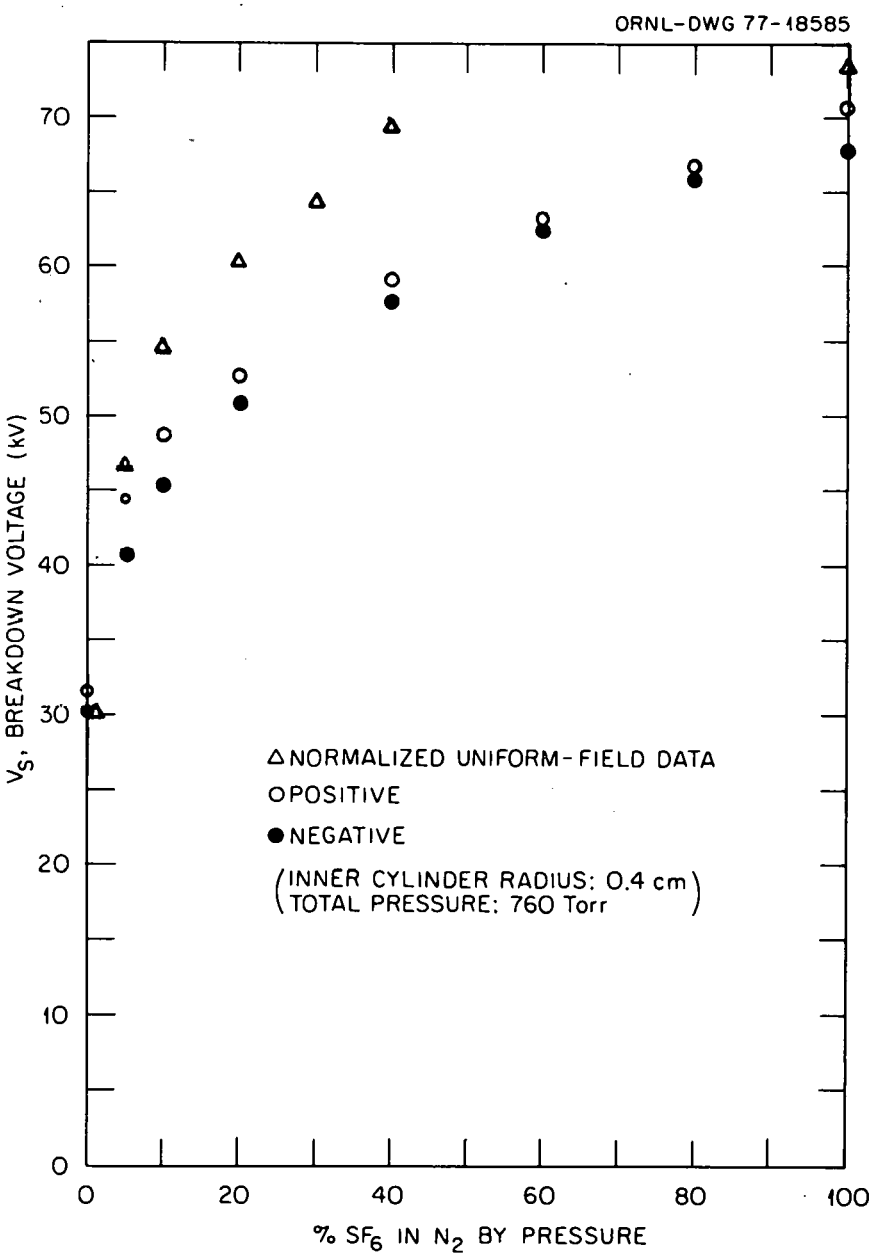

FIG. 11. Breakdown voltages for SF_6-N_2 mixtures with cylindrical electrode radii 0.4 and 2 cm. (o) inner electrode at positive potential, (●) inner electrode at negative potential, (△) normalized uniform field data.

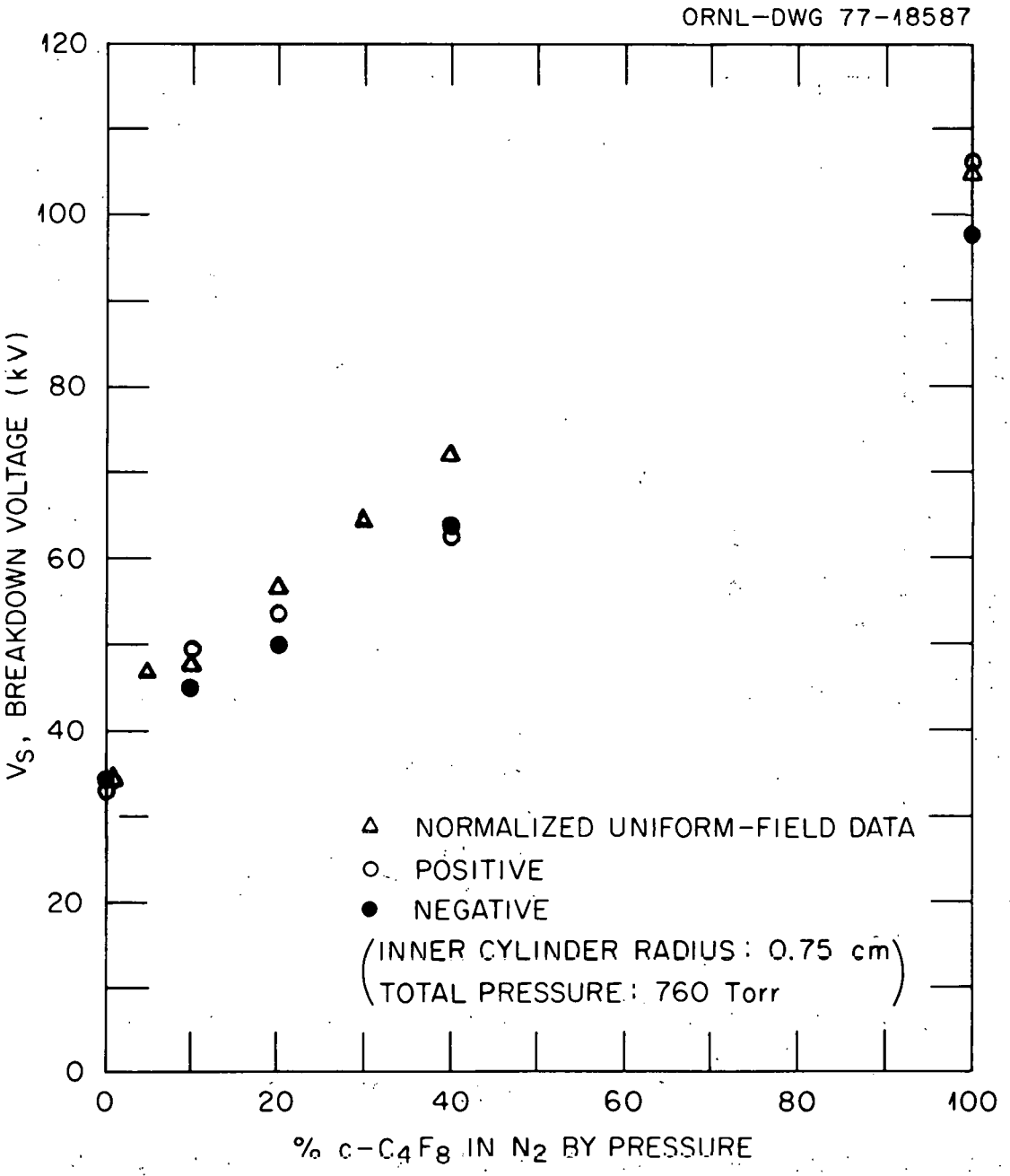

FIG. 12. Breakdown voltages for c-C_4F_8—N_2 mixtures with cylindrical electrode radii 0.75 and 2 cm. (o) inner electrode at positive potential, (●) inner electrode at negative potential, (Δ) normalized uniform field data.

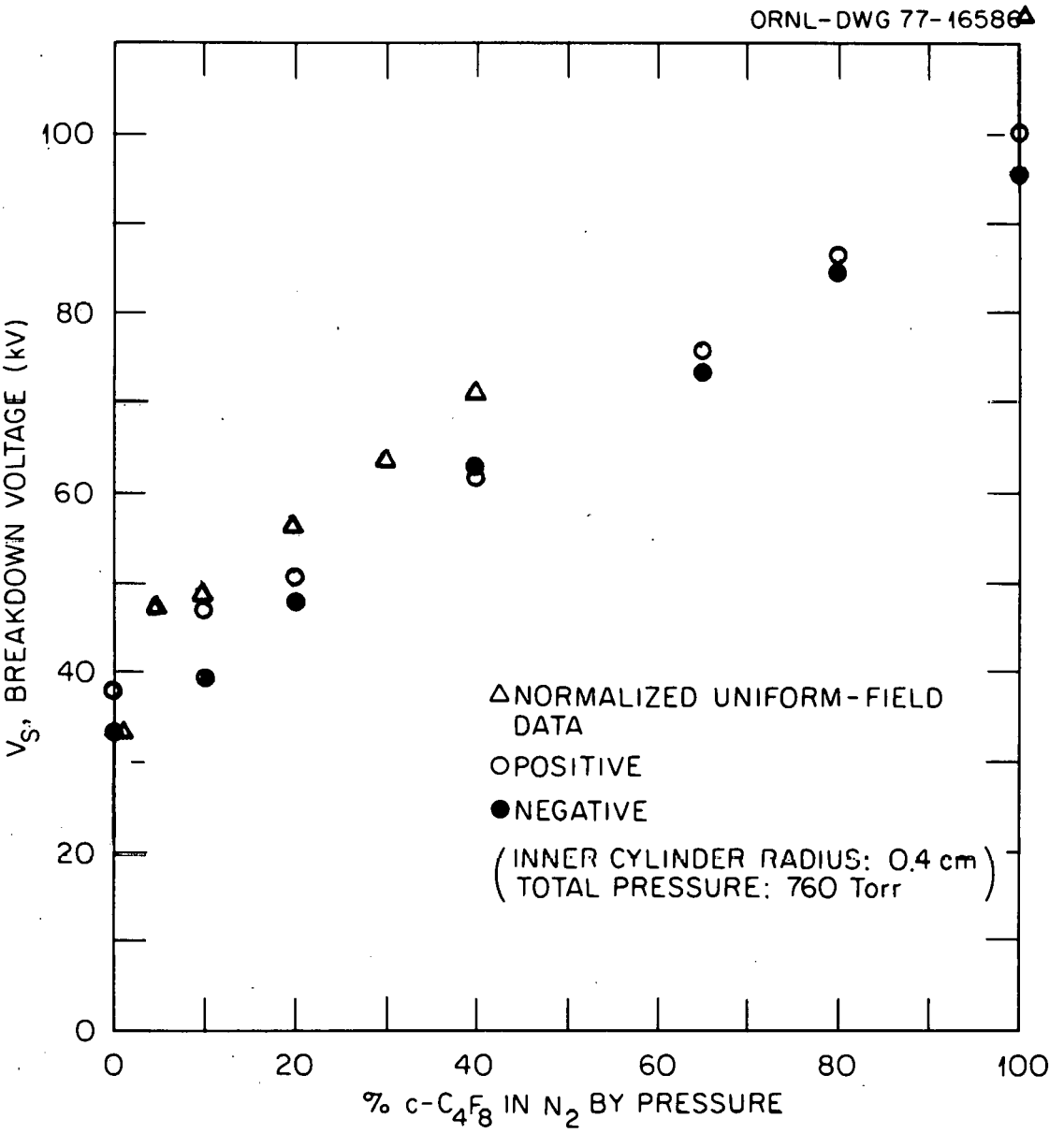

FIG. 13. Breakdown voltages for c-C_4F_8—N_2 mixtures with cylindrical electrode radii 0.4 and 2 cm. (○) inner electrode at positive potential, (●) inner electrode at negative potential, (△) normalized uniform field data.

nonuniform fields of concentric cylinder geometries, the V_s versus % SF_6 curves exhibit less of this saturation. This difference between uniform and nonuniform fields seems to increase with increasing field inhomogeneity (as the radius of the inner electrode decreases; see Figs. 9, 10, and 11). The above findings could be attributed to the fact that the electron energy distribution function is shifted to higher energies in the case of nonuniform fields and to remove the same number of electrons more SF_6 is needed because the electron attachment cross section for SF_6 is small for electrons with energies $\gtrsim$ 0.5 eV (see Fig. 11 in ref. 3; see also Fig. 7 of this report). Consistent with this interpretation are the data in Figs. 12 and 13 where it is seen that when the uniform field data on V_s versus % of c-C_4F_8 in N_2 are normalized to the nonuniform field data on the same system, no significant changes are observed and practically no saturation effect is evident in either. The superior behavior of c-C_4F_8 compared with SF_6 is attributed to the fact that the electron attachment cross section for this molecule extends to higher energies than that for SF_6 (see Fig. 8 in ref. 3). This proposition will be tested further using other systems, such as C_4F_6, for which the magnitude of the electron attachment cross section is also large to much higher energies than for SF_6.

It is finally noted (Figs. 9, 10, and 11) that for SF_6-N_2 mixtures the highest breakdown voltages are obtained with the 0.75-cm inner electrode radius. This agrees with the theory that a ratio of outer

radius to inner radius of $\sim e = 2.72$ is optimum. In Figs. 9 and 11, this ratio takes respective values of approximately 2e and e/2.

These studies are currently being extended to corona inception versus breakdown, to other gases/mixtures, and to the effects of polarity (noted in some of the data in Figs. 9, 10, 11, 12, and 13), surface roughness and electrode composition.

The Problem of Carbon Deposits for Fluorocarbons

One of the practical difficulties of using fluorocarbons as gaseous insulators is the problem of carbon formation caused by a spark in the gas. If carbon is formed, it can deposit on an insulator and cause a continuing short, rendering the insulator unusable.

We have indeed found that using fluorocarbons as unitary gases leads to the formation of carbon upon an electrical discharge, especially at pressures $\gtrsim$ 1 atm. We have also found, however, that one advantage of a multicomponent insulator containing fluorocarbon(s) is that the problem of carbon formation is reduced or even eliminated. For example, we have sparked a mixture of 80% SF_6-20% C_4F_6 (perfluorobutyne) at a total pressure of 3500 torr ($\sim$ 50 psig) at 300 kV with up to 15 Joules of energy in the arc and with a total of over 200 Joules. No carbon deposits were discernible on the electrodes. Similarly, a 50% N_2-40% SF_6-10% C_4F_6 mixture at 3500 torr has been tested with an equal amount of energy dumped into a series of arcs with no carbon deposits observed.

A transmission line breakdown will, of course, dump more energy into the arc. Nonetheless, the above tests indicate that carbon formation may not be a major problem for multicomponent gaseous insulators containing C_4F_6.

VII. ENVIRONMENTAL EFFECTS OF DIELECTRIC GASES: ANALYSIS OF THE BREAKDOWN PRODUCTS OF NEW GASEOUS INSULATORS

The increased usage of dielectric gases and the introduction of superior new gases and gas mixtures for the nation's energy needs imposes on us the responsibility to identify the decomposition products of such systems especially under electron impact. These and their subsequent reaction products may be toxic. Identification of the initial products provides knowledge of the precursors of the final products which being long-lived are of immediate concern to the environment. Such knowledge will not only enable us to identify formation of possible toxic products in the dielectric but will also provide the basis for the possible usage of chemical means to transform or to neutralize the toxic species formed.

We have begun identifying the initial decomposition products of new dielectric gases/mixtures under electron impact as a function of the electron energy using a time-of-flight mass spectrometer. Also, we have begun a mass analysis of samples of actual dielectric gases/mixtures taken from our breakdown apparatus after breakdown, identifying in this manner the final, long-lived species. In this latter effort we have used the facilities of the Mass Spectroscopy Group of the Analytical Chemistry Division of Oak Ridge National Laboratory (ORNL). A study of the reactions the initial products undergo with their gaseous environment and of the reaction pathways leading from the initial (precursors) to the final products is planned for the future, making use of a high-pressure mass spectrometer.

The results of the aforementioned studies are important also in assessing the long-term stability of a gaseous dielectric, even in the absence of breakdown. Low-energy free electrons are always present in the dielectric and these, depending on the molecular structure, can be exceedingly disruptive since (multiple) molecular fragmentation via the process of dissociative attachment can occur very efficiently even with "zero" energy electrons (see Appendix III and ref. 7).

Mass Spectrometric Studies

Using[†] a time-of-flight mass spectrometer we have identified the main negative ions (parent and/or fragment) produced when quasi-monoenergetic electron beams of energies from 0 to $\sim$ 10 eV collide with C_4F_6 (perfluoro-2-butyne). Very interestingly it was found that the parent ion $C_4F_6^{-*}$ is by far the most abundant negative ion formed within this energy range. If other fragment ions are formed, they should have less than 1/200 the intensity of the $C_4F_6^{-*}$ parent ion. From the practical point of view, this is quite significant since it indicates that C_4F_6 does not decompose efficiently upon electron collision, preserving the integrity of the dielectric with time.

The dependence of the yield of the parent negative ion ($C_4F_6^{-*}$) on the electron energy is shown in Fig. 14. It is consistent with the absolute electron attachment cross section as a function of electron energy deduced earlier from our electron swarm studies. The energy scale in Fig. 14 has been calibrated with respect to the position

---

[†]This work has been performed primarily by J. G. Carter and J. Cowan of the Atomic, Molecular and High Voltage Physics Group.

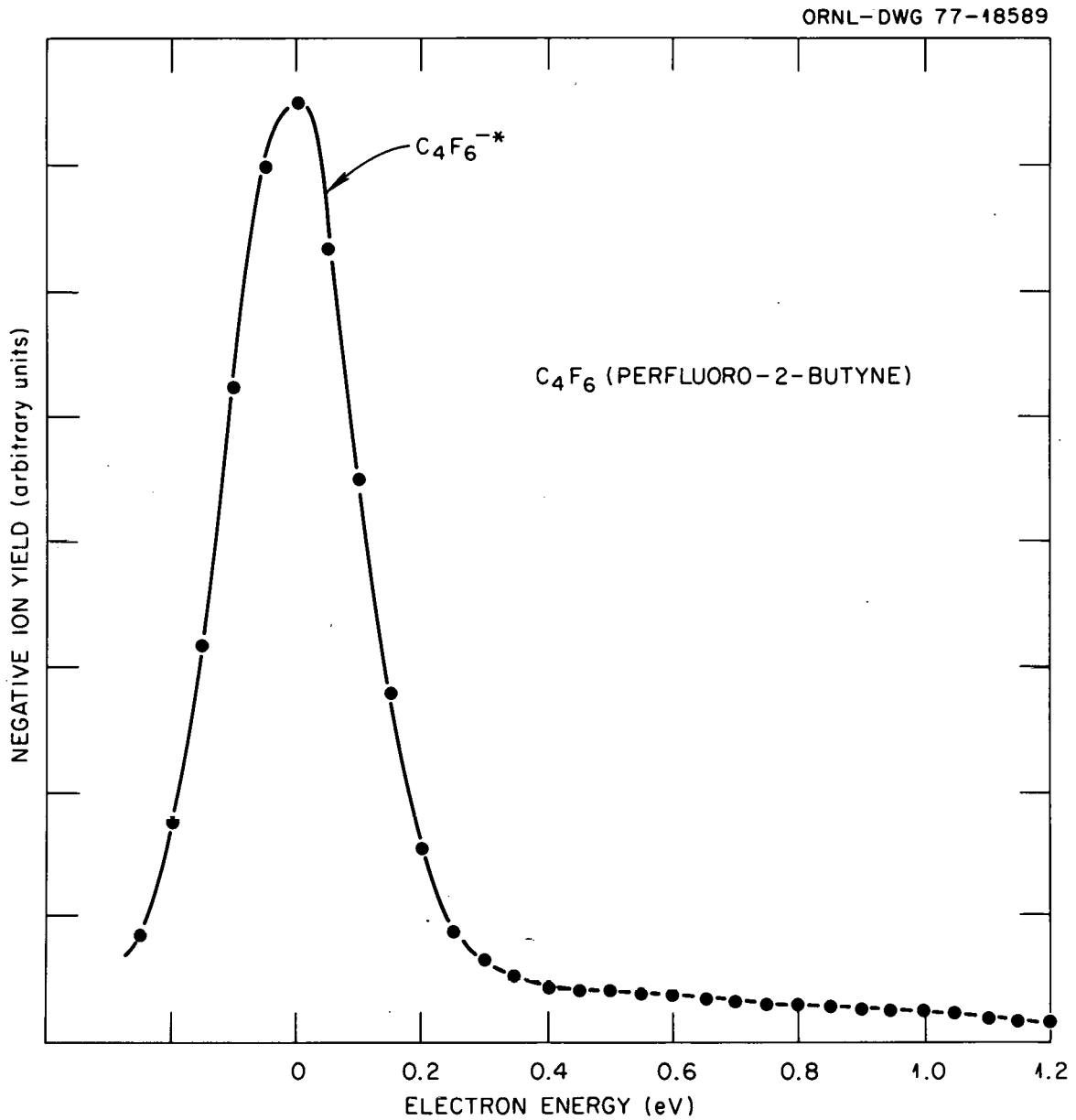

FIG. 14. Production of $C_4F_6^{-*}$ parent negative ions as a function of electron energy for C_4F_6 (perfluoro-2-butyne).

(0.37 eV) of the SF_5^- from SF_6 resonance.[8] The mean autodetachment lifetime of $C_4F_6^{-*}$ at $\sim$ 0.0 eV was found to be $\sim$ 15 μsec. At normal pressures the ion is, of course, completely stabilized via collisions.

Perfluorobutene-2 (C_4F_8) has also been studied using our time-of-flight mass spectrometer. Although in this case the parent ion $C_4F_8^{-*}$ was again found to be the main negative ion with maximum intensity at $\sim$ 0.0 eV, a variety of fragment ions were detected: $C_4F_6^-$ at $\sim$ 0.0 eV and F^-, CF_3^- and $C_3F_5^-$ at higher energies ($\sim$ 5 eV). The relative intensities of the observed fragment ions with respect to the parent ion $C_4F_8^{-*}$ intensity of 1000 are 9, 600, 10, and 8 for $C_4F_6^-$, F^-, CF_3^-, and $C_3F_5^-$, respectively. The lifetime of $C_4F_8^{-*}$ at $\sim$ 0.0 eV was found to be $\sim$ 12 μsec.

Breakdown Product Analysis

When breakdown occurs in a gaseous dielectric, in addition to the dominant electron-molecule interactions, other processes such as physical heating of the gas and resultant molecular decomposition, positive ion formation via higher-energy electrons, and photoionization, take place. The products of these processes and their subsequent reactions eventually lead to the final breakdown products, which must be identified.

In pursuit of such knowledge we began some initial experiments wherein we sparked gases across sphere-sphere electrodes held at fixed distances for varying periods of time (and then varying energy inputs into the gas). Following sparking, the gas was run through a gas chromatograph belonging to the Analytical Chemistry Division of ORNL. In a gas chromatograph, GC, the sample under study is injected into a high-pressure stream of gas (e.g., He or H_2). The gas and the entrained

sample are passed through a column of packed but porous material. With properly chosen column material, various sample components have sufficiently different "throughput" times to be separated at the end of the column where a detector (an ionizer-mass spectrometer in our case) is used to identify each of the separated species.

Preliminary gas chromatography breakdown product analysis on SF_6 indicated that SF_4, a known toxic species, is a prominent breakdown decomposition product. Studies on C_4F_6 are planned, although some preliminary results have been obtained for the multicomponent mixture 10% C_4F_6-40% SF_6-50% N_2. This mixture was sparked at various voltages up to 300 kV and allowed to corona for times to $\sim$ 60 minutes. In Fig. 15, the total ion current of the GC column output as detected in the ionizer-mass spectrometer is plotted as a function of the time after the injection of the sample. A tentative identification of the peaks is shown in the figure. The three major peaks are, as expected, due to the components (N_2, SF_6, and C_4F_6) of the tertiary mixture. The peaks at $\sim$ 470 and 525 sec are identified as reaction products of SF_6 and C_4F_6 possibly $S_2C_2F_2$ (126 amu) and $S_2C_2F_4$ (164 amu). The 610 and 700 sec peaks are attributed to an impurity ($C_4F_6Cl_2$) in the C_4F_6 gas as supplied to us by Columbia Chemical Company. (The chemical $C_4F_6Cl_2$ is used to make C_4F_6 and could be a major impurity in C_4F_6 if proper precautions are not taken.)

Identification of the constituents of insulating gases/mixtures after varied periods of sparking and corona will continue and will include a quantitative analysis as well.

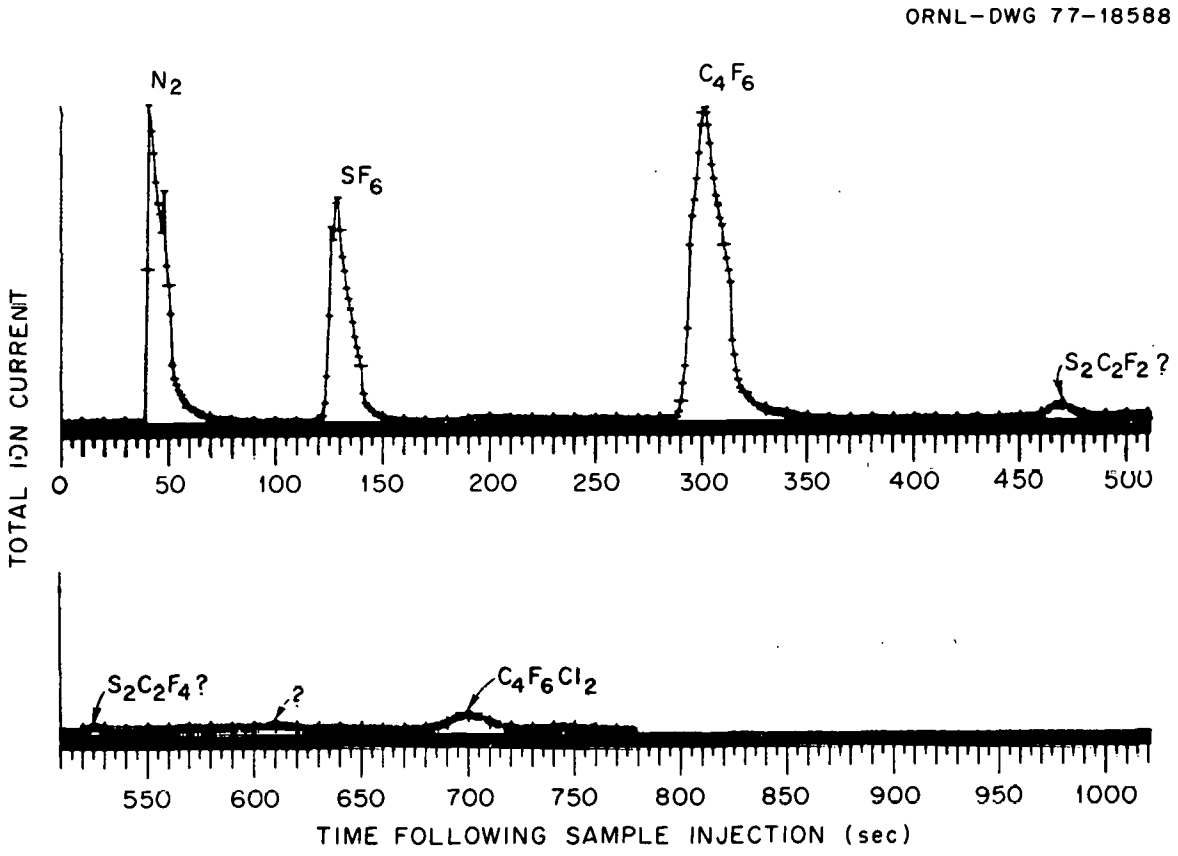

FIG. 15. Total ion current versus time following sample injection in the gas chromatograph column (see text for discussion).

VIII. APPARATUS

High Pressure, Variable Temperature Breakdown Apparatus

During this period, the design and fabrication of a new high-pressure breakdown apparatus were completed. This apparatus should enable us to achieve voltages up to 300 kV using a small volume of gas up to $\sim$ 11 atm of pressure. In addition, the temperature, T, of the test chamber will be controllable ($-$ 50°C $\lesssim$ T $\lesssim$ 150°C) so that actual field use conditions can be approximated.

Figures 16 and 17 show the new chamber partially assembled. It occupies the radio frequency shielding cage which formerly housed the sphere-plane apparatus. The chamber itself is made of 316 stainless steel. It is approximately 19 in. in height and 10-1/2 in. in diameter with six 1-1/2-in.-diameter and two 4-in.-diameter ports around the bottom portion. These ports will be used for pumpout, gas inlets, and as observation windows. The chamber itself mounts on a fiberboard insulator which thermally isolates the chamber from the support stand. The system will be pumped by an oil diffusion pump with a freon refrigerated cold trap and a mechanical roughing pump. A gas inlet manifold system has been constructed to facilitate the handling of gas mixtures; more gas bottles can be attached to the system, and the feedlines can be evacuated separately from the chamber.

The chamber is designed for 150 psig (approximately 11 atm absolute), which covers the practical range of pressures for high voltage devices. The pressure vessel was designed to strict local construction codes and has been approved by the ORNL Pressure Review Committee. Also, all ORNL Quality Assurance procedures were followed throughout the various stages

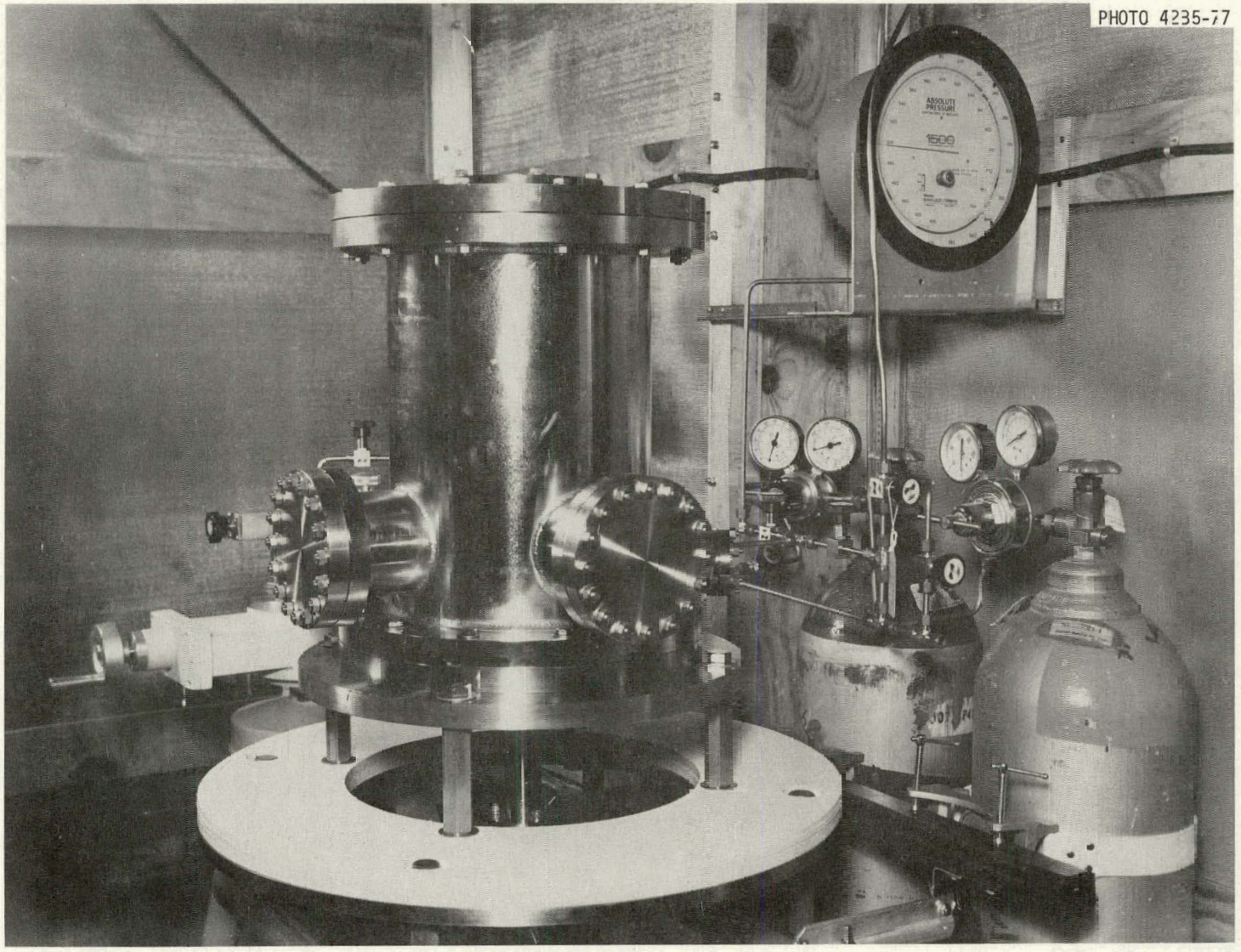

FIG. 16. A view of the high pressure, variable temperature breakdown apparatus.

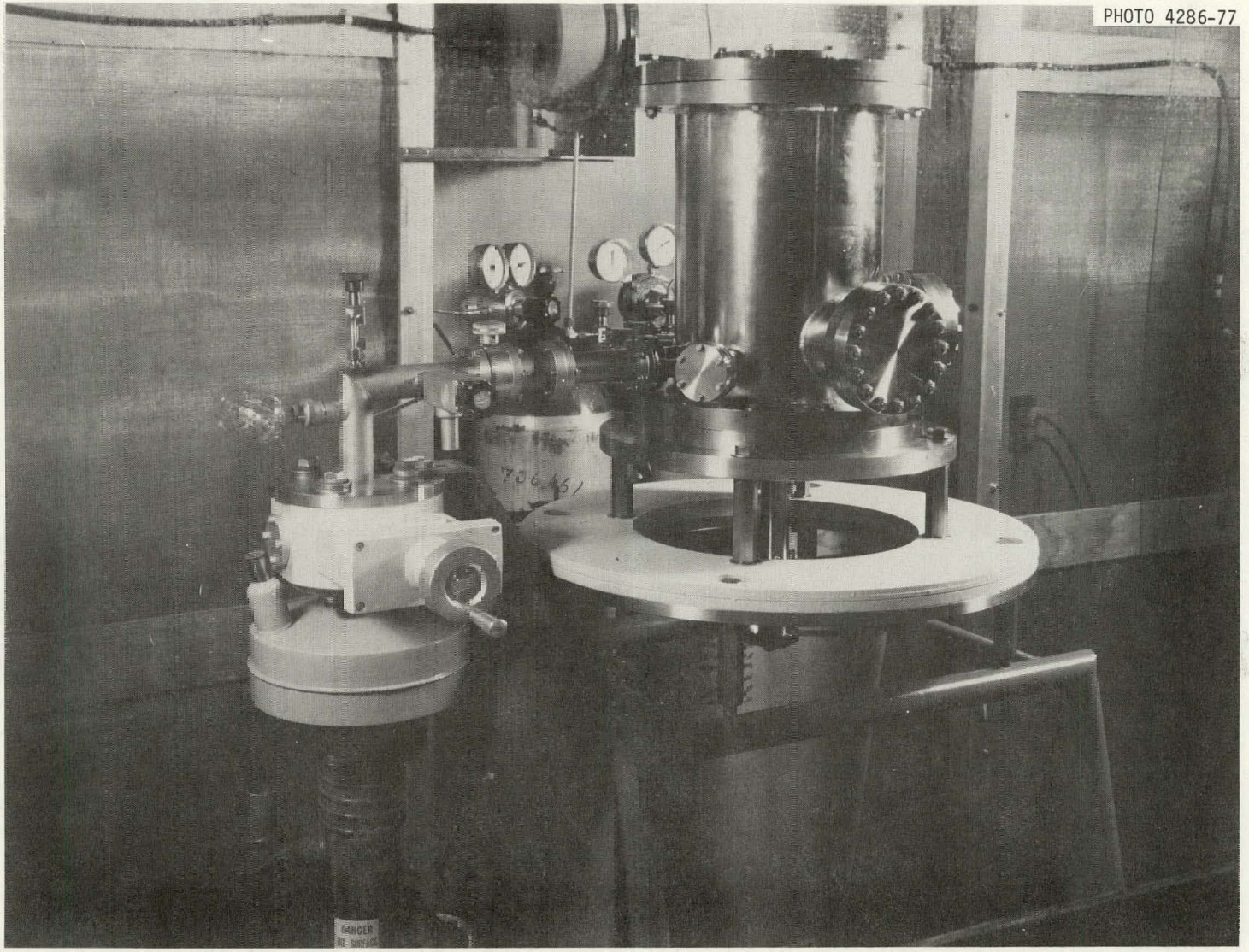

FIG. 17. A view of the test chamber for the high pressure, variable temperature breakdown apparatus.

of construction. The system was hydrostatically tested before being released from the shop. For protection against an accidental over-pressure, we will install a knife-blade-type rupture disc on one of the 4-in.-diameter ports.

The high voltage will be supplied by our Deltatron L300-2C power supply from Delta Ray Corporation. This is a 300-kV DC supply with low ripple ($\lesssim$ 0.01% peak to peak at maximum voltage and current) which we have used on our plane-plane electrode apparatus. It has an internal type HV feedthrough which eliminates the need for a large air external insulator.

An identical feedthrough will be used to bring the high voltage into the test chamber. This type of feedthrough is relatively inexpensive and can be readily obtained from Delta Ray Corporation.

The internal volume of the vessel is approximately 16 liters which includes the volume of the ports. As is seen in Figs. 18 and 19, a specially designed Teflon plug anchored from the top flange surrounds the cable feedthrough and serves both to occupy volume and to provide additional insulation. A small volume is desirable since the amount of gas used is less, and the gas can be pumped out and cycled much faster than in larger chambers.

To study the breakdown voltage as a function of temperature, we have designed an oven for heating the chamber to $\sim$ 150°C. The oven is comprised of sections which can be fitted around the ports and HV feedthrough. It is constructed from thin stainless steel and filled with insulation. Electrical resistance heaters are placed on the inner surface of the oven. The oven is similar to one currently in use in an experiment of our basic

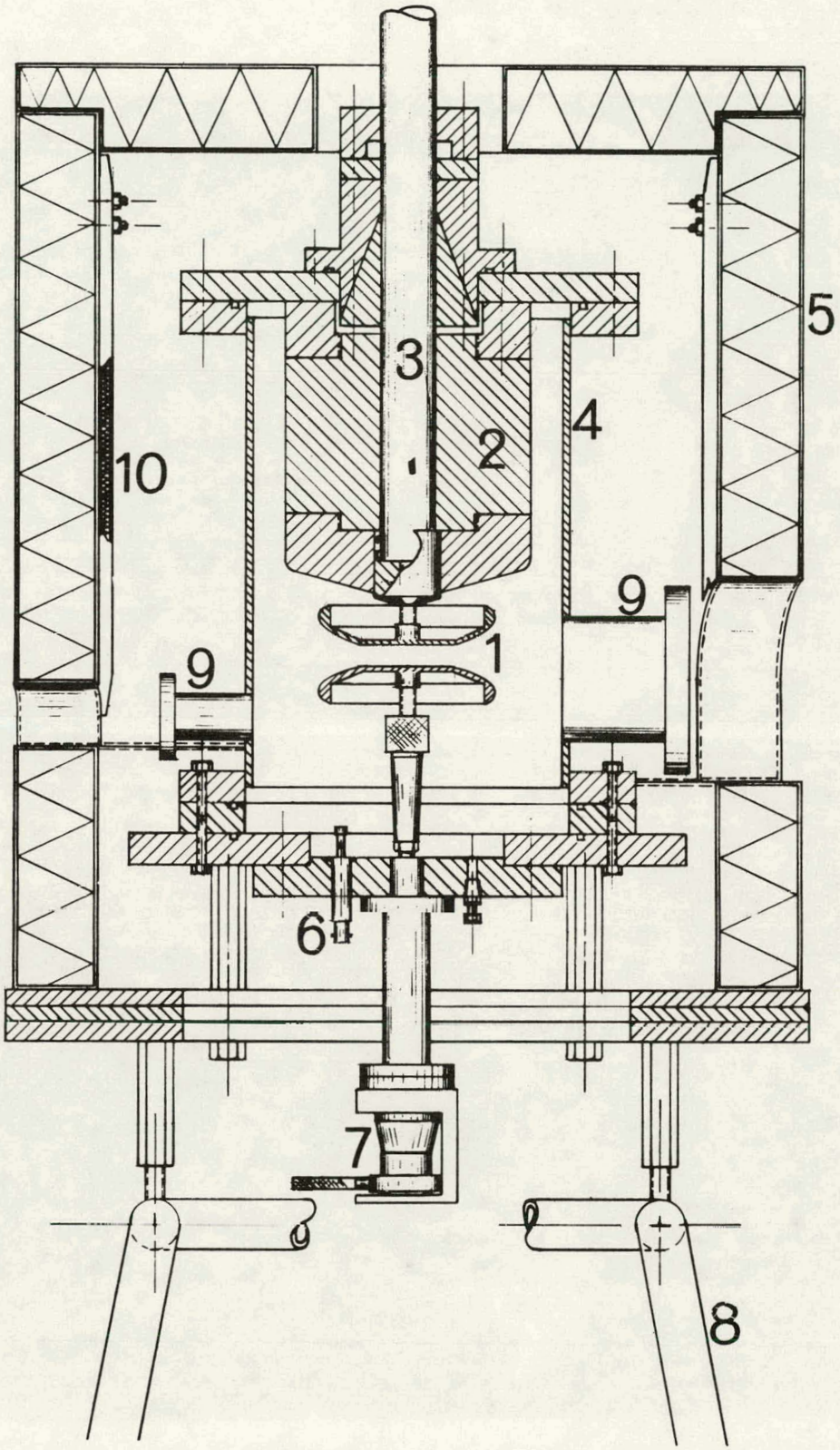

FIG. 18. Cross sectional view of the new high pressure, variable temperature chamber: (1) uniform field electrodes, (2) Teflon spacer, (3) high voltage cable, (4) high pressure chamber, (5) oven, (6) ground feedthrough, (7) linear motion drive, (8) support stand, (9) ports, (10) resistance heaters.

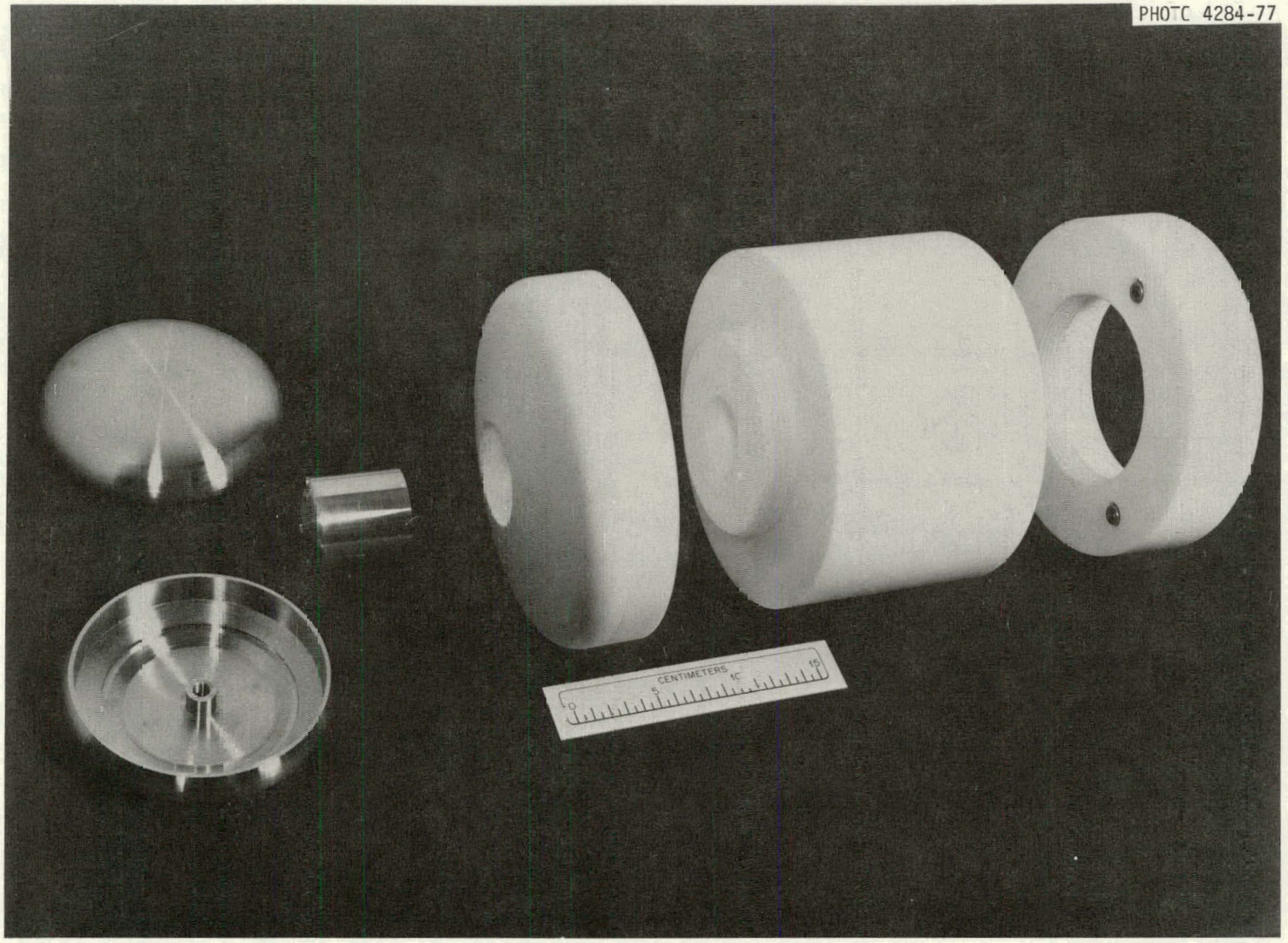

FIG. 19. Teflon plug, cable termination, and electrodes for the new high pressure, variable temperature breakdown apparatus.

research program. Regulation of the temperature to within a degree or less can be achieved by means of a proportional controller. Temperatures will be monitored by sheathed thermocouples of chromel-alumel connected to a digital readout monitor. A cooling jacket fitting snugly around the outside of the chamber has been constructed and tested. The jacket is made in separate sections of copper for the sides, top, and bottom. Liquid nitrogen, liquid nitrogen vapor, or other coolants can be circulated through the jacket. The oven will be used as thermal insulation for the cooling system as well since it will totally enclose the chamber. To prevent condensation of moisture from the laboratory air, a slight positive pressure of N_2 gas will be maintained between the cooling jacket and the oven. Temperatures for the cooling system will be monitored with the same thermocouples.

Initial breakdown measurements on our most promising gaseous systems will be made as a function of temperature using plane-plane electrodes of Pearson-Harrison profile, which we have used in our previous studies.[3]

Applied Studies (Cylindrical Electrode) Facility

In this period the applied studies facility has been built, tested, and put into operation. With this facility, gases/mixtures selected through our basic studies are tested under conditions corresponding to applications, with the results being correlated on the one hand with basic physicochemical data, and on the other hand with engineering design rules for practical apparatus. In the latter case "the scaling factor" still remains a problem.

With this facility, breakdown strength measurements of gases/mixtures in the fields of concentric cylinders with various degrees of roughness

can be made. Such studies will also include the effects of electrode material composition and the action of triggered gaps with various gases/mixtures. The concentric cylinder electrodes are shown in Figs. 20 and 21. The outer cylinder was machined with smoothly tapered ends from a solid brass block to effect a cylinder of 2-cm inner radius and a 10-cm length of central cylinder, plus 11-cm length of tapered ends. Eight inner cylinders of 27-cm length have been made of three materials (stainless steel, copper, and aluminum) and radii 0.107, 0.4, 0.75, and 1.4 cm. The inner electrode is held at the ends and is centered within the outer electrode by Plexiglas discs; in the chamber a high voltage rod is screwed into the inner electrode. The smaller electrodes (Fig. 21) are held in the Plexiglas discs by appropriate Plexiglas bushings.

The concentric cylinder electrodes are mounted in a high vacuum chamber with appropriate gas, optical, and electrical ports (see Fig. 22). The chamber has approximately 60-liters volume but in concentric cylinder tests approximately 20 liters of this volume are occupied by sealed glassware. The electrodes are accessible through a top cover. They are positioned with one end toward the high voltage cable and the other end facing a 2-in.-diameter quartz window facing the rear cage wall. Ultraviolet light from a 60-watt deuterium lamp can be directed onto the inner cylinder through the window via a partially-reflecting, partially-transmitting mirror made by vacuum deposition of aluminum such that the operator has full view through the window from outside the cage.

The chamber receives high voltage via a cable feedthrough of the type used at the output of Delta Ray Corporation power supplies. The ground (outer) electrode is connected only to a 50-kV bushing in the

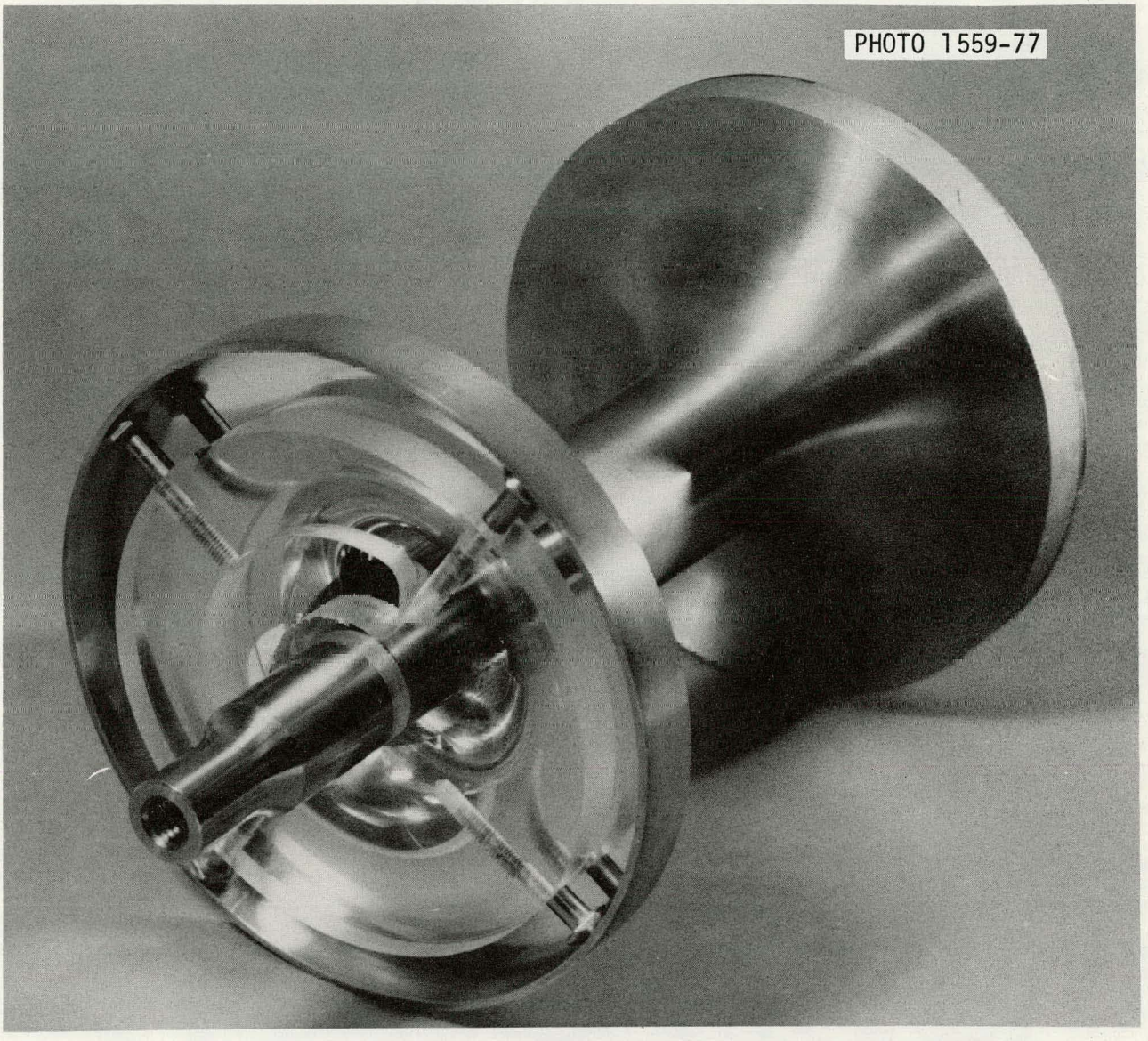

FIG. 20. Concentric cylinder electrodes for applied studies facility.

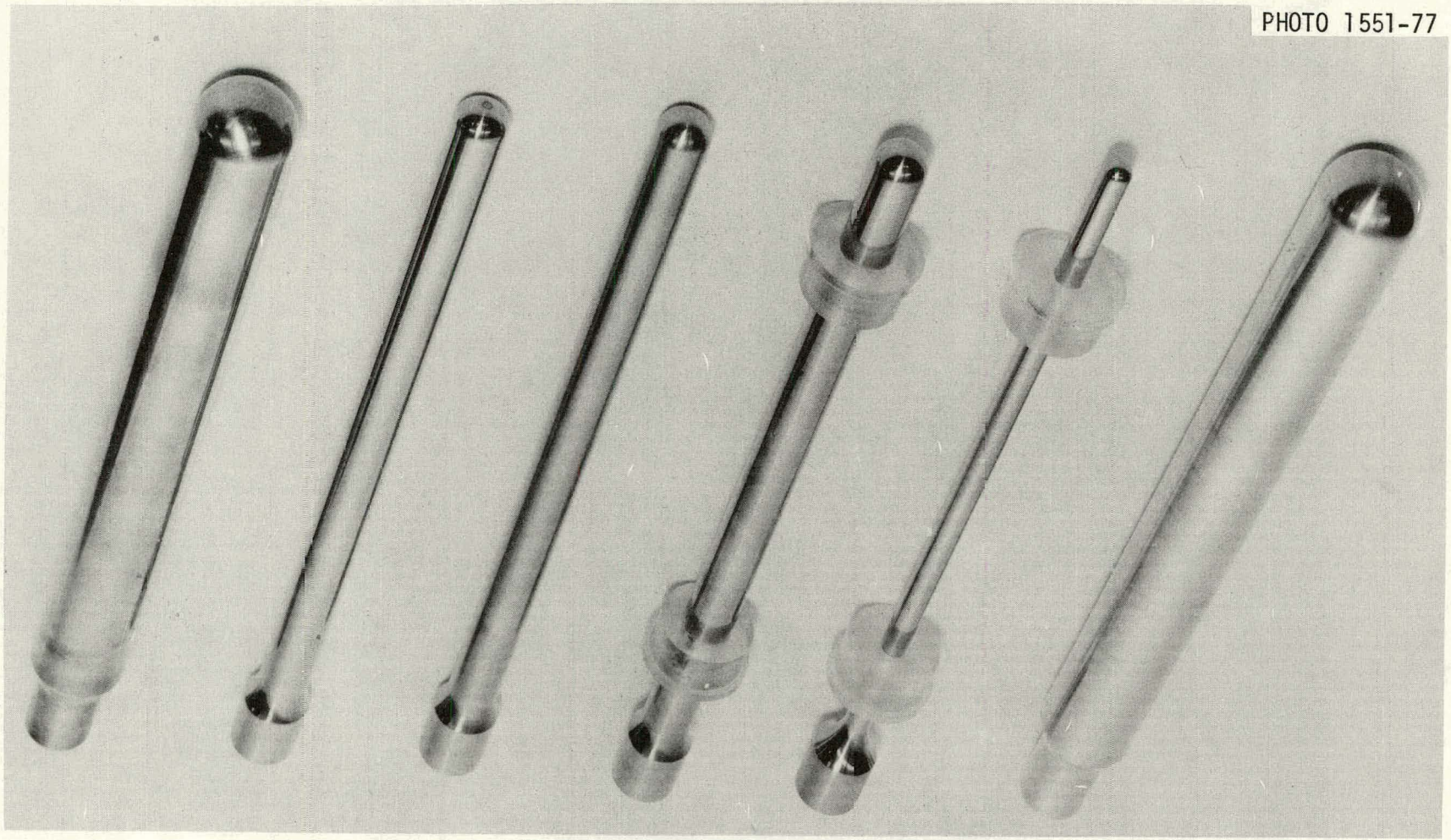

FIG. 21. Inner electrodes for concentric cylinder electrode sets.

chamber wall with electrical connection to ground made outside the chamber through small current-sensing resistors.

Figure 22 provides a view of the apparatus in the shielding cage as seen through its door. The new 300-kV DC supply for this apparatus is expected from the manufacturer in November 1977; a surplus 0 to 150-kV DC supply has been repaired and put into service in the interim. It consists of an oil tank for high voltage components and low voltage controls mounted in the rack outside the cage. These controls make the usual provisions for turn-on sequence, interlocks, and automatic turn-off for overcurrent and overvoltage. The oil tank employs vacuum diodes in a voltage-doubler circuit, charging two 0.006-μF capacitors in series. It also provides a 300-MΩ resistor string for the voltage divider.

The high voltage parts of the equipment are shielded within the wire mesh "cage" to avoid excessive noise effects on the instrumentation. The cage is a two-independent-layers type purchased from Erik Lindgren Company. Its modular construction will facilitate future expansions and/or modifications. High voltage is carried by the 150-kV DC power supply black cable in the left foreground up to an open corona shield topped by a hemisphere (a diverter electrode) and down through another (larger white) cable into the rectangular test chamber (see Fig. 22). The diverter motor and trigger generator and the cage feedthrough panel for carrying cooling water, exhaust gases, power, and instrumentation signals are visible over the chamber.

Figure 23 shows the cage exterior. Outside the cage are seen the experiment controls and the cage feedthrough panel.

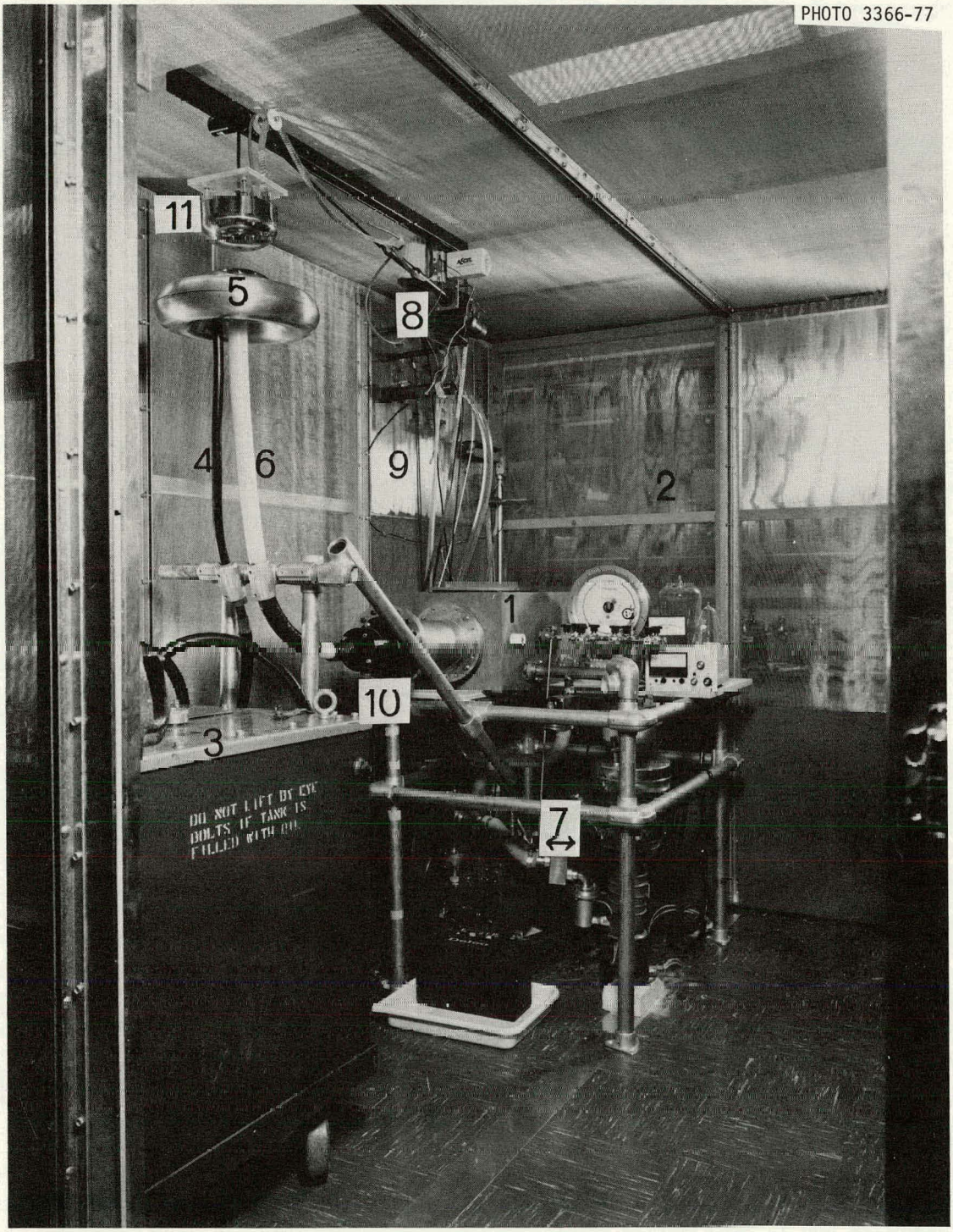

FIG. 22. Interior of shielding cage of cylindrical electrode facility. (1) Chamber, (2) rear cage wall, (3) power supply (4) supply output cable, (5) HV diverter electrode and corona shield, (6) chamber HV input cable, (7) vacuum pumps, (8) diverter motor and trigger generator, (9) cage feedthrough panel, (10) chamber HV feedthrough, (11) diverter ground electrode.

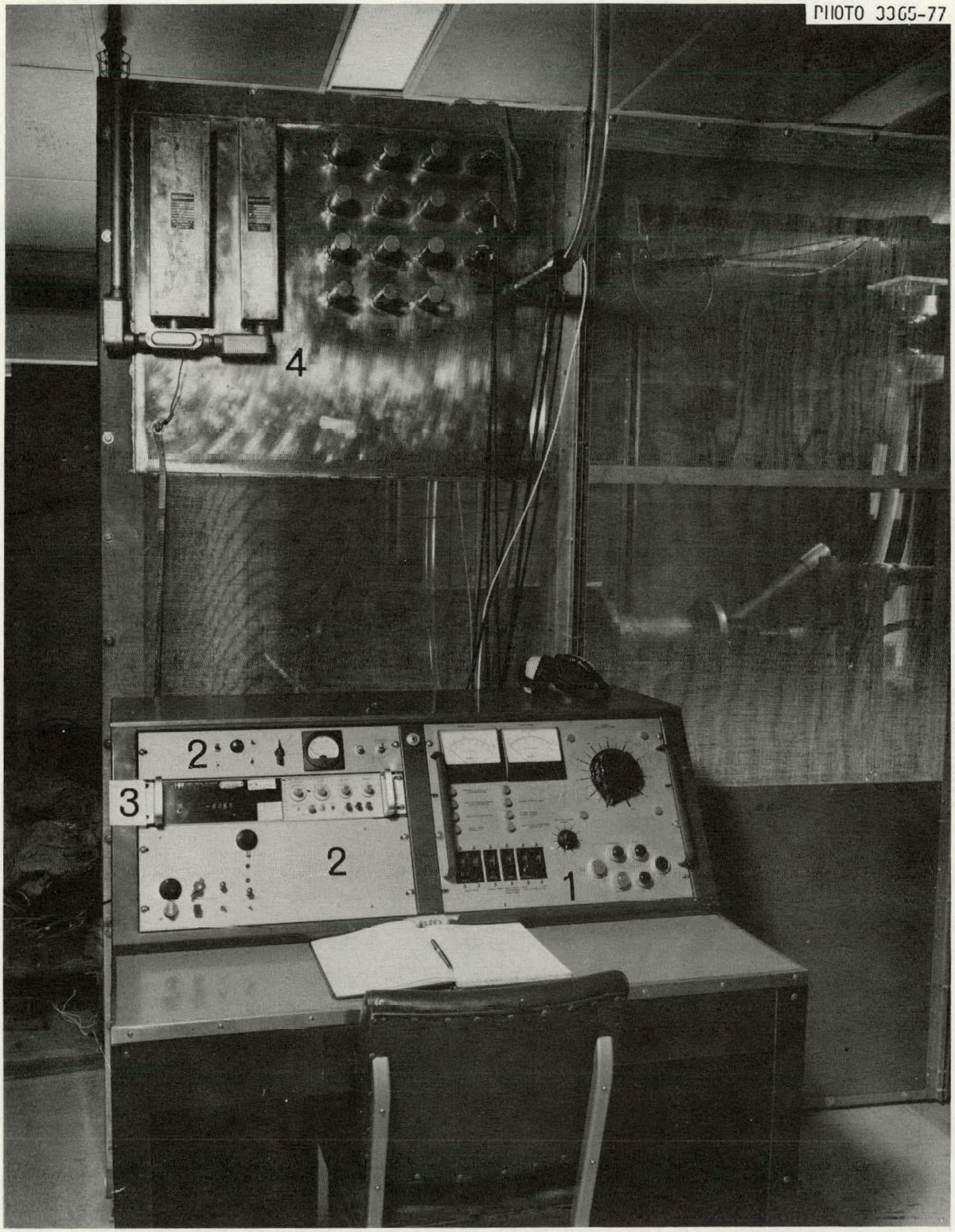

FIG. 23. Exterior view of the shielding cage of cylindrical electrode facility. (1) Power supply controls, (2) automated controller, (3) digital voltmeter, (4) cage feedthrough panel.

Test gases are introduced into the chamber after it is pumped out to a high vacuum (better than $\sim 10^{-6}$ torr) by the mechanical forepump and an oil diffusion pump with liquid nitrogen trap. The vacuum pressures are monitored by a thermocouple gauge and an ion gauge. Test gases are admitted at several valved ports as the chamber pressure is monitored by a Wallace and Tiernan FA-145 pressure gauge; mixtures are formed according to the measured partial pressures of the components.

High voltage DC is applied between the electrodes by a locally produced electronic controller rising at a slow controlled rate, beginning from some selected "base" voltage below breakdown. During this voltage rise, the gap is illuminated by ultraviolet light and the voltage is repeatedly sampled by a digital voltmeter. Breakdown is sensed either by light or by ground electrode current, and the controller causes the digital voltmeter to automatically hold the last voltage reading before the event, while the high voltage is rapidly returned to the lower "base" value. The voltage reading is held for a preset time for recording and then the cycle is automatically repeated.

In order to limit the energy of the breakdown arcs, a "diverter" spark gap across the high voltage supply is triggered within microseconds after the event to lower the voltage until the power supply controls are returned to the "base" setting some seconds later. This diverter gap minimizes spark effects on the electrodes and test gas. The diverter gap is formed by two 6-in.-diameter stainless steel hemispheres, one at high voltage and backed by a corona shield and one at ground potential and fitted with the trigger electrode. The diverter-grounded electrode is suspended from the ceiling by a chain drive so that a linear

actuator motor/gear set can be run to adjust the gap from outside. The trigger spark generator, consisting of a high performance automobile ignition system, is mounted at the ceiling adjacent to the gap-adjustment motor.

Interchangeability of Components Between Our Three Breakdown Apparatuses

With the impending arrival of a new 300-kV DC power supply, the installation of the temperature/pressure effects apparatus, and some remaining minor modifications, the three breakdown apparatuses will utilize interchangeable controls. The test chambers will all be fitted with identical high voltage feedthroughs, and the power supplies will be on rollers so that the supplies can be interchanged. The diverter being developed in the cylindrical electrode facility can be inexpensively built and used for the other apparatuses as well.

Image Converter Camera

Our search for such a camera, to be used for basic studies of breakdown phenomena at very short times and also for studies of the time evaluation of the breakdown process, has been completed. We were visited by Mr. J. Owren of Marco Scientific who demonstrated an Imacon 675 image converter camera. We have just received detailed information and a price list from Mr. Owren. We are studying this along with information on a Quantrad camera for a pending final selection.

Automation of the Time-of-Flight Mass Spectrometer Apparatus

We have completed the first phase of automation of our time-of-flight mass spectrometer in order to speed up the data acquisition for our studies on the fragmentation of dielectric gas molecules under

low-energy electron bombardment. A lock-in amplifier and a signal analyzer have been incorporated in the output phase of the apparatus which greatly improved the quality and quantity of the data. The second stage of automation involves a digital controller. The required devices for this stage are being built; they are scheduled for completion in October 1977. In this way the data-taking process will be speeded up fifty-fold compared with the manual operation of the spectrometer.

IX. RADIOGRAPHY OF ENERGIZED GAS-INSULATED SYSTEMS

Calculations of the effects of radiography on an energized gas-insulated cable have been performed and are outlined in Appendix II. On the basis of these, no effect of radiography is foreseen.

X. INTERNATIONAL SYMPOSIUM ON GASEOUS DIELECTRICS

In May 1977, the initial announcement concerning the Symposium to be held in Knoxville, Tennessee, on March 6-8, 1978, was promulgated. This letter notified about 250 individuals throughout the world of the Symposium and its purpose. Also, it issued a call for papers on specific topics of interest which had been formulated from suggestions from a number of the world's key researchers in gaseous dielectrics.

In late June, the Advance Program was mailed, delineating those individuals invited to be speakers, session chairmen, and panel participants. Also, detailed information on times of sessions, format, registration, fees, and hotel accommodations was included.

By September, numerous abstracts were received and distributed to the Program Committee for review and selection. The final program will be drafted in early October, and appropriate announcements and notifications will be made immediately thereafter.

Detailed arrangements for the Symposium and the Proceedings will remain a continuing endeavor.

XI. PUBLICATIONS AND CONTACTS

Publications

1. "Improved Unitary and Multicomponent Gaseous Insulators," by M. O. Pace, L. G. Christophorou, D. R. James, R. Y. Pai, R. A. Mathis, and D. W. Bouldin, IEEE Trans. Elect. Insul. (in press); also Proc. IEEE Electrical/Electronics Insulation Conference, Chicago, Illinois, September 26-29, 1977.

2. "Elementary Electron-Molecule Interactions and Negative Ion Resonances at Subexcitation Energies and Their Significance in Gaseous Dielectrics," by L. G. Christophorou, Proc. XIIIth International Conference on Phenomena in Ionized Gases (Vol. III, Invited Lectures), Berlin, East Germany, September 11-17, 1977.

3. "Breakdown Voltages of Some New Unitary and Multicomponent Gas Mixtures," by D. R. James, L. G. Christophorou, R. Y. Pai, M. O. Pace, R. A. Mathis, and D. W. Bouldin, Proc. Conference on Electrical Insulation and Dielectric Phenomena, Colonie, New York, October 17-20, 1977.

Contacts

We continued communications with leading researchers in the U.S. and Europe, as well as with users of gaseous dielectrics and manufacturers of laboratory apparatus.

We have been visited by Dr. C. Pollock of Union Carbide, Dr. D. Razem of the Radiation Laboratory at the University of Notre Dame, Dr. R. Keil of Heidelberg University, Dr. A. A. Christodoulides of the University of Ioannina in Greece, and Dr. Y. Ichikawa of the

University of Tokyo. Mr. Joe Owren, Vice President of Marco Scientific Company, visited to demonstrate the Imacon model 675 image converter camera.

Others at ORNL continue to interact with us on the various aspects of the high voltage research project, notably H. Schweinler, H. H. Hubbell, Jr., R. D. Birkhoff, J. G. Carter, and J. J. Cowan. Additionally, the Analytical Chemistry Division of ORNL has aided in analyses of gases and breakdown products. The ORNL Instrumentation and Controls Division has aided in calibration. L. G. Christophorou presented a seminar on our work to those in the ORNL Physics Division concerned with high voltage accelerators.

We corresponded with many colleagues in many countries and discussed the many and varied aspects of gaseous dielectrics with active groups in the U.S. and Europe (especially Denmark, Germany, and Switzerland). Dr. A. Cookson of Westinghouse and Dr. J. A. Rees of the University of Liverpool have contacted us concerning improved gases and mixtures, especially C_4F_6.

In May our program review was held in Washington, providing useful discussions with our Department of Energy and Electric Power Research Institute colleagues. In September we had an interesting meeting with Westinghouse and DuPont colleagues at the EPRI headquarters in Washington.

Two tours of our laboratories were made in September by the secretarial staffs of ORNL's director and associate directors and those from DOE in Washington.

Industrial contacts in this period include those with Maxwell Laboratories, Sorenson, Marco Scientific, Tektronics Research, Inc., RFL Industries, Ross Engineering, Quantrad Corporation, Erik A. Lindgren and Associates, Inc., Continental Disc Corporation, Hamamatsu Corporation, General Engineering and Applied Research, Inc., and Armageddon Chemical Company. Advice on high-speed cameras also came from Mississippi State University and the University of Quebec.

During this period we were joined by Ching C. Chan, an Electrical Engineering graduate student at The University of Tennessee.

XII. REFERENCES

1. L. G. Christophorou, D. R. James, R. Y. Pai, M. O. Pace, R. A. Mathis, and D. W. Bouldin, High Voltage Research (Breakdown Strengths of Gaseous and Liquid Insulators), Fourth Quarterly Report, Oak Ridge National Laboratory Report ORNL/TM-5917 (June 1977).
2. L. G. Christophorou, D. R. James, R. Y. Pai, M. O. Pace, R. A. Mathis, D. W. Bouldin, and D. E. Tittle, High Voltage Research (Breakdown Strengths of Gaseous and Liquid Insulators), Third Quarterly Report, Oak Ridge National Laboratory Report ORNL/TM-5806 (February 1977).
3. L. G. Christophorou, D. R. James, R. Y. Pai, M. O. Pace, R. A. Mathis, and D. W. Bouldin, High Voltage Research (Breakdown Strengths of Gaseous and Liquid Insulators), First Quarterly Report, Oak Ridge National Laboratory Report ORNL/TM-5604 (September 1976).
4. L. G. Christophorou, Atomic and Molecular Radiation Physics, Wiley-Interscience, New York, 1971.
5. L. G. Christophorou, D. L. McCorkle, and V. E. Anderson, J. Phys. B: Atom. Molec. Phys. 4, 1163 (1971).
6. G. J. Schulz, Phys. Rev. A 135, 988 (1964).
7. J. P. Johnson, L. G. Christophorou, and J. G. Carter, J. Chem. Phys. 67, 2196 (1977).
8. L. G. Christophorou, D. L. McCorkle, and J. G. Carter, J. Chem. Phys. 54, 253 (1971).

THIS PAGE

WAS INTENTIONALLY

LEFT BLANK

APPENDICES

Appendix I

STRUCTURAL FORMULAE, SYNONYMS, AND BREAKDOWN STRENGTHS OF SOME UNITARY GASES[†]

Dielectric Gas	Structural Formula	Synonyms	Dielectric Properties		
			Electrode Geometry	Pressure Range (torr)	Pd Range (atm-mm)	$(V_s)_R$ [‡]
Hydrogen (H_2)			sphere-plane	1520	2—6	0.25
Nitrogen (N_2)			plane-plane	500	1.0—5.4	0.40
Carbon Monoxide (CO)			sphere-plane	1520	0.5—4.0	0.50
Carbon Dioxide (CO_2)		carbonic anhydride, carbonic acid	various	$0.075—3.83 \times 10^4$	10^{-3}—187.5	0.37[§]
Dichlorodifluoromethane (CCl_2F_2)		Freon-12, Genetron-12, Arcton-12, Isotron-12, Ucon-12	plane-plane	200—600	1.3—26.3	1.03[‖]
Sulfur Hexafluoride (SF_6)			sphere-plane	500—2065	0.5—3.0	1.0
			plane-plane	500—2000	2.0—33.9	1.0
			sphere-plane	83, 100, 154	0.5—2.0	1.0
Perfluoropropane (C_3F_8)		octafluoropropane	sphere-plane	760	1.0—3.0	0.93
Hexafluorobutyne (C_4F_6)	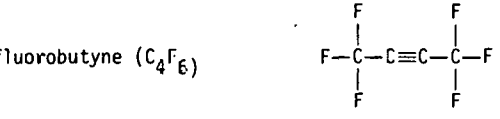	perfluoro-2-butyne	sphere-plane	760—1100	0.5—1.5	2.1—2.2
			plane-plane	500	1.2—3.8	2.2
			sphere-plane	83, 100	0.5—2.0	1.7—1.9

[†]This table will be expanded to include other gases and also the most significant physicochemical properties (such as boiling point, viscosity, thermal conductivity, toxicity, etc.) of gaseous dielectrics in the next semiannual report.
[‡]Breakdown strength relative to SF_6 = 1 as measured by the ORNL group, except where noted.
[§]From H. Winkelnkemper, Z. Krasucki, J. Gerhold, T. W. Dakin, Electra 52, 67 (1977).
[‖]From I. D. Chalmers and D. J. Tedford, Proc. IEE 118(12), 1893 (1971).

Dielectric Gas	Structural Formula	Synonyms	Dielectric Properties			
			Electrode Geometry	Pressure Range (torr)	Pd Range (atm-mm)	$(V_s)_R$
Hexafluoro-1,3-butadiene (C_4F_6)	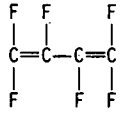		sphere-plane	188, 281	0.5—3.0	1.4
Perfluorobutene-2 (iso-C_4F_8)	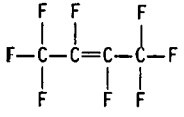	octafluoro-2-butene, perfluoro-β-butylene	sphere-plane plane-plane	500—1600 500—1000	0.5—3.0 1.7—13.4	1.7—1.8 1.7
Octafluorocyclobutane (c-C_4F_8)	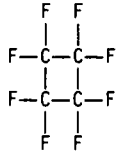	perfluorocyclobutane, Freon C318, cyclic-C_4F_8	sphere-plane plane-plane	760—1850 500-1000	0.5—2.5 2.0—20.1	1.4 1.3
Perfluorocyclopentene (C_5F_8)	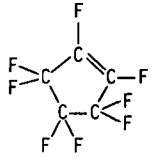	octafluorocyclopentene	sphere-plane	151, 153	0.5—2.0	2.1—2.2
Hexafluorobenzene (C_6F_6)	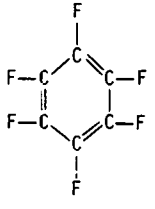	perfluorobenzene	sphere-plane	500	0.5—2.5	¶

¶Pure gas not studied; low percentages of C_6F_6 in SF_6 improved dielectric strength relative to pure SF_6.

Dielectric Gas	Structural Formula	Synonyms	Dielectric Properties			
			Electrode Geometry	Pressure Range (torr)	Pd Range (atm-mm)	$(V_s)_R$
Perfluorocyclohexene (C_6F_{10})	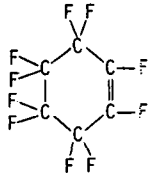	decafluorocyclohexene	sphere-plane	83	0.5—1.75	1.9—2.2
Perfluordimethylcyclobutane (C_6F_{12})	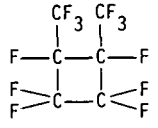 (1,2 isomer)		sphere-plane	140	0.5—2.0	2.3—2.4[††]
Perfluorcheptene-1	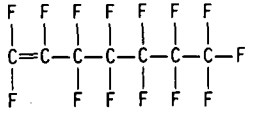		sphere-plane	152	0.5—2.0	1.2
Perfluormethylcyclohexane (C_7F_{14})	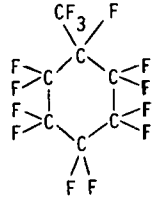	hendecafluorocyclohexane, trifluoromethylcyclohexane	sphere-plane	58	0.1—1.0	2.1

[††]Mixture of 1,2- and 1,3-perfluorodimethylcyclobutane.

Dielectric Gas	Structural Formula	Synonyms	Dielectric Properties			
			Electrode Geometry	Pressure Range (torr)	Pd Range (atm-mm)	$(V_s)_R$
Perfluoro-1,3-dimethyl-cyclohexane (C_8F_{16})	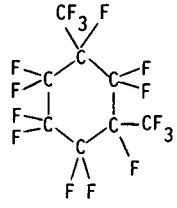		sphere-plane	35	0.07—0.17	‡‡

‡‡$(V_s)_R$ not determined since SF_6 data at 35 torr could not be taken. Strength relative to C_4F_6 (perfluoro-2-butyne) at 35 torr was 1.3.

Appendix II

ESTIMATE OF THE LIKELIHOOD OF ELECTRIC BREAKDOWN DURING RADIOGRAPHY OF HIGH VOLTAGE, GAS INSULATED POWER TRANSMISSION LINES*

I. SUMMARY

Preliminary information has been obtained from workers in the field of gas insulated, high voltage transmission lines on properties of such lines, industry practice in installation of such lines, and radiographic techniques for inspection. Differences of opinion exist as to whether radiography of energized lines will initiate breakdowns. Approximate calculations indicate the order of magnitude of the current of electrons which might be released from the outer pipe wall and in the insulating gas during radiography and the probable electron densities resulting. The conclusion is reached that radiography will not induce breakdown unless a very high intensity, pulsed x-ray source is used or sharp points on the conductors badly distort the electric fields.

II. INTRODUCTION

The use of gas insulated, high voltage transmission lines may permit significant savings in electric power transmission losses. Gamma- and x-radiography can detect unwanted particles or broken insulators which may lead to electric breakdowns within line components. The ionization produced in the insulating gas during radiography might trigger electric breakdowns if the high voltage is on. The purpose of this study is to determine the probability that radiography will cause breakdowns.

---

*Prepared by H. H. Hubbell.

The steps in analyzing the problems are seen to be as follows:

1. Determination of what radiation sources are used for radiography (i.e., the energy distributions and intensities of the sources and the source-to-conductor distances in order to determine the radiation dose).

2. The electron energy spectra released from the inner surfaces of the high voltage conductors into the gas. The spectra will be given as the absolute number of electrons as a function of their energy for given radiation sources.

3. The corresponding spectra of electrons released in the gas.

4. The probability that the electrons can be accelerated to ionization energy by the high voltage and cause Townsend avalanche or the formation of streamers and resultant breakdown.

Additional problems concern the possible chemical decomposition of the insulating gas by the radiation, or the radiation plus the high voltage, the production of chemicals which might corrode the conductors or insulators, or become toxic hazards if the conductor pipe was opened for repairs.

The present discussion will summarize the problems and the present information available and give estimates of the probable number and energies of the electrons released from the walls and gas by radiography. From this information we will estimate the probability of induced breakdown.

III. BACKGROUND

We obtained by phone and letters available information on industry experience with radiography of gas insulated transmission lines. Many people were very helpful in explaining the problems.

The general conclusions from these discussions may be summarized as follows:

1. The purpose of x- and γ-radiography of gas insulated transmission lines is to find contamination particles, broken or distorted insulators, displaced conductors, etc., which may be sources of electric breakdown.

2. The radiographs made so far have nearly always been done on de-energized lines where radiation induced breakdowns could not occur. However, if the technique proves useful, radiographs might be made routinely on energized lines in service to detect possible faults or incipient breakdowns, in which case radiation induced breakdowns could be very serious.

3. The rigid pipe type line with a single central conductor must be assembled in the field, and it is practically impossible to prevent dirt particles, metal sawdust or shavings, etc., from getting into the pipes during assembly. With AC high voltage applied, these particles jump around constantly in the high fields and may end up in such positions that they initiate electrical breakdown. Traps or low electric field regions are therefore built into the lines. If the particles bounce into such places, they will stay there out of harms way, and eventually all particles will be so trapped.

One worker remarked that faults seldom recur at the same place, indicating again that the particles causing the faults probably jump around a great deal.

If DC is applied, however, the particles tend to fly to spacing insulators or to high field regions and cling there, distorting the field and tending to initiate electric breakdown with resultant burning or

shattering of the insulators. For this reason, most workers strongly advise against testing lines with DC. Direct current transmission lines must therefore be much cleaner than those for AC.

One manufacturer is developing a flexible bellows type of transmission line, sometimes containing three conductors separated by spacers and insulated with polyurethane foam saturated with SF_6. The bellows walls are presumably much thinner than the rigid pipes, and much lower energy x rays can be used for radiography. This technique permits visualization of some detail of the insulators and even distortions, etc., in the polyurethane. The advantage of this construction is that the line can be assembled, filled with gas, and sealed in the relatively clean conditions of a factory so that particle and oil or dirt contamination can be greatly reduced and would occur only at infrequent joints made in field assembly of lines. X-ray inspection in manufacture and assembly would be desirable but need not be done when the line is energized. In service, inspection with x rays may still be desirable, especially at substations. Buried lines would have to be excavated, which would only be done if a fault had occurred and had been localized.

4. Other systems than radiography can be used for finding faults on lines not in service, such as radar or sonar signals sent down the line. Unusual reflections could indicate the possible faults. Simple resistance or capacitance tests could indicate the location of short circuits or open circuits. Such tests are done routinely to find faults in telephone lines.

5. Another possible problem in radiography is the potential degradation of the insulating spacers by the radiation. Three types of

spacers are presently in use: ceramic, cyclo-aliphatic epoxy resins, and bisphenol epoxy resins. Radiation damage work in the past has usually indicated that 10^5 to 10^7 rad dosages are needed to produce significant radiation damage in organic materials, while radiography seldom requires more than 1 to 100 rads. Hence, I do not think this is a significant problem. Ceramics are relatively unaffected by the highest dosages mentioned.

6. Bonneville Power Administration is currently contracting with Battelle Northwest to study the effects of x and γ rays on energized transmission lines. It was informally stated that preliminary tests indicated no breakdowns under irradiation.

7. Considerable difference of opinion was expressed on the use of radiography. Several people thought radiation would not significantly decrease the dielectric strength of SF_6 insulated lines, while another person was of the opinion that the use of x or γ rays had initiated breakdowns. Apparently, experimental work is needed.

8. One high voltage equipment manufacturer is reported to have used x irradiation of anode and cathode regions of high voltage, DC machines to discharge contamination particles, thus preventing them from being strongly attracted to charged electrodes and thus initiating breakdowns. If such irradiation were used continuously rather than just in initial "seasoning," then radiation damage to insulators might become a problem. Health physics problems of protecting personnel might also be serious if continuous irradiation of high voltage lines or components were used.

Ideally, the probability of high voltage breakdowns induced by radiography would be analyzed by the steps outlined in the introduction to this section. Considerable effort was expended in trying to determine the spectra of possible x-ray and radioisotope sources, the number of electrons and the electron energy spectra they would produce in the insulating gas, and the rates at which these electrons would be captured or multiply, and hence the probability of induced breakdown. It was evident that this would be a rather long and complex calculation with many assumptions needed where experimental data are lacking. The procedure is outlined in Section V.

IV. APPROXIMATE CALCULATION OF BREAKDOWN PROBABILITY

General Considerations

Because only a simple yes or no answer is required, a much simpler approach is possible. It is well known that during breakdown testing when all the conditions of gas pressure, electric field, electrode shape are satisfied so that a spark is certain to occur, there is always a delay before the spark takes place while the system waits for the inevitable initial electron to appear at a critical point as a result of cosmic rays, background radioactivity, etc. It is customary therefore in testing to provide these initial electrons by irradiating the gas or the electrodes with ultraviolet light or radiations from radioactive substances.

Hence, we may conclude at once that the ionization produced by radiography would not cause any breakdowns which would not occur anyway as soon as background radiation produced the necessary initial electrons

at the critical point. Eventually, usually within a few seconds, these electrons will certainly appear, and breakdown will occur if the other conditions of electric field, pressure, etc., are met. There are one or two important exceptions to this statement. First, if the critical breakdown field occurs because of a contamination particle moving quickly through a particular position, then an electron might not appear at the critical place and time in the absence of irradiation, and breakdowns would not always occur. This event, of course, is unpredictable but will not occur if there are no loose particles inside the pipe.

The second exception would occur if the radiography produced such a high electron density in the insulating gas that the resulting space charge seriously distorted the electric field distribution in the line, producing critical breakdown conditions where they would not otherwise occur.

About 10^8 electrons must be present in a volume of about 1 mm^3 for a streamer to form and propagate, causing a breakdown, or the critical electron density is $\rho_e' \cong 10^{11}$ electrons/cm^3.[1] The remaining discussion is an attempt to see if this density would be produced by radiography.

Sources and Photon Flux Produced

If a radioisotope is used as a source, then the number N_o of photons per cm^2 per sec of energy E reaching the outside of the pipe being radiographed at a distance r cm can be calculated from[2]

$$N_o = (Sf\ A/4\pi r^2)\ \exp(-\frac{\mu_a}{\rho}\rho r),$$

where

A = activity of source in curies

$S = 3.7 \times 10^{10} \frac{\text{disintegrations}}{\text{sec/Ci}}$

f = number of photons of energy E per disintegration

$\frac{\mu_a}{\rho}$ = mass attenuation coefficient of material between source and point of interest for energy E

ρ = density of material between source and point

If several gamma rays are emitted, the N_0's should be separately calculated unless they are close together in energy so that the μ_a/ρ values are essentially the same. This is true for the case considered. For example, a suitable source for radiography of aluminum pipes with about 0.3-in. walls is iridium-192. This isotope has 7 gamma rays from 296 to 612 keV energy with μ_a/ρ values all nearly the same. There are a total of 2.08 photons per disintegration having a weighted average energy of 375 keV. If the pipe has a 30-cm diameter, 0.76-cm wall, and is 70 cm from the source (source to film 100 cm), the absorption coefficient of the aluminum is 0.0945 cm^2/g (ref. 3) and the Al density is 2.71 g/cm^3, we obtain for the irradiation at the inside of the pipe for a 65 Ci source of Ir 192:

$$N_i = 6.7 \times 10^7 \text{ photons/(cm}^2 \text{ sec)}.$$

The pipe wall is assumed flat. The attenuation in air is negligible at this energy and distance, but the attenuation in the pipe wall is included. The number buildup factor for a broad beam in the aluminum for the 0.2 mean free path through the pipe wall is assumed to be 1.0.[4]

Alternatively, one might use an x-ray source instead of a radioisotope. X-ray machines with outputs in the appropriate energy range are large, heavy, and not very portable. They would probably not be used

for field radiography, but we might include a rough estimate of the analogous photon flux for such a machine. The author's data[5] and data in the literature[6,7] for a 250-kV, constant potential therapy machine with window thickness equivalent to 0.661 g/cm^2 of Al gave an absorbed dose rate in air at 1 m of about D_{out} = 0.054 rad/(sec mA). The absorbed dose may be converted to photons/cm^2 sec inside the pipe as follows:[2]

$$N_i = \frac{D_{out}\, i e^{-\left(\frac{\mu_a}{\rho}\right)\rho t}}{(\mu_{en}/\rho)_{air}} \frac{k}{E} \left(\frac{100}{r}\right)^2 ,$$

where

i = x-ray target current = 15 mA;

$k = \frac{100 \text{ ergs}}{g_{air} \text{ rad}} \cdot \frac{1 \text{ eV}}{1.60 \times 10^{-12} \text{ erg}} = 6.25 \times 10^{13} \frac{\text{eV}}{\text{g rad}}$;

E = average photon energy* = 1.2 x 10^5 eV;

$\frac{\mu_a}{\rho}$ = 0.148 cm^2/g, mass attenuation coefficient for aluminum;

r = distance in cm from target to pipe, 70 cm;

t = thickness of pipe, 0.3 in. = 0.762 cm;

ρt = 2.07 g/cm^2;

$(\mu_{en}/\rho)_{air}$ = 0.024 cm^2/g, mass energy absorption coefficient for air.

With these assumptions, we get for the photon flux at the inside surface of the pipe

---

*See discussion in Part V below for the method of determining the average energy.

$$N_i = 2.6 \times 10^{10} \text{ photons/(cm}^2 \text{ sec)}$$

for x rays from a 250-kV, 15-mA machine.

Electrons Produced in the Insulating Gas

The next steps are to calculate the number of electrons released in the insulating gas, SF_6. For this approximate calculation we will assume that the energy absorbed in the gas is all used to produce primary ions and electrons and that these primary electrons produce secondaries at an average rate which is independent of the primary electron energy.[8,9] The number of electrons produced in the gas per photon, n, can then be calculated from

$$n = \frac{E_{av}}{W},$$

where

E_{av} = the average energy per photon, eV;

W = average energy to produce one ion pair in the gas in question, SF_6;

$W = 5.9 + 1.82\ I$ (ref. 10)

where

I = ionization potential of $SF_6 \cong 15.4$ eV (ref. 11)

so

W = 33.9 eV/ion pair.

From these data we get

$n = 3.5 \times 10^3$ electrons/photon absorbed for 250-kV x rays

$n = 1.1 \times 10^4$ electrons/photon absorbed for Ir-192 gamma rays.

The fraction of photons absorbed per cm path in SF_6 is

$$h = \left(1 - e^{-(\mu_{en}/\rho)\rho t}\right)$$

$t = 1$ cm

μ_{en}/ρ for SF_6 is the sum of the mass absorption coefficients for S and F, weighted in proportion to their masses in the molecule:

$$\left(\frac{\mu_{en}}{\rho}\right)_{SF_6} = \left(\frac{\mu_{en}}{\rho}\right)_S \frac{A_s}{A_s + 6A_F} + \left(\frac{\mu_{en}}{\rho}\right)_F \frac{6A_F}{A_s + 6A_F},$$

A_s, A_F = atomic weights of sulfur and fluorine

μ_{en}/ρ = mass energy absorption coefficients.

The mass energy absorption coefficients (in units of cm^2/g) are[12,13]

	120 keV	375 keV
S	0.050	0.030
F	0.024	0.028

hence

SF_6	0.030	0.0284

The SF_6 is assumed to be at a pressure 45 psig, so P = 4 atm absolute. Its density is then

$$\rho_{SF_6} = \frac{P(A_s + 6A_F) \text{ g/mole}}{2.24 \times 10^4 \text{ cm}^3/\text{mole}} = 0.0261 \text{ g/cm}^3.$$

Using the values stated, the fractions of photons absorbed in SF_6 are:

for 250-kV x rays, $h = 7.8 \times 10^{-4}$

for Ir-192 gamma rays, $h = 7.4 \times 10^{-4}$.

The number of ions formed per cm^3 will then be

$$N = n N_i h.$$

So finally we get for the number of electrons released in the gas:

for 250-kV x rays, $N = 7.1 \times 10^{10}$ electrons/(cm^3 sec)

for Ir-192 gamma, $N = 5.5 \times 10^{8}$ electrons/(cm^3 sec).

Electrons Injected from the Walls

The next step is to calculate the number of electrons which will be injected into the gas from the pipe wall by radiation. An exact calculation of the number and energy distribution of such electrons is rather complex. The procedure will be outlined in Section V. Here we employ approximations similar to those used above to get an estimate of the numbers. The range of the most energetic electron which could be produced by the radiations considered is only 0.15 g/cm^2 Al,[14] or 0.05 cm, and for low energy electrons about 10^{-6} cm, so all electrons entering the gas arise essentially at the inner surface of the pipe. Hence, we consider only the situation there and assume that the aluminum medium is infinite in extent so far as the slowing down of electrons is concerned. We assume the same photon intensities and average energies as before incident at the inner side of the pipe.

Nelson et al.[5] and Finston et al.[15] studied the yield and spectra of electrons released from aluminum by x rays up to 250 kV. Finston[15] noted that the total yield of electrons per rad of absorbed dose was nearly constant, independent of the x-ray energy or the material, and amounted in aluminum to

$$I_e = 4.9 \times 10^{-4} \text{ esu/(cm}^2 \text{ rad)}$$

for electrons up to 40 eV. McConnell et al.[16] obtained the slowing-

down flux spectrum of electrons produced inside aluminum by a distributed beta-ray source. Ritchie et al.[17] showed that Finston's and Nelson's data fitted the same curve for electron energy distribution as McConnell's results, although the first two studies used x-ray sources and the last, a beta ray, with totally different energy analysis techniques. The data also fitted the theories as calculated by Ritchie et al. and by Klots and Wright[18] at low energies and by Spencer and Fano,[19] Spencer and Attix,[20] and McGinnies[21] at high energies. We corrected McConnell's spectrum for the transmission barrier from aluminum given by him and integrated first to find the current expected up to 40 eV, getting a result which agreed with Finston's. Then we integrated again up to the end point. The last two figures showed that only about 1% of the total flux of electrons outside the wall was below 40 eV and that a total of about $n_w = 0.043$ electrons/cm^2 emerged from the aluminum per primary electron born/cm^3. The primary electrons in McConnell et al.'s work were produced by an Au-198 source with an average energy of 315 keV distributed throughout the aluminum. All the beta-ray energy was absorbed in the source, so the dose was

$$D_{Au} = \frac{\bar{E}_\beta}{k\,\rho_{Al}} = 1.86 \times 10^{-9} \text{ rad in Al for each primary electron born/cm}^3.$$

Thus we find that the number of electrons emerging from the aluminum, n_e, is

$$n_e = \frac{n_w}{D_{Au}} = \frac{0.043 \text{ electrons emerging}}{\text{cm}^2\ 1.86 \times 10^{-9} \text{ rad}} = 2.3 \times 10^7 \frac{\text{electrons}}{\text{cm}^2 \text{ rad}}.$$

We have assumed from the results of the studies discussed that the number of electrons emerging from the aluminum per rad of absorbed dose

is the same regardless of the radiation source. As shown above, the significant dose for generating electrons is that at the inside of the aluminum pipe.

For x rays then the number of electrons emerging from the walls is

$$s_w = n_e D_{out} i \left(e^{-(\mu_a/\rho)\rho t}\right) \left(\frac{100}{r}\right)^2$$

or

$$s_w = 2.8 \times 10^7 \frac{\text{electrons}}{\text{cm}^2 \text{ sec}} \text{ for 250-kV x rays at 70 cm from the source.}$$

For Ir-192 the corresponding calculation is

$$s_w = N_i E(\mu_{en}/\rho)_{Al} n_e/k,$$

where

E = 375 keV for average Ir gammas,

(μ_{en}/ρ) = the mass energy absorption coefficient for gammas of energy E in aluminum = 2.87×10^{-2} cm^2/g,

N_i = photons/(cm^2 sec) inside the pipe from the Ir source = 6.7×10^7 photons/cm^2 sec,

hence

$$s_w = 2.7 \times 10^5 \frac{\text{electrons}}{\text{cm}^2 \text{ sec}} \text{ for Ir-192.}$$

These additions are negligible compared with the number generated in the gas, which has been shown to be of the order of 10^8 to 10^{10} electrons/(cm^3 sec).

Electron Drift in the Gas and Resultant Electron Density

With the electron source terms calculated above for the gas, we can determine the electron swarm density as it drifts through the SF_6 gas under the influence of the electric field.[23] The first point is that

since the mean free paths of the electrons in the gas at the pressures considered are very short (on the order of 10^{-6} cm) compared with the dimensions of the pipe, the initial fast electrons make many collisions in a very short time and distance, losing energy at each collision, so that they attain their equilibrium energy distribution before they have moved very far regardless of their initial energies. Therefore, we need consider only the equilibrium drift of electrons (and/or ions) in the electric field.

The differential equation for the electron density in the absence of electron capture is

$$\frac{d\rho_e(x)}{dx} = \frac{N}{w} ,$$

where $\rho_e(x) = \frac{Nx}{w}$ is the electron density, N is the rate of electron production by radiation, and w is the electron drift velocity in the gas. In this extreme case where no electrons are captured to form negative ions we may use[†] for $w \underline{\sim} 10^6$ cm/sec[34] and obtain for the maximum electron densities:

for x rays, $\rho_e(10) = 10^5$ electrons/cm^3

for Ir 192, $\rho_e(10) = 10^3$ electrons/cm^3.

Possibility of Breakdown

Since these numbers are 10^6 or 10^8 times smaller than the critical density quoted, 10^{11} electrons/cm^3, we conclude that there is no possibility of the irradiation causing a breakdown unless sharp points,

---

[†]For ions $w_i \underline{\sim} 10^4$ cm/sec and the charge density increases accordingly (by x 100).

particles, etc., greatly increase the local electric fields, or unless flash radiography is done, giving dose rates 10^6 times larger than those possible with continuous exposure devices. As was pointed out earlier, such flash x-ray machines are not ordinarily suitable for routine field radiography.

Effect of Sharp Points

The possible increase in electric field strength due to sharp points may be estimated as follows: Assume the point is actually a very small sphere of radius of curvature a. The surroundings may be approximated as a large sphere of radius b. The electric field at any point a distance r from the center of the small sphere with a potential difference V between spheres is

$$E_r = \frac{V}{r^2}\left(\frac{ab}{b-a}\right).$$

The field is largest at the surface of the small sphere, so

$$E_{max} = \frac{V}{a}\left(\frac{b}{b-a}\right).$$

For small a, b/b-a = 1 so approximately

$$E_{max} = \frac{V}{a}.$$

The field thus increases inversely as the radius of the point.

Since the drift velocity, as a rule, increases with increasing electric field, it is evident from the equation for electron density, $\rho_e = Nx/\mu E$, where μ is the electron mobility, that increasing the field must lower the electron density and thus reduce the probability of breakdown from this cause. The breakdown at higher fields arises because of either cold emission from the point when it is negative, or because electrons in the vicinity gain

more than enough energy to ionize in one free path, leading to avalanches or because both effects occur. If the electric field is large enough for avalanches to occur, the point will exhibit corona and be a problem spot in the line anyway. Neither process, therefore, is likely to be very sensitive to a prevailing electron density of the magnitudes calculated, so we conclude radiography at the dose rates assumed here is unlikely to cause breakdowns which would not otherwise occur.

Effect of Magnetic Fields

So far the discussion has assumed static electric fields and no magnetic fields. Actually, the conductors will be carrying very large currents, perhaps as much as 10^4 A, so the magnetic fields may be quite large. Under vacuum conditions, the free electrons would be trapped and move around the circular magnetic field lines, not getting to the walls at all. However, at high pressures they collide so frequently with atoms and thus suffer direction changes that the net drift is not altered very much. Huxley and Crompton[35] show that the angle θ between the drift direction in crossed magnetic and electric fields is given approximately by

$$\tan \theta \sim \frac{e}{m} \frac{B}{\nu},$$

where

$\frac{e}{m}$ = specific charge of electron = $1.76 \times 10^8 \frac{\text{coulomb}}{g}$,

B here for 10^4 A is of the order of 400 Oe,

ν = collision frequency of electrons about 10^{12}/sec or more at 4 atm pressure.

Hence θ, the angle between the drift velocity and the electric field is very small. Hence, the magnetic field has negligible effect on the electron density.

Summary

We may summarize the numerical calculations in Table 1, referring to Fig. 1. We assume the high voltage is about 100 to 300 kV.

SECTION V. OUTLINE OF POSSIBLE EXACT CALCULATION OF ELECTRON DENSITIES AND PROBABILITY OF INDUCED BREAKDOWN

In view of the large spread between the estimated electron densities produced by irradiation and the critical electron density for breakdown, it does not seem worthwhile to attempt a more sophisticated calculation However, the possible procedure will be briefly outlined.

The essential problem is similar to the derivation of the energy given to the gas in a cavity surrounded by walls of a different composition as given by the Bragg-Gray Principle, which is one of the fundamental bases of radiation dosimetry. Many lengthy studies have been written on this and related subjects (refs. 24-26 and references therein). The present problem is more complex because we wish to know the energy spectrum of the electrons in the gas resulting from the irradiation, and the corresponding spectrum after the electrons have come to equilibrium with the gas under various conditions of pressure, electric field, and gas composition. By contrast, in radiation dosimetry only the energy deposited, and sometimes the linear energy transfer are usually considered. These are simpler, though still rather difficult problems.

The steps in a complete calculation are as indicated in the introductory remarks.

Table 1

Source	Ir 192*	250-kV 15-mA x rays†
E = average source energy, keV	375	120
N_i = photon flux inside pipe, photons/cm^2 sec	6.7×10^7	2.6×10^{10}
N = electron flux produced in gas, electrons/cm^3 sec	5.5×10^8	7.1×10^{10}
s_w = electron current density from walls, electrons/cm^2 sec	2.7×10^5	2.8×10^7
ρ_e = maximum electron density in gas, electrons/cm^3	10^3	10^5
ρ_e' = assumed critical electron density in gas for breakdown, electrons/cm^3	10^{11}	

*Ir = Iridium-192, 65 Ci.

†x = x rays, 250 kV applied, 15 mA, 0.66 mg/cm^2 Al window, average energy 120 keV.

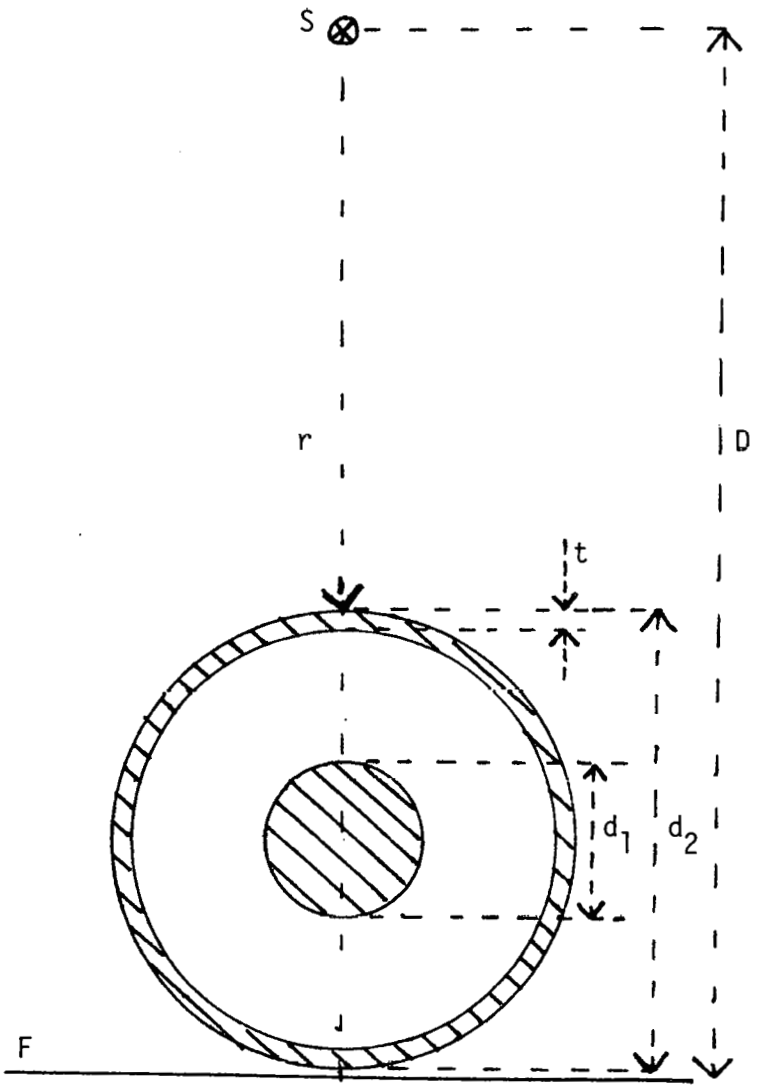

Figure 1

S - source of x or gamma rays
F - photographic film
D - distance to film, 1 m = 39 in.
r - distance to pipe, 70 cm
t - thickness of pipe, 0.76 cm = 0.3 in.
d_1 - diameter of center conductor, 10 cm = 4 in.

d_2 - outer diameter of pipe, 30 cm = 12 in.

P - pressure of SF_6 in pipe = 45 psig = 4 atm absolute

Sources

The identification of all reasonably useful radioisotope and x-ray sources and their outputs must be made. Thulium-170, iridium-192, cesium-137, and cobalt-60 are possibilities. As an extreme case of continuous duty x-ray machine, we will consider one with 250 kV, constant potential at 15 mA, with a tungsten target, having a window equivalent to about 0.66 g/cm^2 of aluminum. Such units are large and require water cooling, so any portable one would probably have lower applied voltage and output. Of the radioisotopes, Ir-192 has been suggested as most suitable for the thickness of aluminum to be radiographed.

It has a number of strong γ-rays as follows:

Energy keV, T_i	Number per Disintegration, L_i
296	0.29
308	0.30
317	0.81
468	0.49
589	0.04
604	0.09
612	0.06
Weighted average: 375	2.08

In Section IV it was assumed that the total number of γ rays emitted was $\sum L_i$, each having the weighted average energy, $E_{av} = \sum L_i T_i / \sum L_i$.

For an x-ray machine, data was used for one originally present in the Health and Safety Research Division. Its output was probably larger than the largest value could reasonably be obtained from portable machines.

However, it consisted of four large pieces, weighed several tons, and required special power and water connections, so it was not portable. The yield was measured with standardized dosimetry instruments and agreed with values in the literature.[6] The output radiation spectrum can be derived using a theoretical result of Kramers.[27] He showed on the basis of semi-classical assumptions that the continuous bremsstrahlung spectrum from a thick target could be expressed in a form that may be written as

$$I(E)\,dE = -\,C(E - E_0)\,dE, \quad E < E_0$$
$$= 0 \qquad\qquad , \quad E > E_0,$$

where $I(E)\,dE$ is the intensity of the x rays per unit energy interval E, E_0 is the applied voltage, and C is a constant. Combining this result with the usual exponential absorption law and the mass absorption coefficient, the shape of the spectrum can be calculated after transmission through the inherent filtration of the x-ray tube and any added filters:

$$N(E)\,dE = -\,C(E - E_0)\,\pi_i \exp\left\{-\left[\frac{\mu}{\rho}(E)\right]_i \rho_i x_i\right\}.$$

In this expression $\frac{\mu}{\rho}(E)_i$ is the mass absorption coefficient of the $\underline{i}$th filter of density ρ_i and thickness x_i for incident energy E. Villforth et al.[28] calculated the spectra for heavily filtered x-ray beams at a number of applied voltages and measured the spectra with a scintillation spectrometer. The calculated and measured spectra agreed very closely, so we have confidence that the calculation method gives good results. The average energy was obtained by integrating the spectrum as usual:

$$E_{av} = \frac{\int_0^{E_o} E\, N(E)\, dE}{\int_0^{E_o} N(E)\, dE} .$$

For the light filtration of the x-ray tube and tube head windows, equivalent to about 0.66 g/cm^2 of aluminum, E_{av} = 120 keV approximately, as used in Section II above. For a detailed study we would use the complete spectrum as calculated this way and derive from it the degraded spectrum in the aluminum pipe and gas for each source, as is discussed below.

Photon Spectrum at Inside Surface of Aluminum Pipe

The photon spectrum at the inside surface of the pipe and its absolute intensity will be degraded by passage through the aluminum and air. For the energies considered, the effect of the air absorption is negligible. Since we are interested only in steady state conditions, the Boltzmann transport equation reduces to a diffusion equation. Some consideration should be given to the solution of this equation under the present conditions to derive the changes in the spectra produced by the passage of the radiation through the pipe wall. The buildup factor[29] should not exceed a factor of 2 at most and will probably be closer to 1, but the increase in the low-energy end of the spectra may be appreciable.

Primary Electron Spectra in the Aluminum of the Pipe

It was pointed out in Section IV that we need calculate only the electrons generated in a very thin layer of aluminum at the inside of

the pipe because of the very short range of such electrons. The number and energy spectra of primary photo and Compton electrons produced by each energy photon should be calculated from the known cross sections.[12,13] The resulting electron spectra should be integrated over the photon spectra to obtain the primary electron source terms in the aluminum, giving the electron spectra as

$$s_e(E)\,dE = \left\{ \int_0^{E_0} \left[\tau_{pe}(E',E) + \sigma_c(E',E) \right] N_i(E')\,dE' \right\} dE,$$

where $\tau_{pe}(E',E)$ and $\sigma_c(E',E)$ are the photoelectric and Compton cross sections for the production of electrons of energy E by photons of energy E'.

Slowing-Down Spectra of Electrons in Aluminum

By the "slowing-down spectrum of electrons," we mean the total number of electrons per eV entering an imaginary probe of 1 cm^2 cross sectional area per primary electron born/cm^3. The resulting dimensions are cm/eV, confirming the statement of Spencer and Fano[19] that the slowing-down flux at an energy E is the track length traveled by the electrons per unit energy range. As these authors showed, the flux can be calculated[30] as the product of the reciprocal stopping power of electrons at kinetic energy T times the sum of all primary electrons born above T and the secondary electrons produced above 2T (T ≡ E here, using Birkhoff's notation)[30]

$$g(T) = \left[S_z(T)\right]^{-1} \left\{ \int_{T}^{T_o} S(T')\, dT' + \int_{2T}^{T_o} k_s(T',T)\, y(T')\, dT' \right\},$$

where $S_z(T)$ is the average stopping power at energy T, S(T') is the primary source spectrum, the same as our $s_e(E)$, and $k_s(T',T)$ is the cross section for production of a secondary electron of energy T by a primary electron of energy T'. This integral equation has been solved numerically, and tables are available[21] at selected primary energies for secondaries down to about 500 eV.

The tabular values can be interpolated for other primary and secondary energies above this value, and the results summed to find the spectrum down to 500 eV. Below this energy more complex calculations must be done to take account of energy losses to excitation and ionization of all the atomic and conduction levels of the aluminum. Ritchie et al.[17] derived such a result for aluminum and showed that it fitted the experimental data, as discussed in Section IV. Thus we may obtain, with a good deal of work, the electron flux spectrum in the aluminum.

Total Electron Spectra Entering Gas from Aluminum Wall Pipe

The electrons going from the aluminum into the gas lose further energy surmounting the potential barrier at the surface, and some are reflected back. Nelson et al.[5] showed that the spectrum after transmission through the barrier is given by

$$n_w(E_{out}) = 2\pi\, y(E_w + E_{out}) \left\{ 1 - \left[E_w/(E_w + E_{out}) \right]^{1/2} \right\} ,$$

where E_{out} is the electron energy in the gas and

$$E_w = E_F + \phi,$$

the sum of the Fermi energy (to the top of the filled band in aluminum) and the work function. This correction was made in the calculations of Section IV for n_w.

Recent work by Sickafus[31] has shown that the basic shape of the spectra derived this way is correct, but that the low-energy end below about 1000 eV is strongly modified by oxide and contamination layers on the surface. Since Nelson et al.'s,[5] Finston et al.'s,[15] and McConnell et al.'s[16] data were taken for normally oxidized surfaces, their results would be applicable here.

Total Electron Spectra Generated by Photons Absorbed in the Gas

Using the same photon spectra from step 3, the procedures of steps 4 and 5 would be repeated using the constants appropriate to SF_6 at the pressure to be used. This procedure would give the initial electron spectrum generated in the gas. This spectrum in the gas would be a source term throughout the gas. At the outer and inner walls it would be added to the spectrum of electrons injected from the walls. Actually, the approximate calculations of Section IV showed that the electrons from the walls were practically negligible compared with those generated in the gas. This is confirmed by the work of Taylor,[32] who found only very small residual currents in ionization chambers when the gas was evacuated. Klots and Wright[18] showed that the electron flux spectra in gases under irradiation were very similar to those in metals.

Drift of Electron Swarm Under the Electric Field and Resultant Electron Density

It was assumed in Section IV that the mean free paths of the electrons of all energies of interest here were so short that the electron energy spectra reached their equilibrium values for the existing E/P before traveling a significant distance. Hence the slowing down and subsequent diffusion of the electrons could be treated as separate problems. An exact solution would combine both phenomena in a single treatment, thus considerably complicating the already very complex Spencer-Fano type calculation. Such a treatment would remove these authors' simplification that the system is independent of space coordinates. The variations in cross sections with energy would include all atomic and molecular resonances, electron capture probabilities, etc., making the problem practically insoluble. Much of the necessary data for SF_6 does not yet exist. In view of this situation and because of the very small electron densities estimated by the approximate method, it does not seem worthwhile to pursue the problem further at this time.

VI. CONCLUSIONS

The study was undertaken to determine whether radiography would cause a breakdown in an energized high voltage, gas insulated electric transmission line. The conclusions are as follows:

1. Radiography with radioisotopes of 100 Ci or so will not initiate breakdowns which would not otherwise occur.

2. Radiography with a 250-kV, 15-mA x-ray machine would give about 100 times the electron density in the insulating gas compared

with radioisotopes. Even this density, however, is at least a million times too small to initiate a breakdown which would not otherwise occur.

3. A very sharp point on one conductor, such as the end of a broken metal particle, might initiate a breakdown under radiography. It would probably cause a spark eventually without radiography.

4. Flash radiography using an x-ray machine which could deliver the dose necessary for a radiograph in 1 or 2 μsec would be marginal and might initiate a breakdown with no sharp points inside the pipe.

VII. REFERENCES

1. J. M. Meek and J. D. Craggs, Electrical Breakdown in Gases, Oxford University Press, London, 1953.
2. K. Z. Morgan and J. E. Turner, Principles of Radiation Protection, p. 275, Wiley, New York, 1967.
3. J. H. Hubbell, National Bureau of Standards Report NSRDS-NBS 29 (1969).
4. R. D. Evans, in F. H. Attix and W. C. Roesch, Radiation Dosimetry, 2nd ed., p. 151, Academic Press, New York, 1968.
5. D. R. Nelson, R. D. Birkhoff, R. H. Ritchie, and H. H. Hubbell, Measurement of Electron Flux in Media Bombarded by X-Rays, Oak Ridge National Laboratory Report ORNL-2521 (1958), pp. 31, 91; Health Phys. 5, 203 (1961).
6. O. Glasser, E. H. Quimby, L. S. Taylor, and J. L. Weatherwax, Physical Foundations of Radiology, 2nd ed., p. 245, Paul B. Hoeber, Inc., New York, 1952.

7. E. V. Condon and H. Odishaw, Handbook of Physics, p. 7, McGraw-Hill, New York, 1958.

8. L. W. Cochran, Principles of Radiation Protection, pp. 157-161, ed. by K. Z. Morgan and J. E. Turner, Wiley, New York, 1967.

9. L. G. Christophorou, "Atomic and Molecular Radiation Physics," Wiley-Interscience, New York, 1971, Chap. 2.

10. L. G. Christophorou, ibid, p. 43.

11. H. M. Rosenstock, K. Draxl, B. W. Steiner, and J. T. Herron, J. Phys. Chem. Ref. Data 6, Suppl. 1, "Energetics of Gaseous Ions," pub. by American Chemical Society and American Institute of Physics for National Bureau of Standards, 1977, p. I-424.

12. J. H. Hubbell, "Photon Cross Sections, Attenuation Coefficients, and Energy Absorption Coefficients from 10 keV to 100 GeV," U. S. Dept. Comm., Nat. Bur. Standards, NSRDS-NBS 29 (1969).

13. E. Storm, E. Gilbert, and H. Israel, LA-2237 (1958).

14. M. J. Berger and S. M. Seltzer, "Tables of Energy Losses and Ranges of Electrons and Positrons," Nat. Aero. Space Admin., NASA-SP-3012 (1964).

15. R. A. Finston, H. H. Hubbell, Jr., W. G. Stone, and R. D. Birkhoff, Measurement of Electron Flux in Irradiated Media by AC Methods, Oak Ridge National Laboratory Report ORNL-2732 (1959).

16. W. J. McConnell, R. D. Birkhoff, R. N. Hamm, and R. H. Ritchie, Radiat. Res. 33, 216 (1968).

17. R. H. Ritchie, C. J. Tung, V. E. Anderson, and J. C. Ashley, Radiat. Res. 64, 181 (1975).

18. C. E. Klots and H. Wright, Int. J. Radiat. Phys. Chem. 2, 191 (1970).

19. L. V. Spencer and U. Fano, Phys. Rev. 93, 1172 (1954).

20. L. V. Spencer and F. H. Attix, Radiat. Res. 3, 239 (1955).

21. R. T. McGinnies, "Energy Spectrum Resulting from Electron Slowing Down," Nat. Bur. Standards Circular 597 (1959).

22. For a short discussion of some of this material, see Christophorou, ref. 9, pp. 4-22.

23. We are indebted to J. K. Baird for this discussion and derivation. An extensive treatment is given by Christophorou, ref. 9, chap. 4.

24. G. J. Hine and G. L. Brownell, eds , Radiation Dosimetry, Academic Press, New York, 1958, especially Chaps. 1, 2, 4, and 12.

25. F. H. Attix, W. C. Roesch, and E. Tochilin, eds., Radiation Dosimetry, 2nd ed., (3 volumes), Academic Press, New York, 1968, although titled a "2nd edition" this is actually a totally different book from ref. 24. See especially Vol. 1, Chaps. 1, 3, 5, 7, and 8.

26. "Stopping Powers for Use with Cavity Chambers," Nat. Bur. Standards Handbook 79 (1961).

27. H. A. Kramers, Phil. Mag. 46, 836 (1923).

28. J. C. Villforth, R. D. Birkhoff, and H. H. Hubbell, Jr., Comparison of Theoretical and Experimental Filtered X-Ray Spectra, Oak Ridge National Laboratory Report ORNL-2529 (1958).

29. H. Goldstein and J. E. Wilkins, Jr., NYO-3075 (1954); see also ref. 2, pp. 268-276.

30. R. D. Birkhoff, in Handbuch der Physik, Vol. 34, S. Flügge, ed., Springer-Verlag, Berlin, 1958, pp. 121-124.

31. E. N. Sickafus, Phys. Rev. B 16, 1436, 1448 (1977).

32. L. S. Taylor, Brit. J. Radiology 24, 67 (1951).

33. F. W. Sears, Thermodynamics, The Kinetic Theory of Gases and Statistical Mechanics, 2nd ed., pp. 258, 266, Addison Wesley, Cambridge, Massachusetts, 1953.

34. See ref. 9, chap. 4.

35. L. G. H. Huxley and R. W. Crompton, The Diffusion and Drift of Electrons in Gases, Wiley, New York, 1974, Chap. 8.

Appendix III

Presented at the XIIIth International Conference on Phenomena in Ionized Gases, Berlin, GDR, September 11-17, 1977

ELEMENTARY ELECTRON-MOLECULE INTERACTIONS AND NEGATIVE ION RESONANCES AT SUBEXCITATION ENERGIES AND THEIR SIGNIFICANCE IN GASEOUS DIELECTRICS

Christophorou, Loucas G.

Oak Ridge National Laboratory, P. O. Box X, Oak Ridge, Tennessee, 37830, USA

ELEMENTARY ELECTRON-MOLECULE INTERACTIONS AND NEGATIVE ION RESONANCES AT SUBEXCITATION ENERGIES AND THEIR SIGNIFICANCE IN GASEOUS DIELECTRICS*

Christophorou, Loucas G.**
Oak Ridge National Laboratory, P. O. Box X, Oak Ridge, Tennessee, 37830, USA

Recent knowledge on low-energy (mostly $\lesssim$ 10 eV) electron-molecule interaction processes in dilute and in dense gases is synthesized, discussed, and related to the breakdown strength of gaseous dielectrics. Optimal design of multicomponent gaseous insulators can be made on the basis of such knowledge.

1. Introduction

Although the field of gaseous dielectrics is old, most of the fundamental knowledge on the underlying basic physicochemical processes which crucially determine what makes a good gaseous dielectric is new. It is a challenge to bring this new knowledge to bear on the field of gaseous dielectrics and on ways to improve them. The need for energy conservation and energy cost reduction dictates the development of better gaseous insulators, especially for electrical energy transmission; transmission line voltages keep going up with projected voltages up to 1.5 MV.

2. The Overall Problem: Main Physical Processes of Direct Significance

What is it that makes a good gaseous dielectric? Figure 1 helps us answer this question from the basic, microscopic point of view.

In a gas under an applied electric field, the ever present free electrons have a distribution of energies, f, which is a function of the gas and the quantity E/P (or E/N), where E is the applied electric field, P is the gas pressure at the temperature T, and N is the gas number density, viz., $f(\varepsilon, E/P, gas)$. The functions $f(\varepsilon, E/P)$ are equilibrium energy distributions even for AC fields since the electron relaxation times (see Section 4) are quite short under normal operating conditions. As the applied voltage is increased, the electrons gain energy, and $f(\varepsilon, E/P)$ shifts to higher energies. This shift is a strong function of the elastic and inelastic processes which absorb the energy input by the field. The distributions $f(\varepsilon, E/P)$ are known for only very few gases. In Fig. 1, $f(\varepsilon, E/P)$ are plotted for N_2 at one E/P value and for Ar at two E/P values. Depending on the gas and E/P, $f(\varepsilon, E/P)$ can peak at any energy from thermal to $\sim$ 10 eV. Knowledge of the electron energy distribution function is necessary for a realistic appraisal of the role

---

*Research sponsored by the Energy Research and Development Administration under contract with Union Carbide Corporation.

**Also, Department of Physics, The University of Tennessee, Knoxville, Tennessee, 37916, USA.

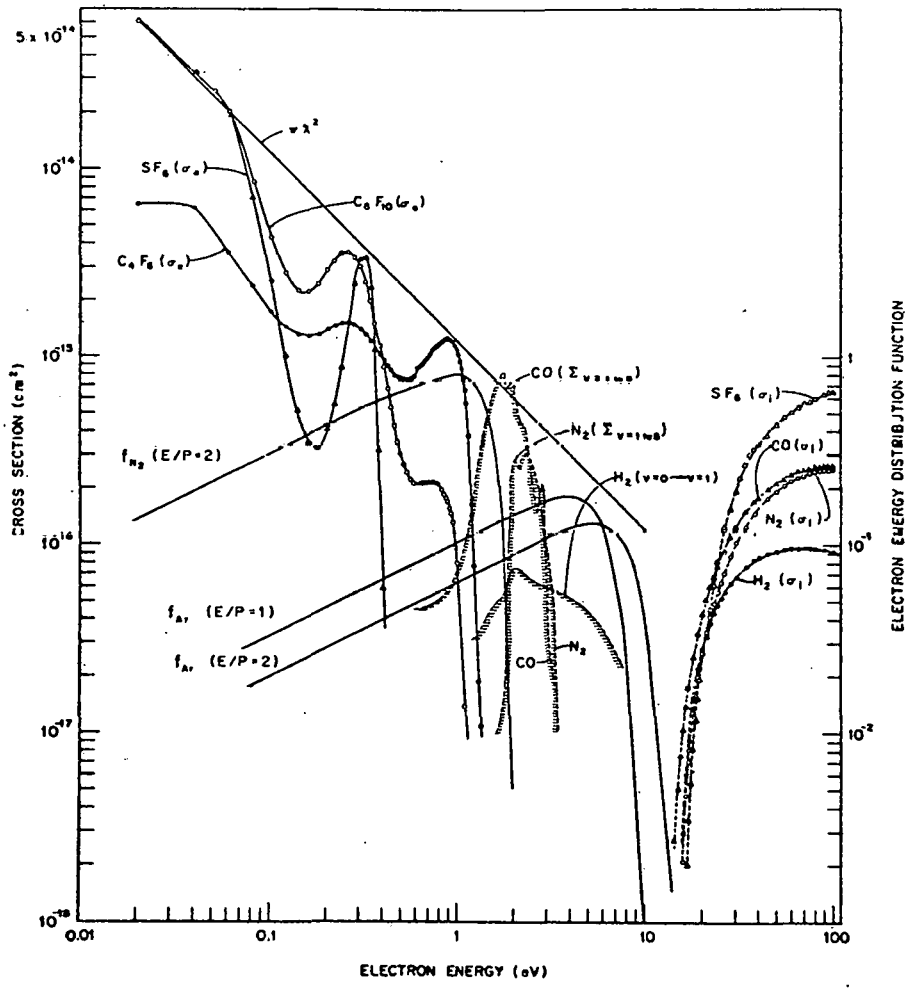

FIG. 1. Electron attachment cross sections, σ_a, as a function of ε for SF_6 [1], C_4F_6 [2], and C_6F_{10} [2]. Vibrational excitation cross sections via the decay of NIRs [3]. CO (Σ υ = 1 to 8) and N_2 (Σ υ = 1 to 8) are the sums of vibrational cross sections for the first eight individual states of CO and N_2, respectively, and H_2 ($\upsilon = 0 \rightarrow \upsilon = 1$) is the cross section for excitation of the first vibrational level of H_2 multiplied by 1.4 (see Ref. [4], p. 347). Electron impact ionization cross sections, $\sigma_i(\varepsilon)$, for SF_6, CO, N_2, and H_2 [5]. See Ref. [4] for information on the electron energy distribution functions, f_{N_2}, for N_2 and, f_{Ar}, for Ar. $\pi\lambda\!\!\!^{-2}$ is the maximum s-wave capture cross section.

of microscopic physical knowledge in understanding and in controlling breakdown.

The most effective way of preventing electrons from initiating breakdown is the removal of the electrons from the dielectric. An effective way of achieving this is to attach the electrons to molecules forming negative ions which, being much heavier than the electrons, do not have kinetic energies high enough to cause ionization. The unattached electrons must be slowed down and be prevented from ionizing the gas and triggering breakdown. The above statements can be formalized as:

$$\int_0^\infty \sigma_a(\varepsilon)\, f(\varepsilon, E/P)\, d\varepsilon \longrightarrow \text{maximum} \qquad (1)$$

$$\int_I^\infty \sigma_i(\varepsilon)\, f(\varepsilon, E/P)\, d\varepsilon \longrightarrow \text{minimum}. \qquad (2)$$

For (1) the electron attachment cross section as a function of ε, $\sigma_a(\varepsilon)$, should be as large as possible over as wide an energy range as possible. Examples of $\sigma_a(\varepsilon)$ for three dielectric gases are shown in Fig. 1 (see also Section 7). Since, as is shown by the straight line in Fig. 1, the maximum s-wave capture cross section $\pi\lambda\!\!\!^{-2}$ ($\lambda = 2\pi\lambda\!\!\!^{-}$ is the electron de-Broglie wavelength) decreases with ε, to optimize (1) $f(\varepsilon, E/P)$ must be shifted to as low energies as possible.

For (2) the electron-impact ionization cross section as a function of ε, $\sigma_i(\varepsilon)$, must be as small as possible and the ionization threshold energy, I, as high as possible. For a given $\sigma_i(\varepsilon)$, $f(\varepsilon, E/P)$ should again be shifted to as low ε as possible to optimize (2). Thus the reduction of the electron energies is of paramount significance because a lower $f(\varepsilon, E/P)$ minimizes (2), but also maximizes (1). Such a reduction in electron energies requires large cross sections for elastic and inelastic electron scattering, especially in the subexcitation energy range.† As will be discussed in Section 4, a most efficient way of slowing down subexcitation electrons is via negative ion resonances (NIR). Vibrational excitation cross sections due to such NIRs are shown in Fig. 1 for CO, N_2, and H_2. Through a combination of gases, NIR states can be positioned over the entire subexcitation energy range keeping in this way the electron energies low. Such a deployment of NIRs is similar to the utilization of neutron inelastic scattering resonances in nuclear reactors to moderate the energies of escaping epithermal neutrons.

The optimum gaseous dielectric is thus envisioned to be not a single gas (unitary system), but rather a combination of gases (a multicomponent system) designed as to components to provide the best effective combination of electron-attaching and electron slowing-down properties to optimize (1) and (2). This optimal design of the multicomponent gaseous insulator can be made on the basis of microscopic, quantitative physicochemical knowledge, especially on low-energy electron-molecule interactions.

3. Electron Attachment

Excluding the ion pair process, negative ion formation by electron impact is viewed as proceeding via a metastable negative ion intermediate which itself

†This is the energy range below the first excited electronic state of the medium.

can be formed by electron capture in the field of the ground or the field of an excited electronic state. The states of such transient anions are nonstationary, i.e., they decay with a characteristic lifetime, τ_a, which varies from 10^{-15} to $> 10^{-2}$ sec [1, 6].

Many authors (e.g., [4], [6-8]) have reviewed the various ways via which slow electrons attach to molecules. In Fig. 2, we illustrate schematically two such basic modes: The shape resonance and the nuclear-excited Feshbach resonance. In the shape resonance the electron affinity, EA, of the molecule is negative (< 0 eV) and the incident electron is trapped in the potential well which arises from the interaction between the electron and the neutral molecule in its ground electronic state. This barrier is the combined effect of the attractive force exerted by the neutral molecule on the incident electron and the repulsive centrifugal force arising from the relative motion of the two bodies. Since the negative ion potential energy curve/surface for a shape resonance lies above that of the neutral, the NIR is subject to autoionization, decaying back to the neutral molecule in its ground electronic state plus a free electron, leaving the neutral molecule with or without vibrational and/or rotational energy; if energetically possible the NIR can undergo dissociative attachment. Such NIRs may involve an excited electronic state and in this case they are called core-excited (type II) resonances.

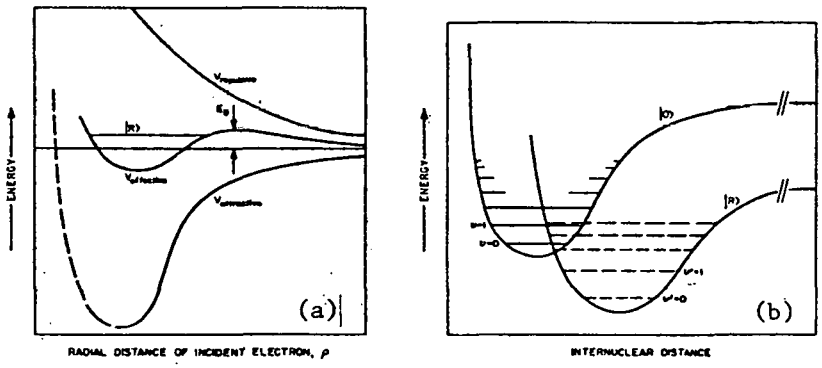

FIG. 2. Schematic illustration of (a) shape and (b) nuclear-excited Feshbach resonances. The symbols $|0\rangle$ and $|R\rangle$ designate, respectively, the electronic ground state of the neutral molecule and the NIR state.

In the nuclear-excited Feshbach resonance, EA is positive (> 0 eV) and the NIR lies energetically below the ground state of the neutral. Thus unless the anion is in vibrational levels v' higher than the lowest vibrational level $v = 0$ of the parent neutral state, the NIR cannot decay into the parent state. This mode of electron capture can involve an electronically excited neutral molecule, in which case the NIR is called core-excited (type I).

Molecular NIR states are abundant. Often they can be described (and their energies [positions] approximated) in terms of the unoccupied molecular orbitals of the neutral molecule [8]. At times also geometrical changes

concomitant with electron impact and portions of a polyatomic molecule can constitute effective modes of electron trapping [6].

The channels of decay of a metastable molecular anion AX^{-*} can be summarized as:

$$e + AX \xrightarrow{\sigma_0} AX^{-*} \begin{cases} \xrightarrow{p_e} AX + e & (3a) \\ \xrightarrow{p_{in}} AX^* + e' & (3b) \\ \xrightarrow{p_{da}} A^{(*)} + X^- & (3c) \\ \xrightarrow{p_{st}} AX^- + \text{energy} & (3d) \end{cases}$$

where σ_0 is the cross section for the formation of AX^{-*}, and p_e, p_{in}, p_{da}, and p_{st} are, respectively, the probabilities for indirect elastic scattering (3a), indirect inelastic scattering (3b), dissociative attachment (3c), and stabilization of AX^{-*} by collision or radiation (3d). Channel (3d) is only possible when EA > 0 eV. All of the above decay processes can be in competition.

In this section we shall discuss reactions (3c) and (3d) and in the next, reactions (3a) and (3b).

From the preceding discussion dissociative attachment can be visualized as proceeding via a negative ion intermediate formed by capture of electrons in a restricted energy range defined by a Franck-Condon transition between the initial state—neutral molecule and electron separated an infinite distance—and the final state representing the compound negative ion, which subsequently dissociates into (multiple) neutral and negative ion fragments. For a diatomic or a "diatomic-like" molecule this is illustrated schematically in Fig. 3, and σ_{da} can be expressed as

$$\sigma_{da} = \sigma_0 \, e^{-\bar{\tau}_s/\bar{\tau}_a}. \tag{4}$$

In Eq. (4), $e^{-\bar{\tau}_s/\bar{\tau}_a}$ is the survival probability of AX^{-*}, $\bar{\tau}_s$ and $\bar{\tau}_a$ are, respectively, the mean times for separation of A and X^- and autoionization of AX^{-*}. Both τ_s and τ_a are functions of the internuclear separation R. For a diatomic molecule initially in the lowest vibrational level $\upsilon = 0$ of the electronic ground state and with a potential energy curve for AX^{-*} as shown in Fig. 3,

$$\sigma_{da}(\varepsilon)_{\upsilon=0} = \underbrace{\frac{4\pi^{3/2}}{(2m/\hbar^2)\varepsilon} \, g \, \frac{\Gamma_a}{\Gamma_d} \exp\left[\frac{\Gamma_a^2 - 4(\bar{\varepsilon}_0 - \varepsilon)^2}{\Gamma_d^2}\right]}_{\sigma_0} e^{-\bar{\tau}_s/\bar{\tau}_a}, \tag{5}$$

where m is the electron mass, $\bar{g}$ is a statistical factor, Γ_a is the partial autoionization width, Γ_d is the width of $\sigma_{da}(\varepsilon)$, $\bar{\varepsilon}_0 = \varepsilon_0 + 1/2\ \hbar\omega$, ε_0 is the electron energy at the peak of $\sigma_a(\varepsilon)$ and $1/2\ \hbar\omega$ is the zero-point energy. Equation (5), due to O'Malley [9], although limited to situations as pictured in Fig. 3, provides an explicit expression for σ_0 and the dependence of σ_{da} on ε, τ_s, τ_a, and the reduced mass of the A—X^- system [4]. Negative ion potential energy curves/surfaces have a variety of shapes, and σ_{da} is affected by these and the competitive decay channels. Also, higher-lying NIRs exist abundantly.

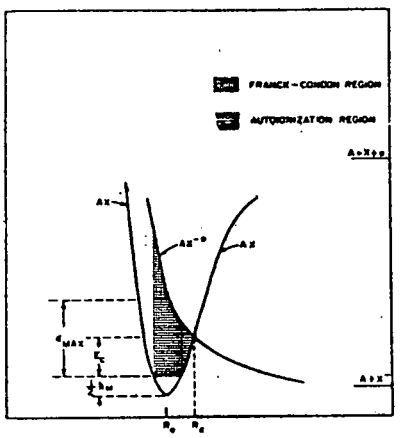

FIG. 3. Schematic potential energy diagram illustrating the process of dissociative attachment for a diatomic molecule.

In Fig. 4, $\sigma_{da}(\varepsilon)$ are shown for a number of molecules. The salient features of the behavior of σ_{da} are:

(i) The magnitude of σ_{da} depends on the position, ε_{max}, of the NIR; the higher the ε_{max}, the smaller the σ_{da}.

(ii) As $\varepsilon_{max} \rightarrow$ thermal, $\sigma_{da} \rightarrow \pi\lambda^2$.

(iii) Many molecules possess a multiplicity of NIRs in the subexcitation energy region. This is clearly illustrated by the recent data [17] on the production of Cl^- from chloroethylenes and chloroethanes. For both groups of molecules, many (five) NIRs were identified below $\sim$ 2.0 eV which were associated [17] with orbitals dominated by the p-orbitals of the chlorine atoms.

(iv) By appropriate combination of gases, mixtures can be developed with dissociative attachment resonances spaced and/or positioned at any energy from thermal to $\sim$ 15 eV.

(v) The cross sections for specific dissociative attachment products and the patterns of (multiple) fragmentation of the metastable anions depend strongly on the details of the molecular structure (e.g., see Figs. 5 and 6). Actually, for the molecules in Figs. 5 and 6 besides the abundant Cl^- ion, Cl_2^- and $(M\text{-}Cl)^-$ (parent molecule, M, less one Cl atom)$^-$ were observed. The relative intensities of these ions depended strongly on the number and relative positions of the Cl atoms in the molecule [17] (for C_2Cl_4, $C_2Cl_4^-$ was also observed). Such studies establish modes of molecular fragmentation (i.e., patterns of molecular "explosion" at the very presence of an electron of suitable energy) and show that slow electrons can be quite disruptive in their impacts with polyatomic molecules.

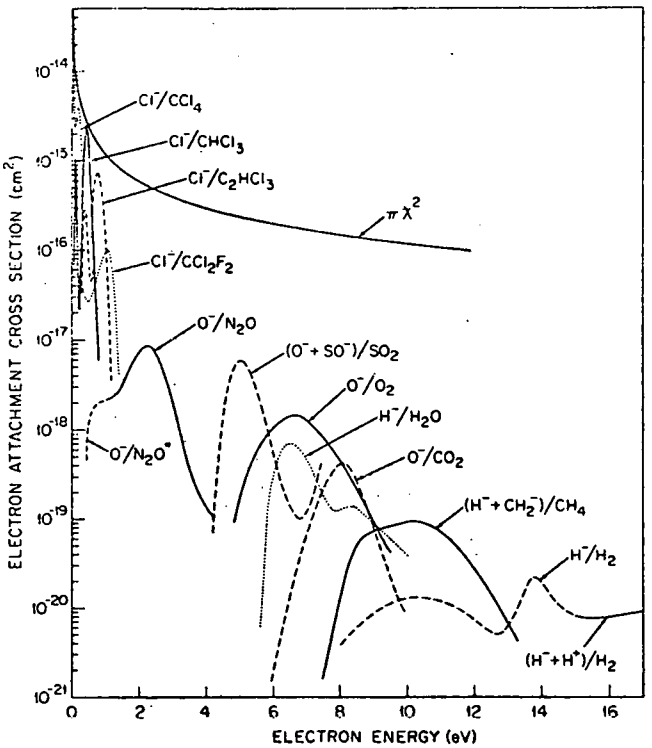

FIG. 4. $\sigma_{da}(\varepsilon)$ for Cl^-/CCl_4 [1], $Cl^-/CHCl_3$ [1], Cl^-/C_2HCl_3 [1], Cl^-/CCl_2F_2 [10], O^-/N_2O [11], $(O^- + SO^-)/SO_2$ [12], O^-/O_2 [13], H^-/H_2O [14], O^-/CO_2 [11], $(H^- + CH_2^-/CH_4$ [15], H^-/H_2 [16]. Some of the plotted $\sigma_{da}(\varepsilon)$ were deduced from swarm experiments and are thus "total" cross sections. They are identified with the specific ions as shown because these were the most abundant in mass spectrometric studies. Some of the molecules shown have other resonances which were not plotted for convenience of display. O^-/N_2O^* denotes dissociative attachment from vibrationally excited N_2O molecules, and $(H^- + H^+)/H_2$ denotes ion pair formation from H_2.

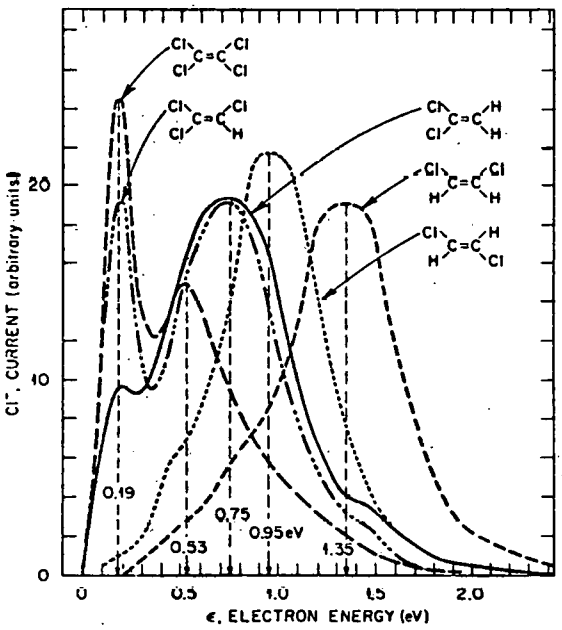

FIG. 5. Cl^- against ε for chloroethylenes [17].

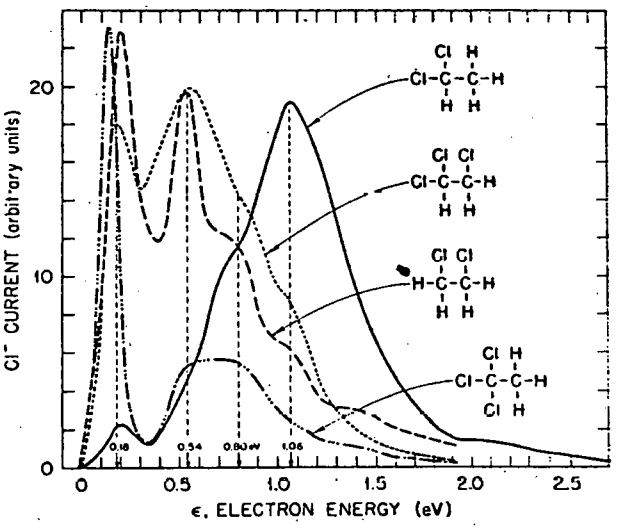

FIG. 6. Cl^- against ε for chloroethanes [17].

(vi) Temperature often has a profound effect on $\sigma_{da}(\varepsilon)$. Figure 7 demonstrates this for the case of O^- from N_2O [18]. This strong dependence of $\sigma_{da}(\varepsilon)$ on ε has been attributed to dissociative attachment from mainly vibrationally excited N_2O molecules [4, 18].

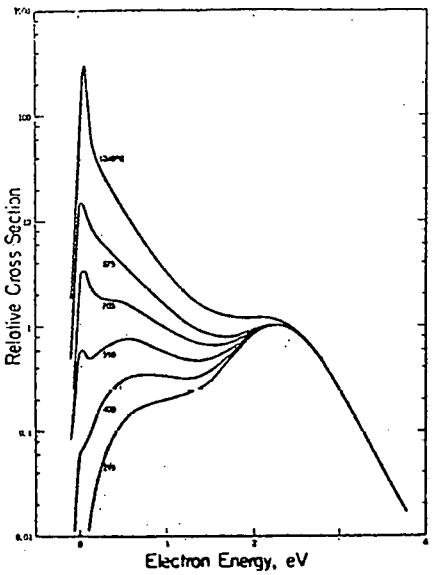

FIG. 7. Relative cross section against ε for O^- from N_2O at the indicated temperatures [18].

(vii) From the dielectric point of view, studies of dissociative attachment identify the initial products (these are the precursors of the final decomposition products in the dielectric) and the energy range of their generation. Such knowledge is necessary to assess the effects of possible toxic fragments, the effects of specific products such as O^- which may lead to explosive reactions, and the deterioration of the dielectric following repeated breakdowns.

Turning now to the nondissociative electron attachment process [channel (3d)], p_{st} is a function of τ_a, P, and the gaseous medium in which the metastable ion is embedded. When τ_a is short, the cross section (or the rate) of attachment depends on P. An example is shown in Fig. 8 for the rate of electron attachment to O_2 in N_2. The lifetime of O_2^{-*} at thermal energies is $\sim 2 \times 10^{-12}$ sec [6, 19]. When, however, τ_a is long, the attachment rate becomes independent of P. A large variety of structures with EA > 0 eV capture slow electrons with large cross sections forming long-lived (> 10^{-6} sec) parent negative ions via a nuclear-excited Feshbach mechanism (see Fig. 2). Among these are some of the best known insulators. In Fig. 9 the attachment rate and cross section for three such systems are presented and are seen to be large and to decrease precipitously with increasing ε above thermal. As a rule, more than one NIR exists below 1 eV (see Fig. 9), some of which (e.g., the SF_5^-/SF_6) may be due to dissociative attachment. In cases where geometrical changes concomitant with electron attachment occur, $\sigma_a(\varepsilon)$ may peak at $\varepsilon > 3/2$ kT (k is the Boltzmann constant) due to the energy required to induce these changes [6]. Such geometrical reorganizations are known to occur for many molecules including CO_2 and N_2O which are bent as negative ions but are linear as neutrals. These systems in undergoing a geometrical change upon electron impact facilitate effective means of electron trapping as well as of electron energy loss.

4. Electron Slowing Down

Electron swarm and electron beam studies have provided useful and complementary information in this area; the former through the electron transport coefficients—the drift velocity[‡] w and the ratio D/μ of the lateral diffusion

[‡]The electron drift velocity in many gases varies (decreases or increases [22]) with gas density.

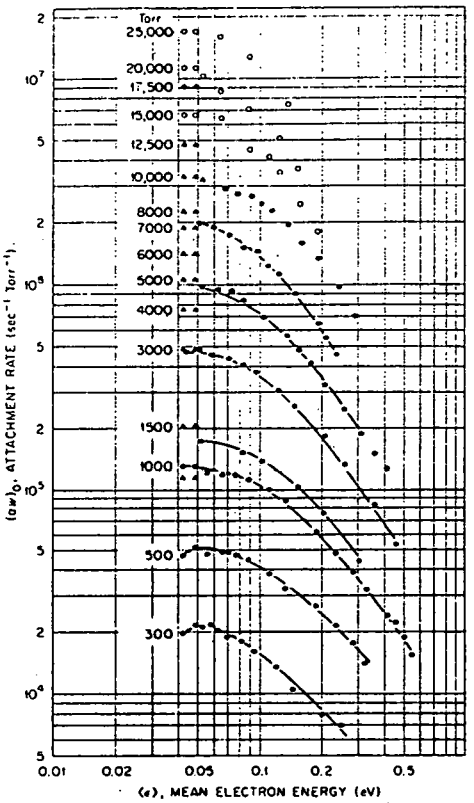

FIG. 8. Attachment rate as a function of the mean electron energy $\langle\varepsilon\rangle$ for O_2 in N_2 at the indicated N_2 pressures [19].

coefficient D to electron mobility μ—and the latter through the direct determination of the cross sections for elastic and inelastic processes.

The quantity $3/2(e\,D/\mu)$ is a rough measure of $\langle\varepsilon\rangle$. The close relation between the functions $D/\mu(E/P)$ and $\langle\varepsilon\rangle(E/P)$ provides an indication as to which gases are effective electron thermalizers and are thus better suited for use as buffer gases in multicomponent insulators. In Fig. 10, $D/\mu(E/P)$ are shown for CO_2, CO, N_2, and H_2. For these molecules swarm, beam, and breakdown data are available and allow for assessment of the effect of their basic properties on breakdown. In the inset of the figure, the momentum transfer cross sections, $\sigma_m(\varepsilon)$, are shown and help in understanding the $D/\mu(E/P)$ functions. All four molecules have NIRs in the subexcitation region [4]: CO_2 at low energies ($\lesssim$ 0.1 eV) and ∿ 4 eV; CO at ∿ 1.75 eV; N_2 at ∿ 2.3 eV; H_2 at ∿ 3.75 eV. By comparing

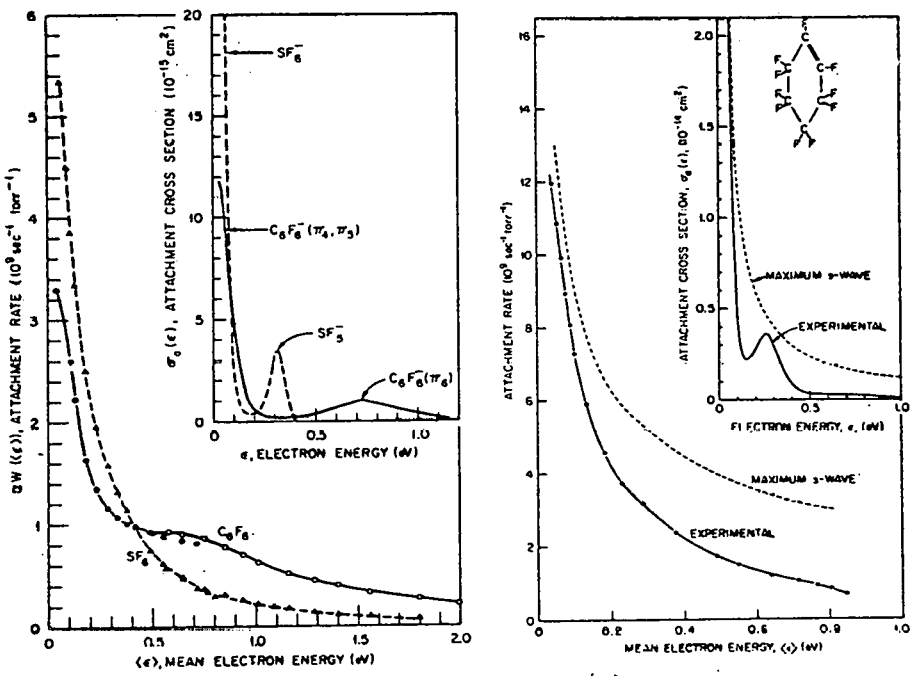

FIG. 9. Attachment rate as a function of $\langle\varepsilon\rangle$ and attachment cross section as a function of ε for SF_6, C_6F_6, and C_6F_{10} [2, 6, 20]. For C_6F_{10} the rate and the cross section is compared with the maximum s-wave capture rate and cross section [6].

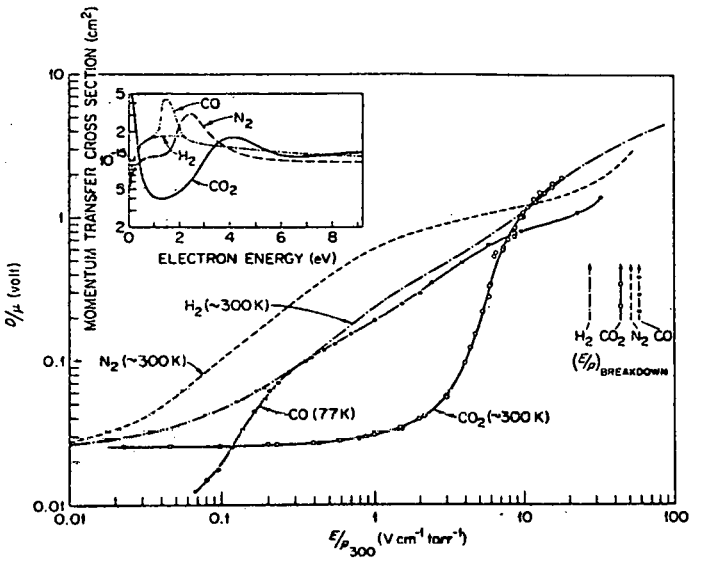

FIG. 10. D/μ versus E/P_{300} for CO_2, CO, N_2, and H_2 (based on data summarized in [4] and [21]); $\sigma_m(\varepsilon)$ for CO_2 [23], CO [24], N_2 [25], and H_2 [26].

the positions of the NIRs for these systems with the $D/\mu(E/P)$ data, it becomes apparent that the dominant process controlling $\langle\varepsilon\rangle$ in the subexcitation energy range is indirect scattering via NIRs. The E/P value, $(E/P)_{Br.}$, at which breakdown occurs in each of these gases is also shown in Fig. 10. In the high E/P region, the lower the D/μ (i.e., the lower the $\langle\varepsilon\rangle$), the higher the breakdown voltage, V_s.

That $\langle\varepsilon\rangle$ is dramatically affected by NIRs and their positions can perhaps be seen by the crude, but revealing, data in Fig. 11 on the mean fractional energy loss per collision, $\eta_M(\langle\varepsilon\rangle)$. η_M is dominated by indirect energy losses via NIRs although at very low energies direct energy losses due to rotational excitation are seen to be significant. Direct vibrational energy losses also contribute to η_M as is seen from similar data on hydrocarbons in Fig. 12. The role of rotational energy losses for polar molecules can be seen from the $\eta_M(\langle\varepsilon\rangle)$ data on H_2O.

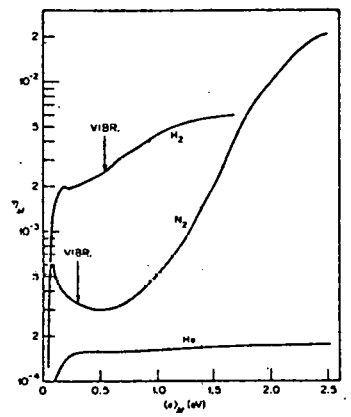

FIG. 11. η_M versus $\langle\varepsilon\rangle_M$ for He, N_2, and H_2. The $f(\varepsilon, E/P)$ was assumed to be Maxwellian. The w and D/μ data used to determine η_M and $\langle\varepsilon\rangle_M$ are from Ref. [4]. The arrows indicate the threshold for vibrational excitation.

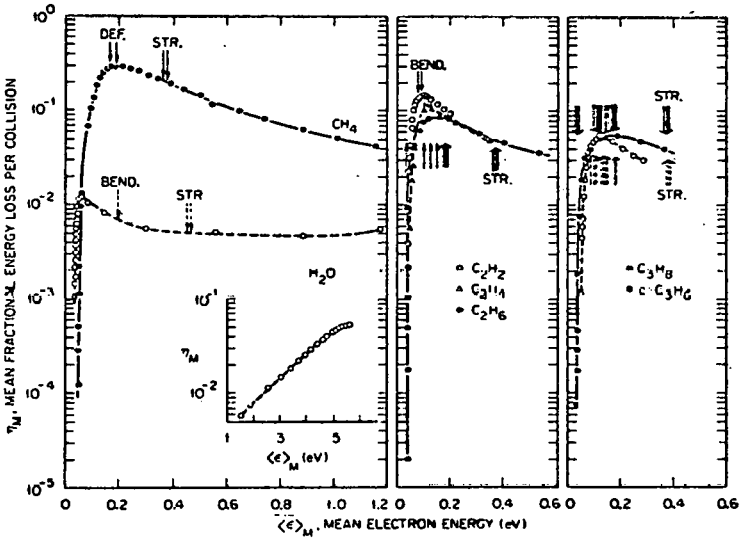

FIG. 12. η_M versus $\langle\varepsilon\rangle_M$ for hydrocarbons and water [27].

The effect of double and triple bonds on $\langle\varepsilon\rangle$ is apparent from the $\langle\varepsilon\rangle$ versus E/P data on a number of hydrocarbons in Fig. 13. For a given value of E/P, $\langle\varepsilon\rangle$ is lower for systems with double and triple bonds. This is consistent with the data in Fig. 14c where the mean scattering cross sections $\langle\sigma_m\rangle$ for thermal and epithermal electrons are seen to increase with increasing number of doubly-occupied π orbitals (i.e., increasing number of double bonds) of the molecule. Interestingly, not only the number but also the relative position of the double bonds affects $\langle\sigma_m\rangle$ (Fig. 14d). For the alkanes which possess only σ bonds, $\langle\sigma_m\rangle$ are small (comparable to the mean geometric cross sections [30]) and increase (Fig. 14b) with increasing static polarizability. For polar molecules at thermal and near-thermal energies, the magnitude of $\langle\sigma_m\rangle$ is determined principally by the size of the molecular electric dipole moment (Fig. 14a; [4, 22, 29]).

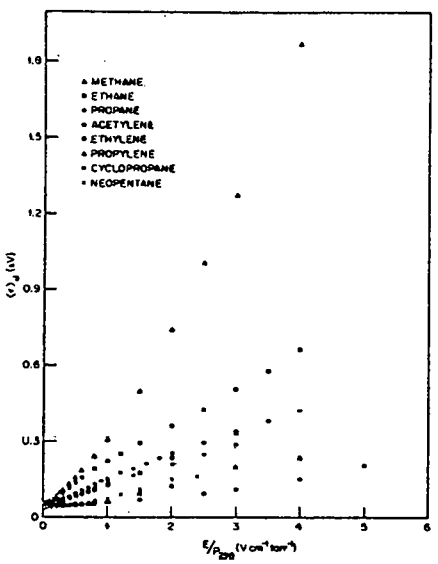

FIG. 13. $\langle\varepsilon\rangle_M$ versus E/P_{298} for some hydrocarbons [28].

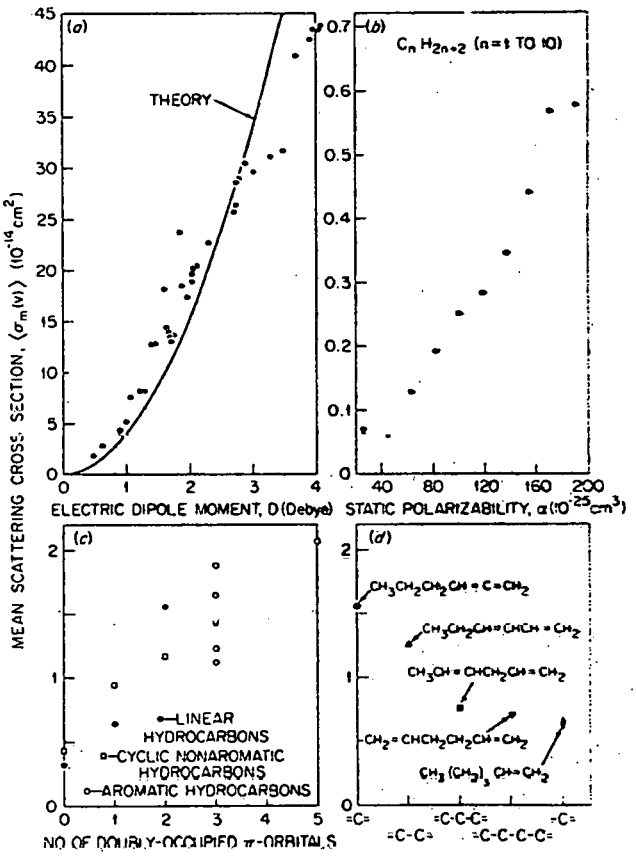

FIG. 14. Mean electron scattering cross sections as a function of (a) permanent electric dipole moment [29]; (b) static polarizability [30]; (c) number of doubly-occupied π orbitals [31]; (d) relative position of the double bonds [31].

Another way of evaluating the significance of the aforementioned processes in slowing-down subexcitation electrons is to consider the time required by an electron of energy, ε_i, to lose energy equal to ε_i - 3/2 kT and be "thermalized." If $d\varepsilon/dt$ is the overall rate of energy loss, the "thermalization time" is

$$\tau(\varepsilon_i) = \int_{3/2\ kT}^{\varepsilon_i} \frac{d\varepsilon}{d\varepsilon/dt}. \tag{6}$$

An estimate, $\tau(\langle\varepsilon\rangle_i)$, of $\tau(\varepsilon_i)$ can be obtained [27] from

$$\tau(\langle\varepsilon\rangle_i) = \int_{3/2\ kT}^{\langle\varepsilon\rangle_i} \frac{d\langle\varepsilon\rangle}{\omega(\langle\varepsilon\rangle)}, \tag{7}$$

where $\omega(\langle\varepsilon\rangle) = e(E/P)w\ P$ is the mean rate at which energy is lost by the electron in collisions with the gas molecules at a pressure P. Such estimates are shown in Fig. 15 for P = 1 torr and show that the time required for subexcitation electrons to be thermalized varies substantially from one gas to another. It increases only slowly with $\langle\varepsilon\rangle_i$ for $\langle\varepsilon\rangle_i \gtrsim 0.4$ eV, and it declines precipitously in the region corresponding to vibrational and rotational excitation thresholds. It is thus seen that the time required for an electron to be thermalized is crucially affected by the energy loss processes in the subexcitation energy region, especially below ~ 0.5 eV.

Electron beam studies have provided absolute cross sections for direct and indirect elastic, rotational and vibrational excitation cross sections and their energy dependence. Important as it is, such basic knowledge is still limited and restricted to simple molecules. In Fig. 16, representative data are shown for H_2 and N_2 whose main features elucidate a number of points directly relevant to breakdown.

(i) Rotational excitation cross sections are substantial to electron energies $\geq$ 10 eV.

(ii) Vibrational excitation cross sections are also substantial to high energies; these decrease with increasing vibrational quantum number.

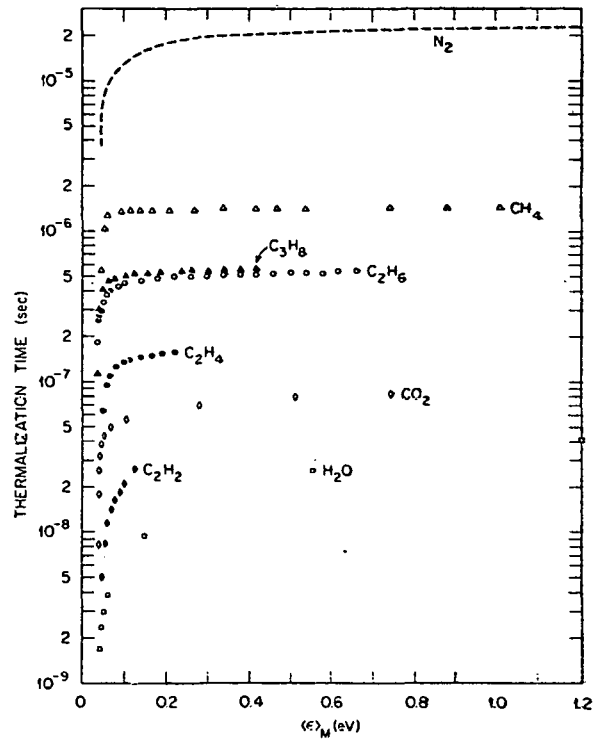

FIG. 15. Electron thermalization time as a function of $\langle\varepsilon\rangle_M$ (P = 1 torr) (present work and Ref. [27]).

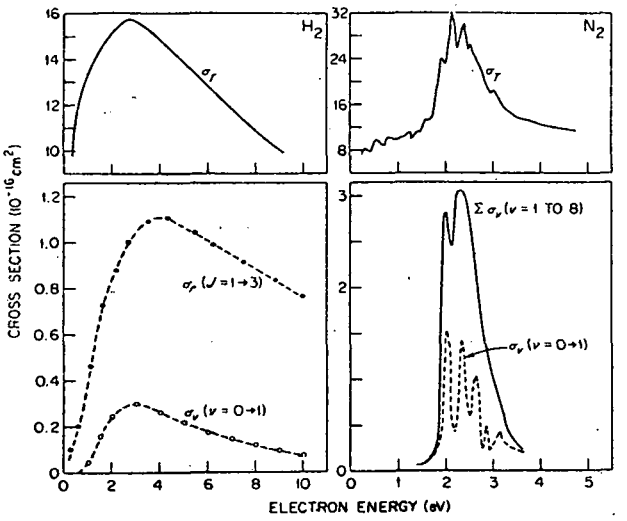

FIG. 16. Energy dependence of electron scattering cross sections for H_2 and N_2: total electron scattering cross section, σ_T, for H_2 [32] and N_2 [33]; vibrational excitation cross section for $\upsilon = 0 \rightarrow \upsilon = 1$ transition, σ_υ ($\upsilon = 0 \rightarrow 1$), for H_2 [34] and N_2 [35]; rotational excitation cross section for the $J = 1 \rightarrow J = 3$ transition, σ_r ($J = 1 \rightarrow 3$), for H_2 [34]. $\Sigma\,\sigma_\upsilon$ ($\upsilon = 1$ to 8) (see text).

(iii) The total cross sections are much larger than the overall inelastic scattering cross section dramatizing the large probability for elastic electron scattering in the subexcitation energy range. Nevertheless, from the dielectric point of view, even elastically scattered electrons may undergo large energy losses if they are scattered in a direction opposite to the applied electric field since they would have to come to rest before they reverse directions and drift in the field direction again.

(iv) The cross sections for elastic, rotational, and vibrational excitation are all strongly affected by NIRs, indicating that a large fraction of these are indirect, via the decay of such resonances. This is particularly dramatized by the N_2 data where $\Sigma\,\sigma_\upsilon$ ($\upsilon = 1$ to 8) is the sum of the vibrational excitation cross sections for the first eight ($\upsilon = 1$ to $\upsilon = 8$) vibrational levels of N_2 via the decay of the N_2^{-*} ($^2\Pi_g$) shape resonance.

(v) At low energies, polyatomic molecules which are good electron scavengers can be simultaneously good electron thermalizers owing to their complex structure and the availability of a multiplicity of rotational, vibrational, and low-lying NIR states.

In closing this section, attention is drawn to Tables I and II where recent data on the shape resonances of complex molecules (themselves not directly significant as gaseous dielectrics) have been selected for the purpose of illustrating how molecules can be tailored to position NIRs at will in the subexcitation energy range.[§] It is seen from Table I that the presence of a

[§]The vertical position of the NIRs is given in these tables. When available, the transition energies from the lowest vibrational level, $\upsilon = 0$, of the neutral molecule to the lowest vibrational level, $\upsilon' = 0$, of the negative ion is given in parentheses and can be considered to give the adiabatic value of EA.

double bond lowers the position of the NIR (i.e., it increases EA). The presence of an additional double bond further lowers the position of the NIR, but this lowering is a function of the distance between the two double bonds. It is evident from the data in Table I that the replacement of an H atom by a CH_3 group raises the NIR (lowers EA). For aromatic molecules, the NIR is raised (EA more negative) when an electron donating group is added to the ring. For both aliphatic and aromatic molecules, replacement of an H atom by an electron withdrawing group or a halogen lowers the position of the NIR. This lowering increases with increasing number of halogens (or electron withdrawing groups) so that EA eventually becomes > 0 eV and long-lived parent negative ions can form.

It can thus be concluded that by changing the number and the position of double bonds, and especially by changing the number and the nature of the substituent(s) to a basic structure (ethylene in Table I, benzene in Table II), NIRs can be positioned at will in the subexcitation region. From the dielectric point of view, multiple fluorine substitution in the various basic hydrocarbon structures can be employed for this purpose.

TABLE I: Effect of Structure on the Position[†] of the Negative-Ion Shape Resonances of Polyatomic Molecules

Molecule	Formula	Position of First NIR	Position of Second NIR or Comments
Ethane	H_3C-CH_3	~-2.3[a]	
Ethylene	$H_2C=CH_2$	-1.78 (-1.55)[b]	
Propene	$CH_3HC=CH_2$	-1.99[b]	
cis-Butene	$CH_3HC=CHCH_3$	-2.22[b]	
1,3-Butadiene	$H_2C=CH-CH=CH_2$	-0.62 (-0.62)[b]	-2.80[b]
Cyclohexene		-2.07[b]	
1,3-Cyclohexadiene		-0.80 (0.80)[b]	-3.43[b]
1,4-Cyclohexadiene		-1.75 (-1.75)[b]	-2.67[b]
1,5-Cyclooctadiene		-1.83[b]	-2.33[b]
Ethylene	$H_2C=CH_2$	(-1.55)[b]	Isoelectronic sequence; replace CH_2 by united atom equivalent, O
Formaldehyde	$H_2C=O$	(-0.65)[b]	
Oxygen	O_2	(+0.44)[‡]	
Ethylene	$H_2C=CH_2$	(-1.55)[b]	
Tetracyanoethylene	$(CN)_2C=C(CN)_2$	(+2.88)[‡]	
Tetrachloroethylene	$Cl_2C=CCl_2$	(+2.12)[‡]	

[†]The uncertainty in the position is usually ± 0.1 eV.
[‡]Equated to the EA. EA values: O_2 [38]; $(CN)_2C=C(CN)_2$ [39]; $Cl_2C=CCl_2$ [40].
[a]Ref. [36].
[b]Ref. [37].

TABLE II: Effect of Structure on the Positions of the Negative-Ion Shape Resonances of Benzene and Some of Its Derivatives[†]

Compound	Formula	First (π_1^*)	Second (π_2^*)	Third (σ_3^*)	π_{CO}^*
Benzene		-1.4[a] (1.15)[b]	-1.4[a] (1.15)[b]	-4.85[b]	
Phenol		-0.61[a] (-1.01)[b]	-1.67[a] (-1.73)[b]	-4.92[b]	
Aniline		-0.55[a] (-1.13)[b]	-1.88[a] (-1.72)[b]	-5.07[b]	
Benzaldehyde		-0.71[a]	-1.12[a]	—	-2.22[a]
Benzoic Acid		-0.63[a]	-1.33[a]	—	-2.64[a]
Nitrobenzene		>+0.51[a]	-1.06[a] (-0.72)[c]	-4.6[c]	—
Fluorobenzene		-1.27[a] (-0.89)[b]	-1.74[a]	-4.77	
1,2,4,5-Tetrafluorobenzene		(-0.29)[d]	(-1.24)[d]	-4.46[d]	
Hexafluorobenzene		+1.8[e]	+1.8[e]	-0.73[e]	

[†]The first three NIRs are associated with the three unoccupied π orbitals. The π_{CO}^* is associated with an additional orbital resulting from an interaction of the carbonyl π* orbital with one (symmetric) of the two lowest degenerate π orbitals of benzene. The lowest two NIRs for benzene and hexafluorobenzene are degenerate. For a complete discussion, see Ref. [8].
[a]Ref. [41].
[b]Ref. [42].
[c]Ref. [43].
[d]Ref. [44].
[e]Ref. [20].

5. Electron-Impact Ionization

Although most of the discussion in this paper is on processes occurring below ∿ 10 eV, it is essential that the role of the electron impact ionization cross section, $\sigma_i(\varepsilon)$, is assessed. From the breakdown point of view, it is the behavior of $\sigma_i(\varepsilon)$ close to I (say to within ∿ 20 eV) which is of interest, since at higher energies $f(\varepsilon, E/P)$ is very small and the contribution of the "high-energy tail" of $f(\varepsilon, E/P)$ to Eq. (2) is negligible. In the energy range close to I, ionization proceeds directly or indirectly via superexcitation [4].

Examples of $\sigma_i(\varepsilon)$ are shown in Fig. 17. It can be seen from the expanded portion of Fig. 17 that close to I, $\sigma_i(\varepsilon)$ varies considerably from molecule to molecule and often in a different manner than at higher energies. It is this low-energy portion of $\sigma_i(\varepsilon)$ which is the most significant from the dielectric point of view.

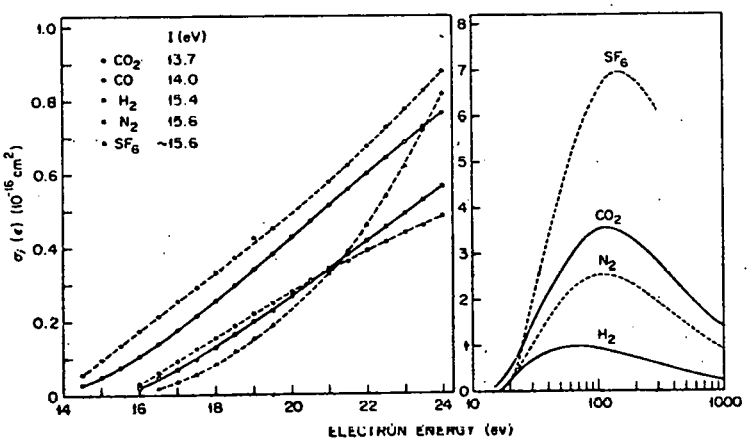

FIG. 17. $\sigma_i(\varepsilon)$ for SF_6 CO_2, N_2, and H_2 [5].

6. Other Processes

No discussion is given of the processes of ion-pair formation, recombination or ion-molecule reactions. A comment on electron detachment, especially collisional detachment, is, however, in order since this process can be significant for weakly bound anions. Although it is desirable that the EA of the insulator molecule be large so that the attached electron is tightly bound to the molecule, the EA need not be too high to avoid collisional detachment since ion-neutral collisions under normal conditions involve small relative kinetic energies.

7. Recent Breakdown Strength Measurements and Their Relation to Basic Electron-Molecule Cross Section Data

A. Effect of $\sigma_a(\varepsilon)$

In Fig. 18, $\sigma_a(\varepsilon)$ for C_4F_6, c-C_4F_8, and iso-C_4F_8 are shown. These extend to much higher energies than the $\sigma_a(\varepsilon)$ for SF_6 but are lower below ∿ 0.1 eV. The relative DC dielectric strengths of these fluorocarbons are shown on the

same figure. Similar data are presented in Fig. 19 for C_6F_{10} and C_6F_{12} whose $\sigma_a(\varepsilon)$ also extend to higher energies than the $\sigma_a(\varepsilon)$ for SF_6 but are comparable below $\sim$ 0.1 eV. The relative DC breakdown strengths are shown on the figure. The results in Figs. 18 and 19 suggest that: (i) All these gases are excellent dielectrics because of their very large $\sigma_a(\varepsilon)$. (ii) C_4F_6 in Fig. 18 and C_6F_{12} in Fig. 19 exhibit the best breakdown strength because their $\sigma_a(\varepsilon)$ is large to substantially higher energies than the rest. (iii) The superior dielectric strength of the two forms of C_4F_8 (Fig. 18) and of C_6F_{10} (Fig. 19) can be attributed similarly to their ability to capture electrons over a wider range of energies than SF_6. The rather better breakdown strength of iso-C_4F_8 compared with the c-C_4F_8 may be associated with the slight extension of its $\sigma_a(\varepsilon)$ to higher ε, although its double bond must influence the value of V_s. (iv) The superior breakdown strengths of all five compounds in Figs. 18 and 19 (see also Refs. [28, 45, 46]) compared with SF_6 seem to suggest that effective electron attachment in the energy range $\sim$ 0.5 to $\sim$ 1.5 eV is very significant in controlling breakdown. Since $\sigma_a(\varepsilon)$ for SF_6 becomes quite small above $\sim$ 0.4 eV, it may be inferred that SF_6 is a poorer dielectric because it loses effective control of free electrons with $\varepsilon \gtrsim 0.4$ eV. It is seen from Fig. 1 (see also D/μ versus E/P data in Fig. 10) that a much larger fraction (21% for Ar at $E/P = 2$ V cm^{-1} torr^{-1}) of electrons will have energies 0.5 to $\sim$ 2.0 eV at pre-breakdown E/P values than in the region < 0.4 eV ($\sim$ 1% for Ar at $E/P = 2$ V cm^{-1} torr^{-1}) where $\sigma_a(\varepsilon)$ for SF_6 is substantial. Conversely, the importance of basic data on the ε dependence of σ_a is clearly borne out by these findings.

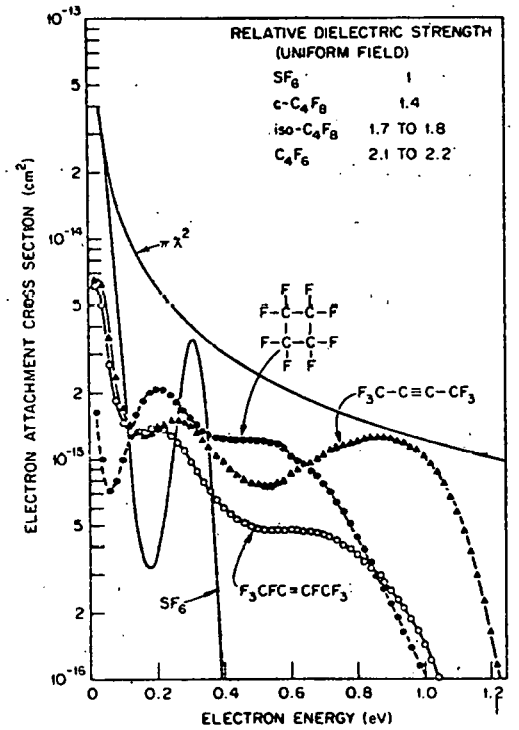

FIG. 18. $\sigma_a(\varepsilon)$ for SF_6 [1], c-C_4F_8 [2], iso-C_4F_8 [2], and C_4F_6 [2]. Relative DC dielectric strengths measured with a plane-plane electrode geometry [45].

Support for the above propositions is provided by the data in Fig. 20, where V_s is plotted as a function of the percentage of the fluorocarbon additive in N_2 at a fixed total pressure (500 torr). Although for each case the V_s of the binary mixture increases with increasing additive concentration, SF_6 suffers, in contrast to the rest, a marked saturation effect. It appears that this behavior can again be attributed to the ε dependence of the σ_a for SF_6: a modest amount ($\sim$ 200 torr on the basis of Fig. 20) of SF_6 captures virtually all electrons with $\varepsilon \lesssim 0.4$ eV so that additional amounts of SF_6 serve little purpose.[‖] On the other hand, the fluorocarbons capture electrons over a wider part of $f(\varepsilon, E/P)$ and increasing their proportions provides additional electron removal. For the same reason, it would seem that free electron control by SF_6 in nonuniform fields would tend to be inferior to free electron control by a gas or a gas mixture which attaches electrons over a wider energy range, since nonuniform fields imply local distortion of $f(\varepsilon, E/P)$ toward higher energies.

Additionally, mixtures of C_6F_6 (hexafluorobenzene) and c-C_4F_8, and C_6F_6 and SF_6 were found [47] to have a higher V_s than, respectively, pure c-C_4F_8 and SF_6. This again underlines the

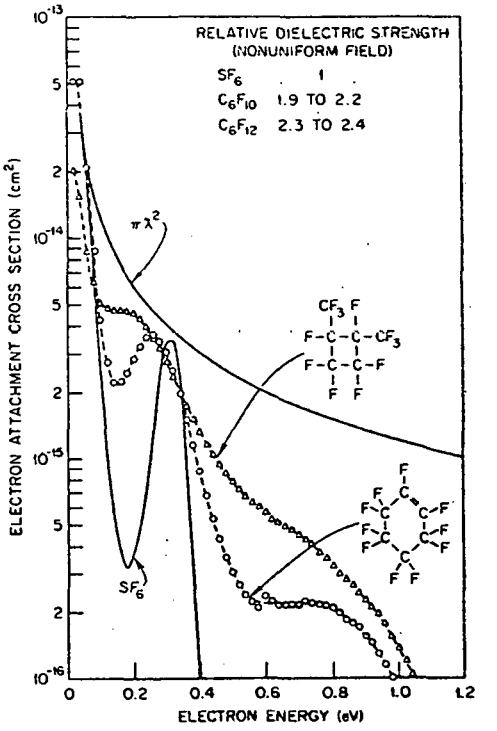

FIG. 19. $\sigma_a(\varepsilon)$ for SF_6 [1], C_6F_{10} [2, 45], and C_6F_{12} [22]. The relative DC dielectric strengths shown in the figure were measured [45] with a sphere-plane electrode geometry and correspond to slightly nonuniform fields.

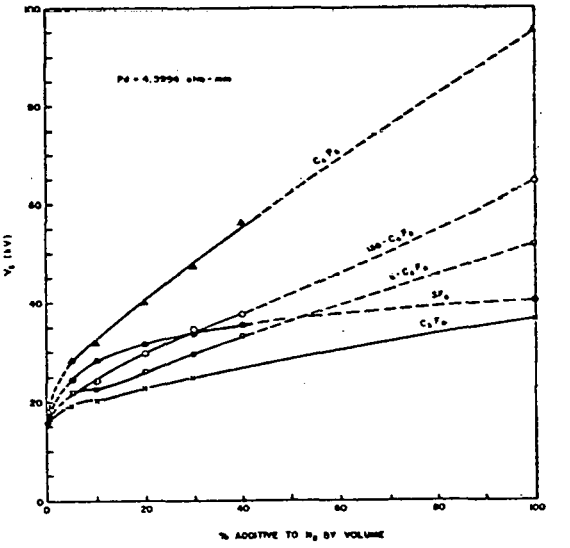

FIG. 20. Breakdown voltage, V_s, versus percent of electron attaching additive to N_2 (total pressure = 500 torr; plane-plane electrode geometry) [45].

[‖] If we assume that $f(\varepsilon, E/P)$ for the SF_6–N_2 mixtures just before breakdown resembles that for pure Ar at E/P = 2 V cm^{-1} torr^{-1}, then only about 1% of the electrons will have energies < 0.4 eV. If 10^8 electrons/cm^3 are present, then $\sim$ 150 torr of SF_6 would be sufficient to remove 10^6 electrons/cm^3.

importance of the high-energy region of the electron energy distribution, since C_6F_6 has three π bonds, and its $\sigma_a(\varepsilon)$ extends to higher energies than the $\sigma_a(\varepsilon)$ of either c-C_4F_8 or SF_6. The extreme effectiveness of systems with large $\sigma_a(\varepsilon)$ extending to high energies as additives to cheap and inert gases and their significance in designing multicomponent gaseous insulators can perhaps be indicated by the data in Table III (see also Refs. [28, 45-47]).

B. Effect of NIRs

Christophorou et al. [45] obtained what seems to be the first direct experimental evidence of the influence of NIRs on breakdown. A series of breakdown strength measurements on CO, N_2, and H_2 and on binary mixtures of these with C_4F_6 (hexafluorobutyne) have been made [45] and preliminary results are shown in Table IV. The $\sigma_a(\varepsilon)$ of C_4F_6 and the cross sections for vibrational excitation of CO, N_2, and H_2 via NIRs are shown in Fig. 21. The position of the NIRs decreases in the order CO < N_2 < H_2 and the magnitude of the scattering cross sections in the order CO > N_2 > H_2 (σ_m [see Fig. 10] and σ_T [4, 45] decrease in the same order). The cross section data in Fig. 21 compared with the results in Table IV show the direct effect of the inelastic properties of the gas via NIRs in the subexcitation energy range—especially $\sim$ 1 to $\sim$ 4 eV—on breakdown; the higher these cross sections are, the better the breakdown strength. This conclusion is consistent with the findings in part B of this section and indicate the strong effect of the energy loss processes in the subexcitation range on breakdown.

TABLE III: Relative Breakdown Strengths* of Some Two- and Three-Component Gaseous Mixtures

Gaseous Mixture			$\Delta V_s/\Delta(Pd)$ (kV/atm-cm)
N_2	C_4F_6	SF_6	
100%	—	—	2.94
—	—	100%	8.65
—	100%	—	19.76
90%	10%	—	6.77
80%	20%	—	8.71
70%	30%	—	10.18
80%	—	20%	6.53
80%	10%	10%	7.60
60%	20%	20%	9.51
50%	30%	20%	11.51

*Plane-plane, uniform-field geometry. The total pressure was 500 torr (Ref. [28]).

TABLE IV: Breakdown Strengths of N_2, CO, H_2, and Binary Mixtures of These with C_4F_6*,†

C_4F_6 (%)	N_2 (%)	CO (%)	H_2 (%)	$\Delta V_s/\Delta(Pd)$ (kV/atm-cm)
100	—	—	—	17.5
—	100	—	—	2.74
—	—	100	—	3.52
—	—	—	100	1.55
33	67	—	—	8.93
33	—	67	—	10.7
33	—	—	67	8.76

*Measured using sphere-plane electrodes at a total pressure of 2 atm.
†Under identical conditions $\Delta V_s/\Delta(Pd)$ for pure SF_6 is 8.49 kV/atm-cm.

8. Concluding Remark

The breakdown strength of gaseous dielectrics can be improved by reducing the numbers of free electrons in the dielectric and by reducing the energies of those electrons remaining free. The best gaseous insulating systems are envisioned to be appropriate combinations of compounds blanketing a wide range of energies with maximal electron attachment and electron scattering cross sections. Both the basic and the applied aspects of the multicomponent insulator need intense further investigation.

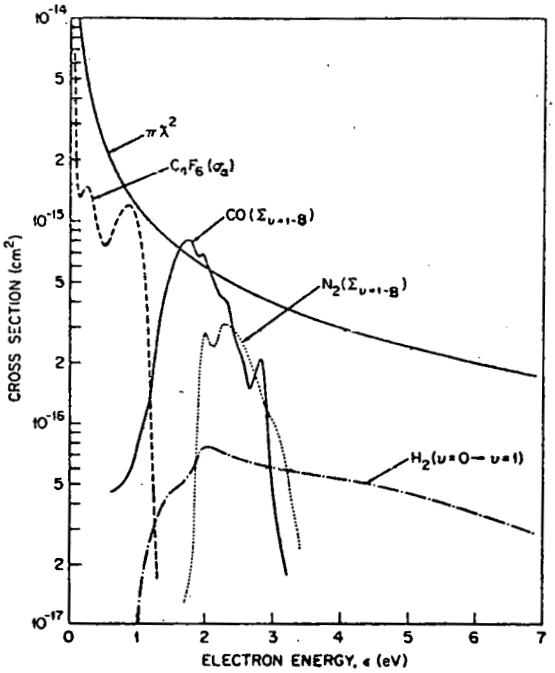

FIG. 21. $\sigma_a(\varepsilon)$ for C_4F_6 [2] and vibrational excitation cross sections via the decay of NIRs for CO, N_2, and H_2 (see caption of Fig. 1).

9. Acknowledgement

I wish to acknowledge useful discussions with Drs. D. R. James, R. Y. Pai, M. O. Pace, and H. Schweinler.

References:

[1] L. G. Christophorou, Chem. Revs. 76, 409 (1976).

[2] R. Y. Pai, L. G. Christophorou, and C.-M. Tung (to be published).

[3] G. J. Schulz, Phys. Rev. A 135, 988 (1964).

[4] L. G. Christophorou, Atomic and Molecular Radiation Physics, Wiley-Interscience, New York, 1971.

[5] D. Rapp and P. Englander-Golden, J. Chem. Phys. 43, 1464 (1965).

[6] L. G. Christophorou, "The Lifetimes of Metastable Negative Ions," Advances in Electronics and Electron Physics, L. Marton (Ed.), Academic Press, New York (in press).

[7] G. J. Schulz, Rev. Mod. Phys. 45, 378, 423 (1973).

[8] L. G. Christophorou, M. W. Grant, and D. L. McCorkle, Advances in Chemical Physics 36, 413 (1977), Wiley-Interscience, New York.

[9] T. F. O'Malley, Phys. Rev. 150, 14 (1966).

[10] L. G. Christophorou, D. L. McCorkle, and D. Pittman, J. Chem. Phys. 60, 1183 (1974).

[11] D. Rapp and D. D. Briglia, J. Chem. Phys. 43, 1480 (1965).

[12] J. Rademacher, L. G. Christophorou, and R. P. Blaunstein, J. Chem. Soc. Faraday Trans. II 71, 1212 (1975).

[13] L. G. Christophorou, R. N. Compton, G. S. Hurst, and P. W. Reinhardt, J. Chem. Phys. 43, 4273 (1965).

[14] R. N. Compton and L. G. Christophorou, Phys. Rev. 154, 110 (1967).

[15] T. E. Sharp and J. T. Dowell, J. Chem. Phys. 46, 1530 (1967).

[16] D. Rapp, T. E. Sharp, and D. D. Briglia, Phys. Rev. Lett. 14, 533 (1965).

[17] J. P. Johnson, L. G. Christophorou, and J. G. Carter, J. Chem. Phys. (in press).

[18] P. J. Chantry, J. Chem. Phys. 51, 3369 (1969).

[19] R. E. Goans and L. G. Christophorou, J. Chem. Phys. 60, 1036 (1974).

[20] K. S. Gant and L. G. Christophorou, J. Chem. Phys. 65, 2977 (1976).

[21] J. Dutton, J. Phys. Chem. Ref. Data 4, 577 (1975).

[22] L. G. Christophorou, Int. J. Radiat. Phys. Chem. 7, 205 (1975).

[23] R. D. Hake and A. V. Phelps, Westinghouse Research Laboratory Sci. Paper 66-1E2-GASES-P1 (1966).

[24] J. E. Land, private communication (1977).

[25] A. G. Engelhardt, A. V. Phelps, and C. G. Risk, Westinghouse Research Laboratory Sci. Paper 64-928-113-P4 (1964).

[26] R. W. Crompton, D. K. Gibson, and A. I. McIntosh, Austr. J. Phys. 22, 715 (1969).

[27] L. G. Christophorou, K. S. Gant, and J. K. Baird, Chem. Phys. Lett. 30, 104 (1975).

[28] L. G. Christophorou, D. R. James, R. Y. Pai, M. O. Pace, R. A. Mathis, D. W. Bouldin, and D. E. Tittle, Oak Ridge National Laboratory Report ORNL/TM-5806 (1977).

[29] L. G. Christophorou and A. A. Christodoulides, J. Phys. B 2, 71 (1969).

[30] L. G. Christophorou, M. W. Grant, and D. Pittman, Chem. Phys. Lett. 38, 100 (1976).

[31] L. G. Christophorou, R. P. Blaunstein, and D. Pittman, Chem. Phys. Lett. 22, 41 (1973).

[32] D. E. Golden, H. W. Bandel, and J. A. Salerno, Phys. Rev. 146, 40 (1966).

[33] D. E. Golden, Phys. Rev. Lett. 17, 847 (1966).

[34] F. Linder and H. Schmidt, Z. Naturforsch. 26a, 1603 (1971).

[35] G. J. Schulz, Phys. Rev. 135A, 988 (1964).

[36] M. N. Pisanias, L. G. Christophorou, and J. G. Carter, Oak Ridge National Laboratory Report ORNL-TM-3904 (1972).

[37] K. D. Jordan, J. A. Michejda, and P. D. Burrow, Chem. Phys. Lett. 42, 227 (1976).

[38] R. J. Celotta, R. A. Bennett, J. L. Hall, M. W. Siegel, and J. Levine, Phys. Rev. A 6, 631 (1972).

[39] A. L. Farragher and F. M. Page, Trans. Faraday Soc. 63, 2369 (1967).

[40] A. F. Gaines, J. Kay, and F. M. Page, Trans. Faraday Soc. 62, 874 (1966).

[41] L. G. Christophorou, D. L. McCorkle, and J. G. Carter, J. Chem. Phys. 60, 3779 (1974).

[42] K. D. Jordan, J. A. Michejda, and P. D. Burrow, J. Am. Chem. Soc. 98, 7189 (1976).

[43] D. Mathur and J. B. Hasted, J. Phys. B 9, L31 (1976).

[44] J. Frazier and L. G. Christophorou (unpublished results, 1977).

[45] L. G. Christophorou, D. R. James, R. Y. Pai, M. O. Pace, R. A. Mathis, and D. W. Bouldin, Oak Ridge National Laboratory Report ORNL/TM-5917 (1977); also (unpublished results).

[46] L. G. Christophorou, D. R. James, R. Y. Pai, M. O. Pace, R. A. Mathis, D. W. Bouldin, and D. E. Tittle, Oak Ridge National Laboratory Report ORNL/TM-5713 (1976).

[47] L. G. Christophorou, D. R. James, R. Y. Pai, M. O. Pace, R. A. Mathis, and D. W. Bouldin, Oak Ridge National Laboratory Report ORNL/TM-5604 (1976).

THIS PAGE

WAS INTENTIONALLY

LEFT BLANK

ORNL/TM-6113

INTERNAL DISTRIBUTION

1-2. Central Research Library
3. Document Reference
4-6. Laboratory Records
7. Laboratory Records, R.C.
8. ORNL Patent Office
9. M. A. Baker
10. R. D. Birkhoff
11. D. W. Bouldin
12. J. G. Carter
13-57. L. G. Christophorou
58. F. L. Culler
59. H. H. Hubbell
60-64. D. R. James
65. C. M. Jones
66. S. V. Kaye
67. T. A. Lewis
68. H. M. Long
69. R. A. Mathis
70. M. M. Menon
71-76. M. O. Pace
77-81. R. Y. Pai
82. H. Postma
83. C. R. Richmond
84. M. W. Rosenthal
85. H. C. Schweinler
86. S. W. Schwenterly
87. J. H. Whealton
88. M. K. Wilkerson
89. H. A. Wright
90. N. F. Ziegler
91. A. Zucker

EXTERNAL DISTRIBUTION

92. D. Allen, Division of Electric Energy Systems, Department of Energy, Washington, D.C. 20545.
93. K. Dimoff, Institut National de la Recherche Scientifique, Universite du Quebec, Case Postale 1020, Varennes, Quebec, JOL 2PO, Canada.
94. J. Gracia, Research and Technical Support Division, Oak Ridge Operations, Department of Energy, Oak Ridge, Tennessee 37830.
95. Director, Research and Technical Support Division, Oak Ridge Operations, Department of Energy, Oak Ridge, Tennessee 37830.
96. O. Farish, Department of Electrical Engineering, University of Strathclyde, Glasgow, G1 1XW, Scotland.
97. R. W. Flugum, Division of Electric Energy Systems, Department of Energy, Washington, D.C. 20545.
98. T. F. Garrity, Division of Electric Energy Systems, Department of Energy, Washington, D.C. 20545.
99. J. M. Googe, Department of Electrical Engineering, The University of Tennessee, Knoxville, Tennessee 37916.
100-114. N. P. Laguna, Division of Electric Energy Systems, Department of Energy, Washington, D.C. 20545.
115. D. Mayhew, Office of the Controller, Department of Energy, Washington, D.C. 20545.
116. J. McKeown, Assistant Administrator for Conservation, Department of Energy, Washington, D.C. 20545.
117. J. J. Phillips, Tennessee Valley Authority, 1310 Commerce Union Bank Building, Chattanooga, Tennessee 37401.
118. L. L. Radcliffe, Research and Technical Support Division, Oak Ridge Operations, Department of Energy, Oak Ridge, Tennessee 37830.
119. V. Tahiliani, Electric Power Research Institute, P. O. Box 10412, Palo Alto, California 94303.
120. J. P. Vora, Division of Electric Energy Systems, Department of Energy, Washington, D.C. 20545.
121-147. Technical Information Center.

☆ U.S. GOVERNMENT PRINTING OFFICE: 1977-748-189/301